PRESSURE DISTRIBUTION AT THE STUMP SOCKET INTERFACE IN TRANS-TIBIAL AMPUTEES

By

SUJAY SAPHIRE GALEN

This thesis is submitted in partial fulfilment of the requirements for the degree of Master of Science in Bioengineering

August 2001

Bioengineering Unit
University of Strathclyde
Glasgow

Copyright

ABSTRACT

The patellar tendon bearing prosthesis is one of the most popular prosthesis for trans-tibial amputees. However an ideal patellar tendon bearing socket is one which has an even pressure distribution and at the same time the sensitive areas of the stump are adequately guarded.. Although many studies have been carried out to investigate the pressure distribution at the stump socket interface, the fabrication of the socket still relies mostly on the skill of the prosthetist. In a patellar tendon bearing prosthesis, load is mainly taken by the patellar tendon bar.

This study was aimed at investigating the stump/socket interface pressures at various horizontal displacements of the patellar tendon bar. This was thought to simulate the pressure the prosthetist applies while taking the cast. A special transducer was developed in this university in a previous study (Osman, 1999), which was capable of displacing the patellar tendon bar forwards and at the same time measuring the forces along three orthogonal directions. However the design of this transducer restricted its use to only one subject. The present study aimed to investigate more than one subject, and so a Patellar tendon bar (Mark-II) transducer was developed, which was capable of being used in more than one subject. This study also aimed at identifying areas of high pressure around the socket and studying the pressure variations in them in different displacements of the patellar tendon bar. Six Entran transducers were used for this purpose and initially areas of high pressure were determined using force sensing resistors (Rincoe socket fitting ssytem)

The results obtained in this study which was done on two subjects showed that pressures around the socket did not vary significantly with horizontal displacements of the patellar tendon bar. Subject:2 who had a shorter stump recorded high pressures and his peak pressures during dynamic gait reached up to 800 kPa. It was discussed later that these high pressures were due to the short stump, and the hard socket that was used to carry out this study. The transducer that was developed showed good linearity and repeatability and had minimal cross talk effects.

Acknowledgements

I would like to thank Professor J.M. Courtney as the Head of the Department, for providing me with an opportunity to pursue my MSc in Bioengineering at the University of Strathclyde. I would also like to thank Professor Barbenel, who had helped me in my decision to come to the University of Strathclyde.

I am very grateful to both my supervisors Mr. W.D.Spence and Mr. Solomonidis, with their help I was able to complete my project successfully.

I would also like to thank Mr. Ian tullis and Mr. David Robb for their contribution in making the PTB mark-II transducer. My thanks also goes to Mr. William, Mr. Rob and Mr. Steven for all their help.

I would also like to thank Mr. Buis for providing the calibration equipment for the Rincoe system. I would like to thank Mr. Sheriff for providing me the 'Acquire' labview program, and Mr. Kevin Holmes for helping me in working with labview.

I would like to thank my friend Dr. Ted Nyunt, whose valuable help made me finish this project successfully.

Last but not the least my parents, without whose help I am sure I would not have made it to what I am today.

TABLE OF CONTENTS

Appendices

Chapter:1

Introduction

1.1 Background

Amputation is a surgery, often performed as a life saving measure. One of the most common amputations performed is the trans-tibial amputation. A suitable prosthesis helps in restoring the functional capabilities of the amputee. Buis (1997) stated that 3 to 4 million people in the developing world require a lower extremity prosthesis, of which 70% are trans-tibial amputees, and the prosthesis of choice in this case is the patellar tendon bearing prosthesis. This prosthesis has proved biomechanically, clinically and in functional restoration, as one of the best. However, it takes quite sometime before the amputee is comfortable with the prosthesis. This can be precipitated due to lot of underlying factors. But the solution probably lies in the right socket fabrication. The difficulty in getting the right socket in the first instance is proving to be a difficult task, because of the lack of data on the distribution of the mechanical stresses at the interface of an amputee's residual limb and prosthetic socket. This often leads to the rejection of the prosthesis by the patient or when used it causes pain and leads to pressure sore formation.

Radcliffe and Foort (1961) have described the design of a prosthetic socket as one whose contours must be able to provide a comfortable and functional connection between the stump and the prosthesis under the conditions of dynamic loading when the prosthesis is used. But to obtain such a design the pressure distribution around the socket must be well understood, before the socket is fabricated. Although CAD/CAM devices have been developed (Oberg et al 1989) to assist prosthetist in socket fabrication, it still has not addressed all the issues, and socket fabrication often relies on the skills of the prosthetist.

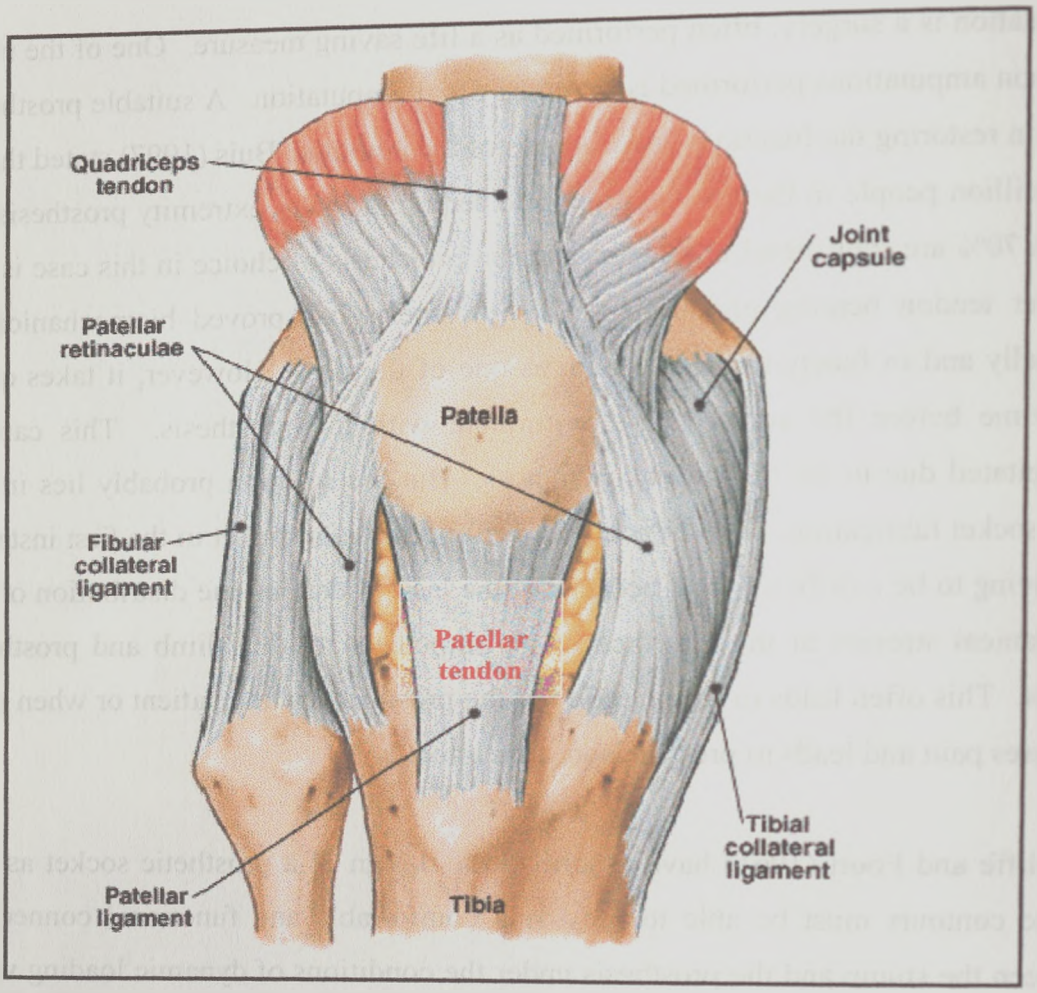

Figure 1.1 Anterior view of the knee joint showing the patellar tendon area
(Adapted from Martini, on-line resources 1999-2000)

A successful rehabilitation program mostly relies upon the functional independence that the patient acquires, and this is achieved not only by the physical condition and pre-morbid status of the patient, but also on the prosthesis that the patient is being trained to use. When a prosthetic socket fails to achieve a good functional and comfortable connection between itself and the stump, it results in abnormal mechanical loading of surface tissue resulting in skin breakdown. This significantly impairs the functional performance of the amputee and limits mobility. Interface pressure measurement studies are of utmost importance in preventing these problems.

The patellar tendon bearing prosthesis primarily loads the patellar tendon area below the apex of the patella (figure 1.1), and prevents the end bearing of the stump and evenly distributes the pressure across the socket. This is achieved by altering the contour of the socket in the patellar tendon region, by providing an indentation. This indentation is usually incorporated in the socket during its fabrication, by the prosthetist. This totally relies on the skill of the prosthetist to provide the right amount of indentation. This study explores the pressure variations across the socket at various position of the patellar tendon bar, starting from a position of minimal indentation.

1.2 Aims of the study

This study was performed to investigate the interface pressures in a trans-tibail amputee, and had the following aims and objectives

- To design a transducer which could measure forces in three orthogonal direction at the patellar tendon region, and also be able to displace the patellar tendon bar horizontally, into the socket.
- To determine areas of high pressures around the socket
- To monitor the pressure variations in these areas of high pressure and the patellar tendon region at various horizontal displacements of the patellar tendon bar.
- To address the disadvantages that were described by similar studies carried out in this area i.e. eliminate the effects of liner material, and to test in a hard socket.

1.3 Structure and outline of thesis

This thesis comprises of seven chapters in all. This chapter (chapter:1) provides an introduction to the study and highlights the background against which the study was carried out. Chapter:2 presents the literature review on the study and outlines the various features of the patellar tendon bearing prostheses, skin response to mechanical loading and finally gives a review of most of the transducers used in the interface pressure measurement studies. Chapter:3 provides a description of the instrumentation and design of the sensors and transducers used in this study, especially the design of the patellar tendon bar transducer. Chapter:4 presents the experimental methodology that was used to achieve the aims of this study. This includes the validation of the Rincoe system, calibration of the Entran and patellar tendon bar transducer and a description of the subject tests. Chaper:5 presents the experimental results. Chapter:6 presents the discussion and analysis of the results. Chapter:7 presents the conclusions and the outcome of the study and also gives suggestion for any future work to continue in this area.

Chapter:2

Literature Review

2.1 Trans-tibial Amputation

2.1.1 Introduction

Amputation is one of the oldest surgical procedures, and amputation of one kind or another has been performed since time immemorial. The first evidence of amputation can be traced back to the Neolithic age (Robinson 1991). Trans-tibial amputations have been described by miracles of Saints Cosmos and Damian as early as 1500. In 1669, Pierre Verduin described a Trans-tibial amputation in detail and he designed a prosthesis, consisting of a thigh corset with side irons and wooden foot.

Trans-tibial amputation is one of the most common forms of lower limb amputations that are performed today. It is most common in elderly patients with diabetes and peripheral vascular disease (PVD). Some of the other causes include trauma, osteomylitis, tumours and congenital deformity. Amputations performed in the elderly due to peripheral vascular disease accounted for about 77% of which 58% also suffer from diabetes, and the average age of patients undergoing amputation is 58 years. Patients with trauma as the cause of amputation were much younger than the patients with PVD as the cause of amputation (Berbrayer, 1996).

Trans-tibial amputation is one of the most important amputations in the category of lower limb amputation (Murdoch, 1969). It is particularly important due to the preservation of the knee joint ensuring better function and cosmesis. From a biomechanical point of view, it may just be a little more than a loss of foot. In terms of rehabilitation the patient with trans-tibial amputation can be expected to achieve a higher functional level compared to one who has undergone a trans-femoral amputation.

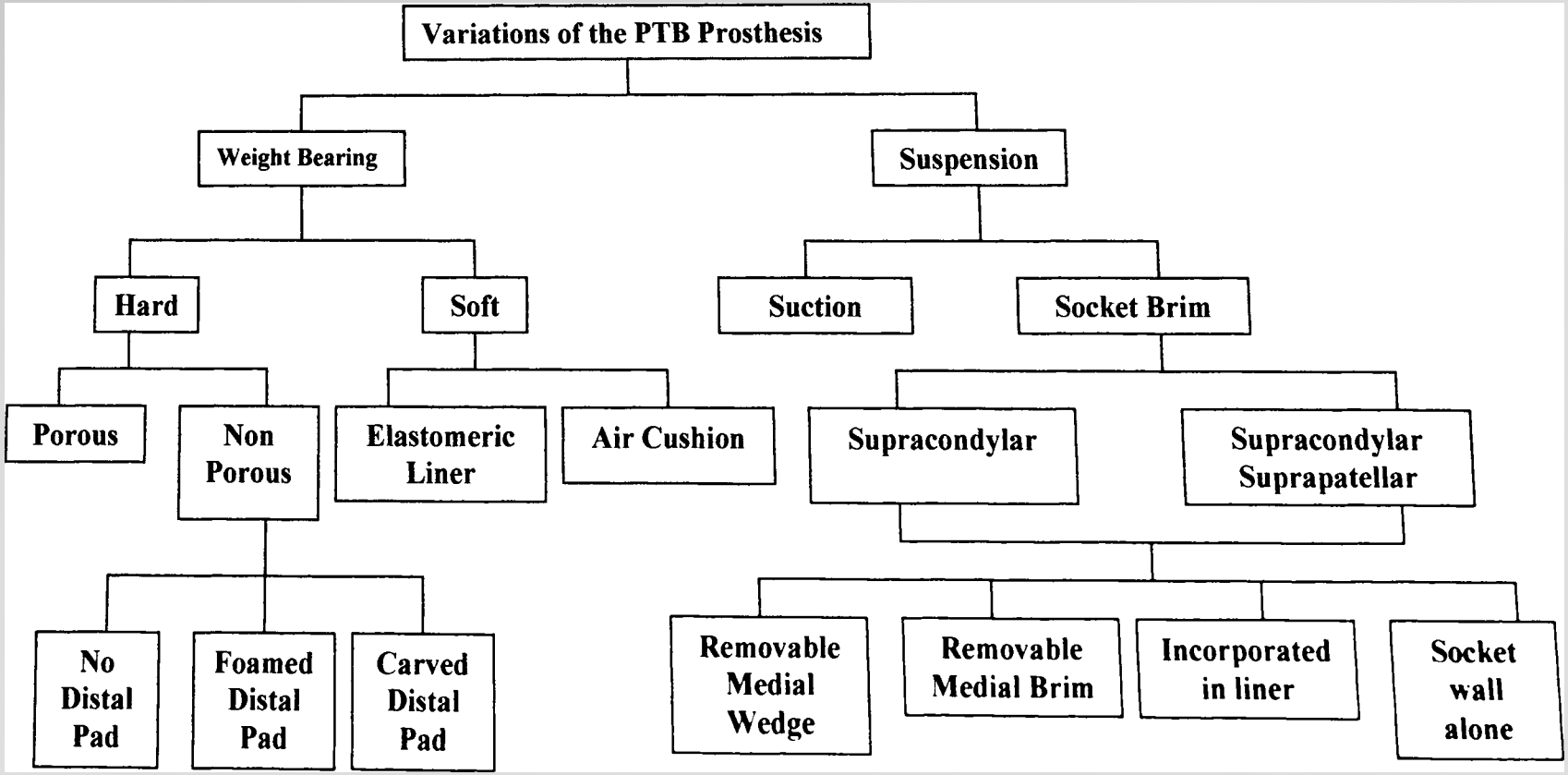

Figure 2.1 Summary of variations of the PTB prosthesis (Reproduced from Pritham (1979)

2.1.2 Indications of amputation

Amputation can be performed for a number of reasons, some of the indications, which warrant an amputation, are as follows:

- Peripheral Vascular Disease
- Trauma
- Burns
- Tumour
- Sepsis/Gangrene

However amputations can also be performed as a treatment in some cases such as:

- Painful limb
- Gross malformation
- Recurrent sepsis
- Severe loss of Function

2.1.3 Trans-Tibial Amputation: Surgery

The Surgical procedures followed in a trans-tibial amputation are varied and beyond the scope of this thesis, however it is important to understand some of the principles involved. The main aim of the amputation is always to leave a stump that will encourage uncomplicated healing. The stump should also be left with good muscular control and should be able to withstand pressures experienced in the stump socket interface. The ideal length of bone that is required to be left behind in a stump is usually between 12.5 and 17.5cms. Although stumps might be shorter or longer than this due to variety of reasons, its generally found that stumps of shorter length contribute less in terms of function and longer stumps have a tendency to breakdown. Another important consideration in a trans-tibial surgery is the retention of the fibular head, because this ensures a stump shape that provides maximum contact with prosthesis thus aiding in a successful and rapid rehabilitation.

2.1.4 Complications following an amputation

Following amputation some complications might occur, and these have a direct impact on early prosthetic fitting and rehabilitation. These complications can be broadly classified as 'Early' and 'Late' complications (Solomon and Warwick, 2001). The 'Early' complications being

- Secondary Haemorrhage
- Infection
- Breakdown of skin flap
- Gangrene

Some of the 'Late' complications are

- Ulceration and skin breakdown
- Bulky muscle cover leading to unstable cushion inducing instability with prosthesis.
- Poor circulation
- Phantom limb sensation and pain
- Stiffness and deformity of joints
- Adherent scars

2.1.5 Prosthesis for trans-tibial Amputation

The first leg prosthesis was a bronze leg (bronze plate with wooden core) found at Pompeii, dated at 300BC (Robinson KP 1991). From that time prosthetics has evolved both in design and in the materials used. One of the most popular prostheses that was used for a long time was one which encased the thigh in a corset attached rigidly through a single axis joint to the shank accommodating the stump. The drawbacks of this prosthesis are the mechanical restriction precluding the possibility of normal action of the knee joint. Because of the lack of understanding of the transmission of forces through the corset, the side joint and the socket, comfort and effectiveness was largely neglected.

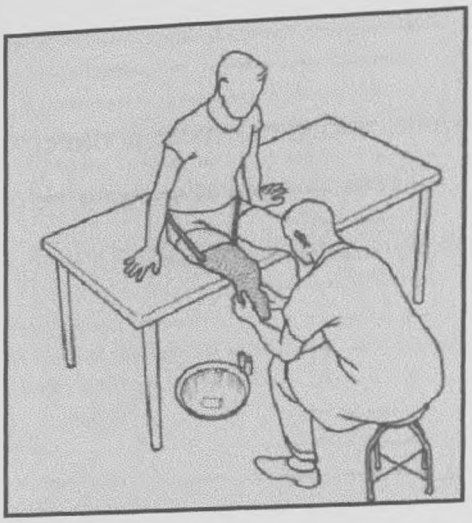

(a)

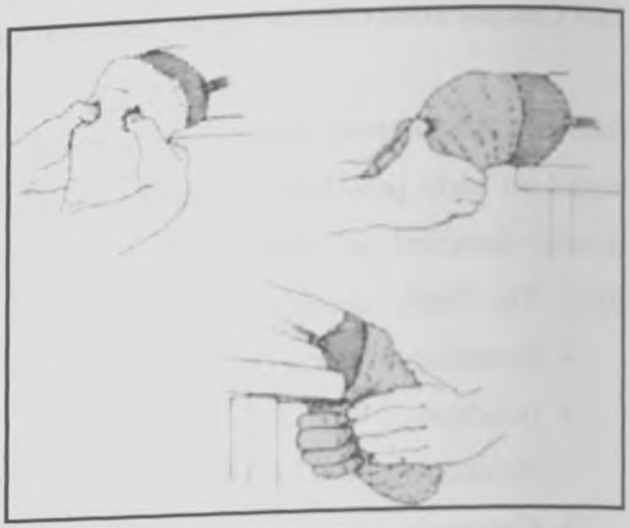

(b)

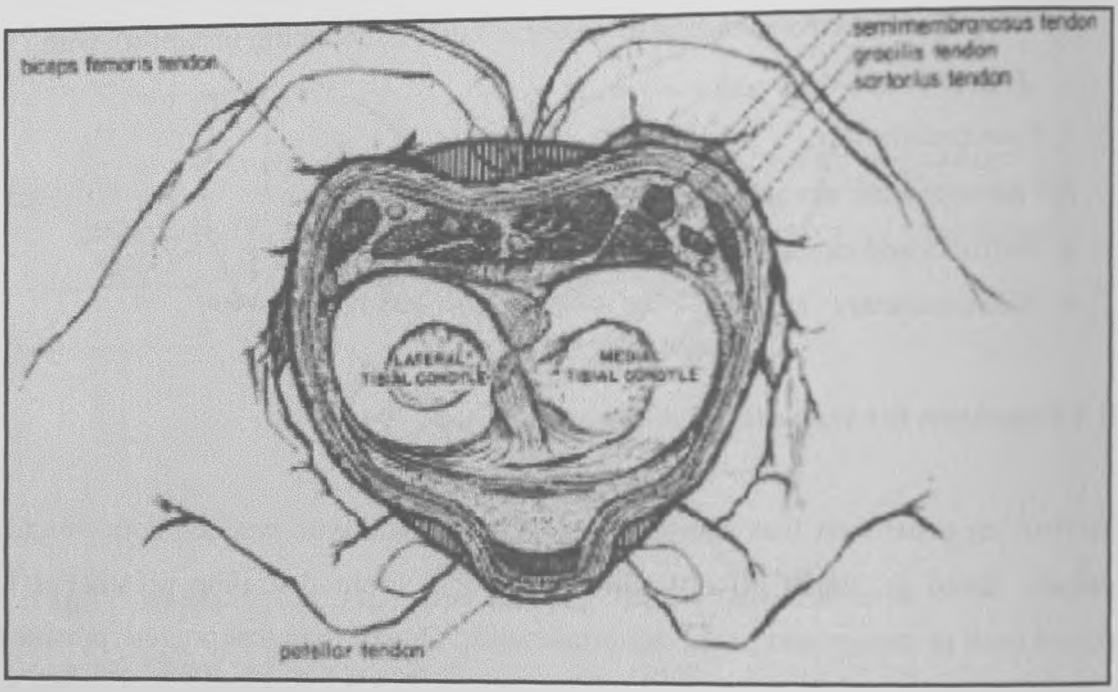

(c)

Figure 2.2 Application of pressure by prosthetist during fabrication of patellar tendon bearing prosthesis
(Reproduced from Radcliffe and Foort (1961)

In the late 1950's the University of California commenced a program to provide an effective prosthesis for the below knee amputee, and came up with the Patellar tendon bearing Prosthesis (PTB). This was thought to be a significant advancement in prosthetic design for trans-tibial amputees (Radcliffe and Foort 1961). Like most prostheses for trans-tibial amputation the PTB consisted of three major parts: a socket, a shank or shin and a foot. However the PTB prostheses differs from the other prostheses in a way that the vertical support load may be largely borne by the patellar tendon, which is a tough area and well suited physiologically for this function. There are many number of variations of the PTB prosthesis based on the type of socket, type of liner and suspension used as shown in figure.2.1

2.1.6 Fabrication of a PTB socket:

The PTB socket is usually hand made by a qualified prosthetist, although modern day technologies have made it possible to fabricate using CAD/CAM devices (Oberg et al., 1989). To fabricate a PTB socket by the manual method the following steps are followed (figure 2.2 a,b,c)

- A wet cast sock is applied over the stump, ensuring a snug fit. The stump during this process is held in about 30° of flexion in order to appreciate all the bony prominences.
- The dimensions of the stump are next measured, and the bony prominence are then marked, including the hamstring tendons
- Wrapping it with a wet plaster-of-Paris bandage makes a negative mould of the stump, and during this process a light thumb pressure is applied on either side of the patellar tendon and the popliteal area is indented by finger pressure.
- Filling the cast with a mixture of plaster-of-Paris and water makes a positive model of the stump.
- After modifications have been made to the model by the prosthetist to make sure that the pressures in the socket will be correct, a test, or check socket, is made by forming a heated sheet of clear plastic over the model.

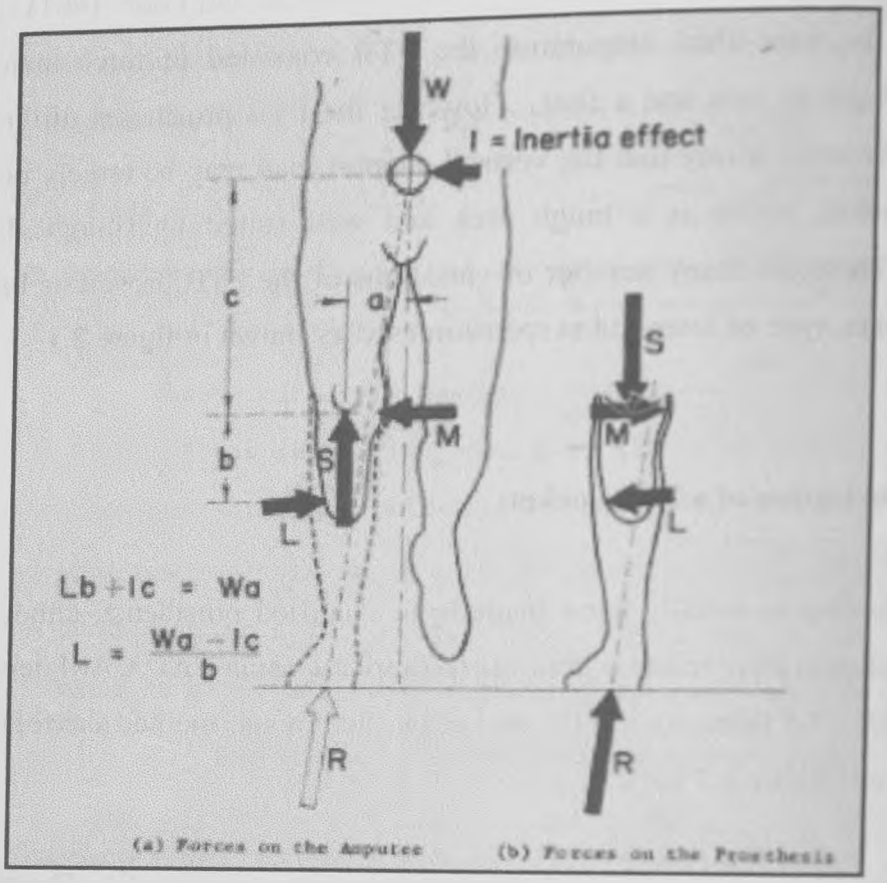

Figure 2.3 Medio-lateral force diagrams in a patellar tendon bearing prosthesis
(Reproduced from Radcliffe and Foort (1961)

- The clear plastic socket is tried on to make sure that it fits properly.
- Filling the clear socket with a mixture of plaster-of-Paris and water makes a new positive model.
- The socket to be used on the definitive prosthesis is formed over the model by using either a mixture of plastic resin and cloth or by forming a heated sheet of plastic over the model.
- The definitive socket is attached to a pylon that can be adjusted for alignment and walking trials can be made.
- The finished prosthesis may be either exoskeletal or endoskeletal.

2.1.7 Biomechanics of the PTB Prosthesis

The PTB socket and prosthesis often helps trans-tibial amputees to achieve gait pattern which is almost near normal and this is mostly attributed to its design. In order to understand this further a force analysis at the interface between the socket and the stump is required. This can be done individually during both the Static phase i.e. standing and Dynamic phase i.e. walking.

2.1.7 a. Static Phase (Standing)

Looking at the forces acting during standing (static phase), the forces inside the socket can be summated to form three distinct force vectors. As shown in figure 2.3, they are named as **S, L, M**, and they act in the vertical, lateral and medial directions respectively. The external forces acting on this system are **W**, which is the force due to the gravitational pull on the body, and **R** is the reaction force from the ground to the prosthesis. The ground reaction force **R** is medially directed and in order to oppose it there is a laterally acting inertial force **I** equal to the horizontal component of **R.** The force **W** acting through the centre of mass of the body acts on the stump through a lever arm **a**, and this brings about a toppling effect which is balanced by the lateral and Medial forces, **L** and **M** acting at the appropriate points of the stump

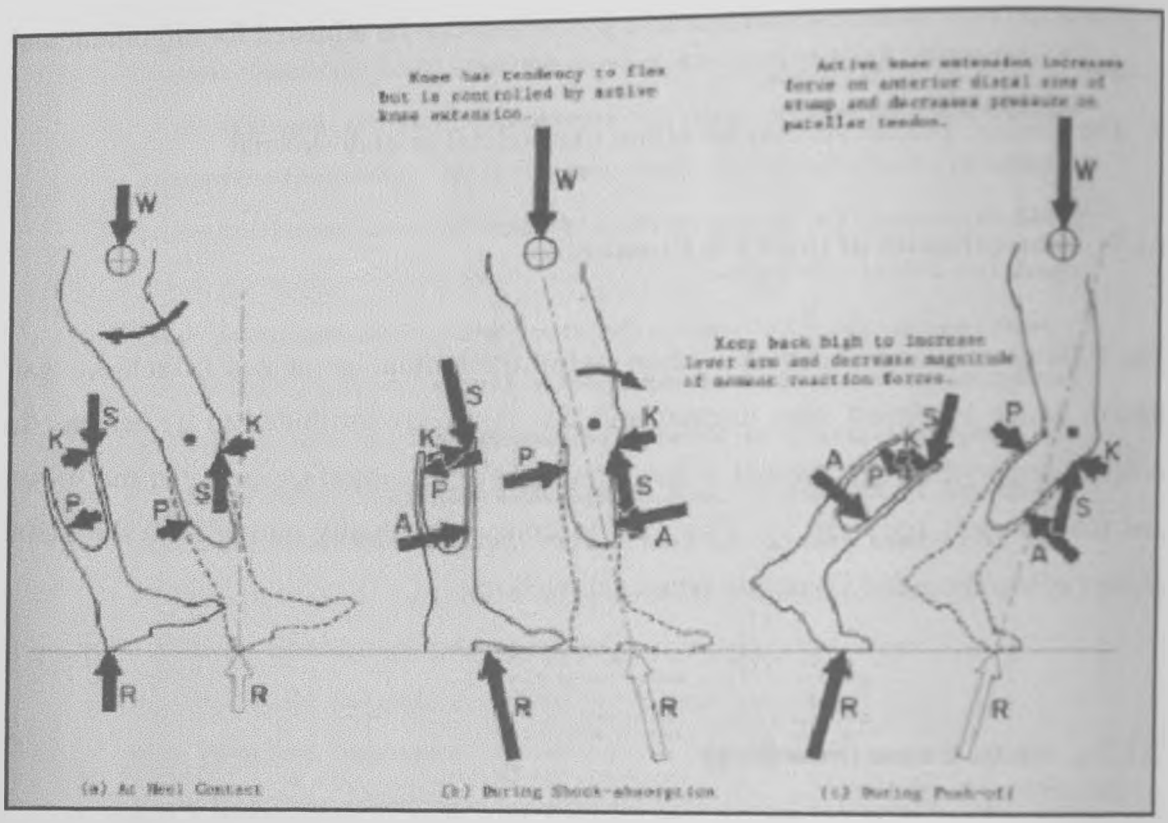

Figure 2.4 Anteroposterior force diagram in patellar tendon bearing prosthesis

(Reproduced from Radcliffe and Foort (1961)

as shown in the figure1.3, and the inertial force **I**. So the summation of about the support point gives the relationship

$$L = \frac{Wa - Ic}{b} \qquad \text{------Equation 2.1}$$

From the above relationship it can be seen that the lateral force **L** depends upon **b** which is the distance between the point of application of **L** and the support point. It can also be seen that it depends on the force **I** which can increase with the lateral positioning of the shoe, in order to compensate for the more medially acting **R.** So a longer stump or a laterally positioned foot can significantly reduce the lateral force.

2.1.7 b. Dynamic Gait

The action of these forces can be seen clearly during the phases of gait cycle from the saggital view, as shown in the figure 2.4. The force pattern during the heel strike, midstance and toe off phases of the gait cycle entirely depend on the position of the resultant force **R** relative to the axis of rotation of the knee. When it is anterior to it causes an extensor moment, which needs to be counterbalanced by the force, patterns in the socket and vice-versa when it acts posterior to it. During heel strike the resultant force **R** passes anteriorly to the knee joint causing an extensor moment and this result in hamstrings acting to counter balance and resulting in a force pattern as shown in the figure2.4. During midstance and toe-off the resultant force **R** acts posterior to the axis of rotation of the knee, there by causing a flexor moment. This is counter acted by the action of quadriceps and the force pattern in the socket changes as shown in figure 2.4

Knowledge of these forces in the socket is taken into account in the designing of the socket, so that they are transmitted comfortably between the socket and stump. The Pressure tolerant areas and the sensitive areas in the socket have been identified as shown in the figure 2.5 (Radcliffe and Foort 1961). The areas of contact through which these forces are transmitted are chosen in such a way that they relieve sensitive areas and at the same time compress only areas that could take up load adequately.

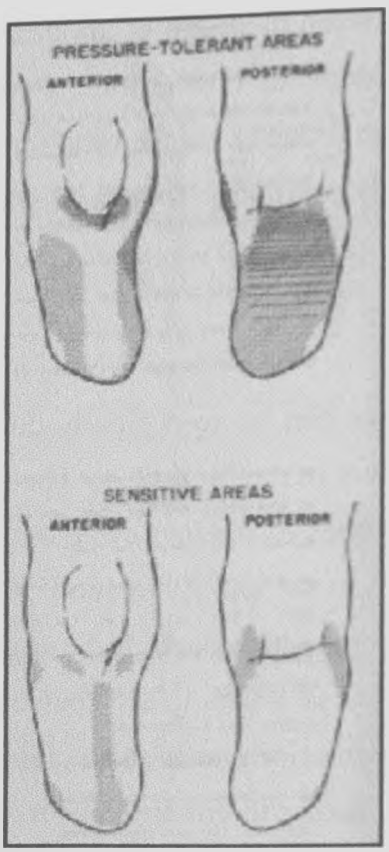

Figure 2.5 Pressure sensitive and tolerant areas in a trans-tibial amputee

(Reproduced from Radcliffe and Foort (1961)

2.1.8 Summary

In the past decade trans-tibial amputation has risen in comparison to the trans-femoral amputation due to the preservation of the knee and its biomechanical significance. It has also less energy demands during prosthetic ambulation as compared to the trans-femoral amputation. The Patellar Tendon Bearing prosthesis and its development has helped many trans-tibial amputees return back to almost normal lives. However a clear understanding on the effect of the patellar tendon bar in the distribution of pressure needs to be understood from a scientific basis. This might lead to better understand its role in trans tibial amputation rehabilitation.

Figure2.6 Structure of skin

1. Hair
2. Stratum corneum
3. Stratum lucidum
4. Stratum granulosum
5. Stratum spinosum
6. Stratum germinativum
7. Papillary dermis
8. Apocrine sweat gland
9. Arrector pili muscle
10. Eccrine sweat gland
11. Adipocyte
12. Hair cuticle
13. Inner root sheath
14. Outer root sheath
15. Hair bulb
16. Follicular papilla
17. Cortex
18. Medulla
19. Sebaceous gland

2.2 Effects of Pressures on the skin of a Trans Tibial Amputee

2.2.1 Introduction

The soft tissues of the residual limbs of individuals with trans-tibial amputation are subjected to significant loading that would otherwise be supported by the feet. The result of abnormal mechanical loading on surface tissue is breakdown. Ideally an effective rehabilitation program aims at preventing this breakdown and encourages load tolerance and adaptation. However, if the abnormal loading continues, tissue breakdown is seen leading to irreversible injury and necrosis. This may further be complicated by formation of pressure ulcers, which may extend deeper into the subcutaneous tissues.

The incidence of pressure ulcers increases with age (Norton et al., 1962). Most of the amputees are elderly and are at high risk of developing these pressure ulcers. The etiology of amputation in most of these elderly amputees being Peripheral Vascular disease (PVD) and diabetes, which bring about sensory changes in the residual limb. In this case the amputee fails to perceive sensory cues about the status of the residual limb at its interface with the socket, resulting in skin breakdown and pressure ulcers.

2.2.2 Basic Structure of Skin

The skin is the largest organ in the body. An average man's skin covers more than 1.7 square meters and weighs 4.53 kg. The skin is divided into 3 distinct layers, the superficial layer is called the epidermis the deep part is called the dermis and below that lies the subcutaneous tissue (Figure.2.6).

The epidermis is a stratified epithelium whose cells get flattened as they mature and rise to the surface. It varies in properties depending upon the region i.e., on the palms of the hand and the soles of the feet the epidermis is thicker and withstands the

wear and tear that occurs in these regions. In the other areas like the arms and forearms it is much thinner.

The dermis is composed of dense connective tissue containing many blood vessels, nerves and lymphatic vessels. The dermis varies in thickness in different parts of the body, tending to be thinner on the anterior than the posterior surface. It is thinner in women than in men (Snell 1992). The dermis of the skin is connected to the underlying deep fascia or bones by the superficial fascia, otherwise known as the subcutaneous tissue.

2.2.3 Mechanical Properties of Skin

In the epidermis the cells migrate from the basement membrane at the junction of the dermis and epidermis towards the surface of the skin. This turnover of the epidermal cells contributes to the maintenance of its mechanical tolerance. As the cells migrate they undergo the process of keratinization (Sanders et al., 1995). During this process the epithelial cells die and the keratin remains and these molecules are reinforced by formation of several disulfide bonds. This makes it strong, insoluble and resistant to enzymes and breakdown. However the mechanical strength of the epidermis is provided by the desmosomes which are plaque like attachments between the cells. At the intercellular level the tonofilaments form the cytoskeleton and are in turn attached to the desmosomes.

The dermo-epidermal junction is the interface between the epidermis and the dermis and is mainly recognised for the mechanical attachment it provides between these two layers. The dermo-epidermal junction is made up of the basement membrane and a sub layer called the lamina lucida, which is considered the weakest point in this interface (Briggaman and Wheeler, 1975).

The dermis consists of elastin (0.2–0.6%), Collagen (27 - 39 %), Glycoamiloglycans (0.03-0.35%), water (60-72%) and cells. The elastin forms a mesh like network in the skin, giving its mechanical integrity when minimal forces are applied (Daly

1982). The skin loses its recoil capability at low force levels with the degradation of this protein elastin. Collagen however, provides integrity to the skin at high force levels, and acts as a principal load-bearing component of the skin. The molecules are arranged in a staggered array giving them a striated appearance. The collagen molecules are attached via crosslinks, covalent bonds between lysine residuals. The collagen modelling occurs based on the distribution of the stresses, the reinforcements in areas of maximum stresses and degeneration in areas of less stress. Glycoaminoglycans along with water contributes the visco-elastic property of the skin. The proteins like elastin and collagen are produced by fibroblasts, and hence play a major role in the laying down of these proteins according to the distribution of mechanical stresses (Clark, 1985).

2.2.4 Tissue Response to Mechanical Loading

The application of external forces to the tissues causes the tissues to deform, the interstitial fluids to flow, ischemia, reactive hyperemia, pain, change in skin temperature and colour (Bader 1990). Within physiological limits these reactions do not disrupt tissue functions. Skin trauma can occur either as a result of metabolic defect such as ischemia or due to accumulated micro damage. The application of forces in a improper way leads to damage of the structure and loss of functions. A large force when applied for a short duration can cause direct skin breakdown. However when forces of a moderate magnitude are applied the underlying blood vessels and lymphatic channels become occluded, hampering the delivery of oxygen and other essential nutrients for the cells and also causes metabolites to be accumulated in the cells (Micheal and Gillot 1990). This result in cessation of cells functions, leading to tissue breakdown both in the superficial and deep levels. The duration during which this process takes place directly depends on the magnitude of the force and frequency of repetition. A frequently repetitive load leads to micro damage causing inflammatory reaction and tissue necrosis leading on to its breakdown.

In a trans-tibial socket the stump is exposed to variety of forces, depending on the relationship of the socket interface with that of the stump contour. These forces or loads are dynamic or repetitive during locomotion. Thus these loads bring about the skin breakdown. Some of the other factors that also leads to skin breakdown are excessive slip between the skin and socket leading to tissue abrasion and generation of heat (Mak et al., 2001). Secondly the high humidity environment in the socket due to accumulation of sweat and lack of circulation of air generates irritability of the skin and breakdown. Thirdly, skin breakdown can also occur due to chemical or mechanical reactions or allergic reactions due to various socket and interface materials (Levy, 1980).

Loading in a trans-tibial socket can be considered under three configurations, and they are pressure, shear and friction and tension (Sanders et al., 1995)

2.2.4.a Pressure:

Pressure may be defined as a uniformly applied force acting perpendicular over an area of skin. Pressure ulcers and skin break down occur as a result of these uniformly distributed forces acting on the skin or load bearing areas for a long duration. In a review of pressure related studies by Sanders et al., (1995) the study on application of pressure and skin changes (Husain, 1953) has been reported. It has been demonstrated in the above mentioned study that an ischemic histological change was found in the underlying muscles when a pressure of 100mmHg (13Kpa) was applied for 2 hours and a complete muscle necrosis was observed when the same pressure was applied for 6 hours. It has also been proven that a relationship exists between pressure and duration, particularly in the regions of bony prominence (Krouskop et al., 1983). As this mechanism of tissue breakdown is irreversible attention must be paid to this pressure-time relationship. Since trans-tibial amputees wear the prosthesis for a considerable amount of time these pressures must be kept at moderate levels.

It has also been proven that deeper tissues are more vulnerable to injury from pressure than the superficial skin (Daniel et al 1981, Nola and Vistnes, 1980). So pathological changes first take place in the muscle and then progress on to the skin. Some of the factors that hasten this process of skin breakdown are moisture, humidity and temperature, as these decrease the stiffness of the epidermis and dermis and thereby loading the deep lying tissues directly.

2.2.4.b Shear and Friction

This a force that is applied along the plane of the surface of the skin. Frictional force comes into play when there is a relative displacement between the skin and the supporting surface. These forces occur often in the stump-socket interface of the trans-tibial amputee, due to the pistoning motion of the stump into the socket. The action of shear and frictional forces on the surface of the skin can bring about blister formation. Concentration of shear and frictional forces are higher over the bony prominence. A combination of shear forces and pressure lead to occlusion of the blood supply and tissue breakdown and at higher magnitudes of shear force a minimal pressure can bring about skin breakdown and ulcers (Bennett et al 1979). Most of the studies have been conducted on animals due to ethical considerations, but earlier studies done by Naylor (1955) on human beings developed a relationship between frictional forces and blister formation. He used different materials and loads to quantify the threshold of blister formation. Through his work on human subjects he stated that the lower the frictional force the greater was the work needed to break down the epidermis i.e. formation of blister. Other parameters on which blister formation depends are thickness and temperature of the skin. Sweating also promotes blister formation, as it increases frictional force. Blisters usually occur as a result of shearing between the epidermis and the deeper anchored layers of skin, resulting in a cleavage between them filled with fluid.

2.2.4 c Tension

Tensile loading is said to occur when the skin is stretched or pulled across a surface. In a trans-tibial amputee tension can be located near adherent scar tissue or at the distal end of the stump due to the action shear forces. Tension can be induced in

trans-tibial amputees without even the stump coming in contact with the socket. This can be observed over the anterior tibial crest due to the anterior shear stresses. (Sanders et al 1992). Such excessive tension can lead to tissue breakdown. However studies to investigate the effects of tension on the skin have been carried out on animals and on healing surgical wounds. This comes into application when suture wounds experience tension inside the socket. As healing wounds have less tensile strength, tension can cause breakdown to occur easily.

2.2.5 Clinical manifestations of mechanical loading

The mechanical loading of tissues first comes to the notice of a clinician through the complaints of the patient, and an extensive clinical investigation would reveal the following at the site of loading

2.2.5a Pain

This is the first response that a human body registers due to mechanical loading, it is generally perceived as a discomfort. In an amputee with intact sensation this is perceived immediately when the skin is loaded with a large abnormal force and the reflex mechanism avoids further application of this force by a change in gait pattern or posture. However in an amputee where sensation is affected this leads to irreversible damage, as they are not able to perceive the pain eg. Diabetic patients.

Some of the other clinical manifestations that occur due to mechanical loading are Microvascular responses and changes in the perfusion of the skin, accumulation of metabolites in the sites of loading and occlusion of lymphatic channels causing oedema, and changes in skin temperature.

2.3 TRANSDUCERS USED FOR PRESSURE MEASUREMENTS

2.3.1 Introduction:

Pressure measurement studies in Trans-tibial prostheses is not a new development, but has been investigated methodically for about 50 years (Mak et al., 2001). As a result of these studies, various changes in the socket design have taken place i.e thigh-lacer side joint, patellar tendon bearing prosthesis rtc.,. The information obtained from these investigations has also brought about better understanding of socket load transfer and to validate information obtained through computational modelling. Measurement of interface pressures is usually done using pressure transducers, sensors and various other pressure measurement techniques. As a result of the extensive investigations carried out in this area many pressure transducers and sensors have been developed to get an accurate picture of the pressure distribution at the stump socket interface. These techniques have also been reviewed by various investigators such as Sanders (1995) and Silver-thorn et al., (1996). Although, at first glance this may look to be an area that has been well investigated and reviewed, infact still a good understanding of the distribution of these pressures is lacking and still relies on the skill of the prosthetist.

The study of the interface pressures in a residual limb is thus inevitable. The transducers used for this purpose can be classified based on their operation as follows (figure 2.6).

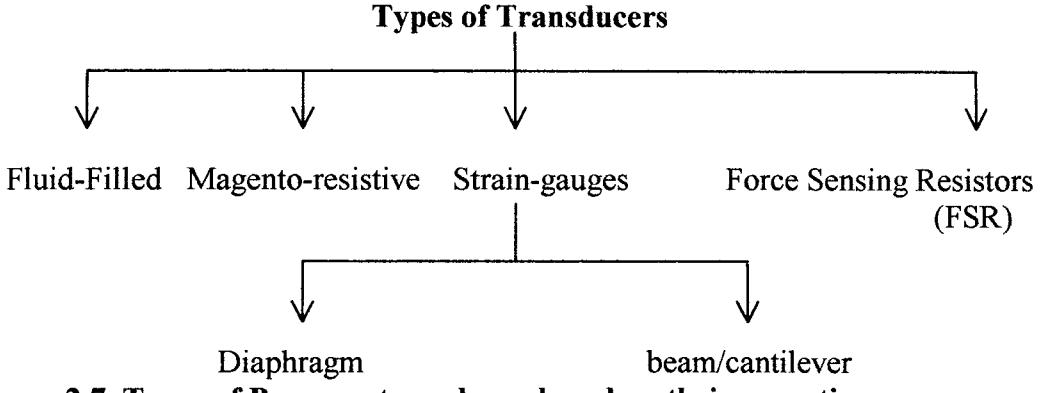

Figure 2.7. Types of Pressure transducer based on their operation

2.3.2 Fluid-Filled Sensor:

Fluid-filled sensors have been used for interface pressure measurements in sockets. These sensors were placed between the skin and the socket liner. The advantage offered in comparison to kulite transducer is that, the edge stress concentration is reduced, because it is more flexible. They were fabricated by Van Pijkeren and were used in various socket interface pressure measurement studies (Van Pijkeren et al., 1980 , Naeff and Van Pikeren, 1980)

2.3.2.a Design:

The sensor was made from Poly-vinyl chloride sheets and it consisted of a 0.25mm thick, 7mm diameter, cylindrical liquid chamber attached to a 1.2mm nylon tube, that exited at the socket brim to a pressure sensing diaphragm. The external sensor was 0.6mm in thickness and 30mm in diameter. This transducer was not used to collect data in walking due to its limited dynamic response. The nylon tube loading in the socket caused a loss of sensitivity, because of its large fluid volume compared to the volume of the fluid in the sensor.

2.3.3 Magneto-Resistive Transducers:

These transducers work on the principle of transduction. The resistance of the semi-conductor resistor varies according to the magnetic field applied to it. The resistor is thus arranged in a bridge configuration, and a magnet is placed over them. The displacement of the magnet by a force proportionally alters the resistance, and thus gives out an electric signal. Transducers using this principle were first developed by Tappin et al (1980). This was a single axis-transducer but this principle was later used by Williams et al.(1992) to develop a triaxial force transducer to investigate stresses at the stump socket interface.

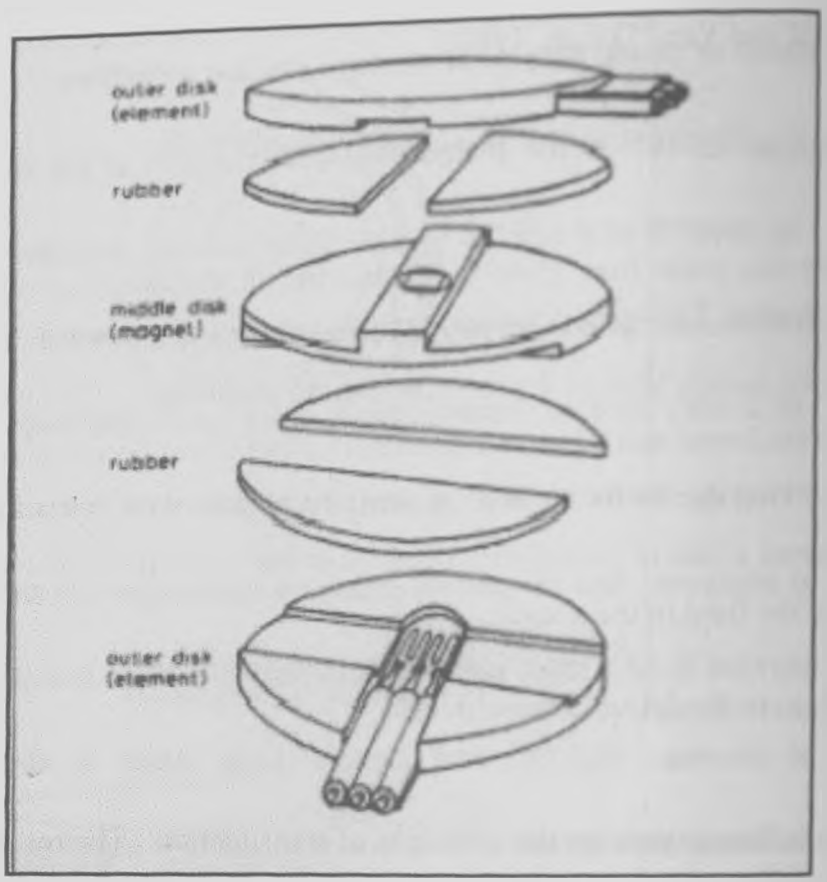

Figure 2.8 Magneto-resistive transducer
(Reproduced from Williams et al, 1992)

2.3.3 a Design of the Transducer:

The design of the transducer is shown in figure 2.8

In the triaxial force transducer, the two shear forces were measured simultaneously. The transducer consisted of 3 disks constrained by ridges and grooves, so that the outer two slide orthogonally with respect to the inner disk. Each outer disk contained magneto-resistor elements. The inner disk contained the magnet. A FP1111100 Siemens differential magneto-resistor was chosen, for its good temperature stability, although it has reduced magnetic field sensitivity. The reduced sensitivity to the magnetic field is addressed by using a neodymium boron iron (NdBFe) magnet for its optimal magnetic field saturation, and using a clearance of 0.1mm between the magnet and the element. Once the magnet was set to accurately move to the shear force over the element, a restoring force was required to bring it back to its original position, this was done by an elastic medium made of Natural rubber. The rubber was glued to the aluminium disk using an epoxy adhesive. The overall thickness of the shear section of the transducer was 3.8mm, with a diameter of 16mm.

To measure normal force an in-house strain gauged diaphragm technique was used. A Technimeasure QF DPF 9-350 full bridge foil gauge mounted on a silver steel diaphragm was used. This particular strain gauge was chosen for its sensitivity and stability with temperature. The normal force transducer was assembled with the shear transducer, but was oriented away from the stump surface, so that an indenter could be incorporated. This measure was taken to avoid any artefacts in the measurement due to variable tissue characteristics. However the problem with the indenter is the chance of overloading of the diaphragm, this was overcome by using a overload protection mechanism, which distributes the load evenly over the diaphragm. The thickness of the normal section was 1.1mm making the overall thickness of the transducer to be 4.9mm.

2.3.3 b Data Collection:

The signals obtained from the transducer were amplified, and then filtered using a four-pole Bessel filter, to filter frequencies above 250Hz. The signals were then converted to digital using a 12-bit A/D converter attached to a micro-computer. The sampling frequency for the data collection was 25Hz.

2.3.3 c Properties of the Transducer:

Although Williams et al. (1992) stated that the transducer had met its original specification, it has been commented by themselves and Sanders (1995) that the transducer has a hysteresis of 8% of the full scale output for shear forces. In the case of the direct stress, a hysteresis of 2% of the full scale output was noted. Due to the overload protection incorporated in the transducer, there was a progressive reduction in the sensitivity to higher loads. For the normal axes, creep was practically negligible. The transducer had a force resolution of 0.2N in the shear axes and a 0.1N in the normal axes. The temperature sensitivity drift was less than 0.7% per degree C for the shear axis, and 0.15% per degree C for the normal axis.

2.3.4 Strain-Gauged Pressure Transducer

2.3.4 a Diaphragmatic type: Kulite Transducer :

The kulite transducer is a diaphragm deflection strain gauge transducer. The kulite transducer was used in many interface pressure measurement studies in sockets (Sonck et al., 1970, Pearson et al. 1973, Burgess and Moore, 1977)

The sensing element was 3.2mm in diameter and 0.8mm in thickness. This was designed to measure only pressure. It was a monolithic integrated circuit wheatstone bridge formed directly on a silicon diaphragm. A stiff backing was provided to prevent it from bending. A four-conductor ribbon cable of 0.5mm thickness was

attached to its bottom surface. The symmetry of the sensor in respect to the disk central axis makes it insensitive to all loading except in the normal direction. The transducer was also light weight. It has good sensitivity, and so does not require amplification. But there are lot of limitations associated with this transducer such as, it underestimates the stress at skin which is thin and over the bone. The sensor movement during ambulation makes stress comparison difficult. The kulite transducers were inserted between the skin and the socket liner, so the cables inside the socket, distort the pressure measurements. Due to a stationary data acquisition facility, the amputee cannot move around much.

2.3.5 Cantilever/beam Strain gauge with Diaphragmatic combined

This is a type of transducer that uses a strain gauged beam or cantilever to measure the shear stresses and a diaphragmatic strain gauge to measure the pressure. The two components were first developed separately by Appoldt and Bennett (1967). However later Sanders and Daly (1993a) and was subsequently used for various socket pressure measurement studies in trans-tibial amputees (Sanders and Daly 1993b, Sanders et al., 1993 and Sanders et al., 1998). The transducer developed by Sanders and Daly (1993a) has been discussed in detail in the following section.

2.3.5.1 a Design:

This transducer had a 6.35mm diameter-sensing surface, and it records forces in three orthogonal directions. Shear measurements in two orthogonal directions in the plane of the transducer were measured by metal-foil strain gauges (EA-06-031DE-120, micro measurements, Raleigh, NC). These strain gauges were mounted on 1.52 mm square cross-section aluminium beam. Two gauges were mounted on each face so that the distance between gauge centres was 12.7mm. A wheatstone bridge was configured, using the gauges in the opposite faces. Thus shear force measurements were in sensitive to off-centre normal forces.

The force normal to the sensing surface was measured using a full-bridge diaphragm strain gauge (EA-13-182JB-350, Micro measurements, Raleigh, NC). The gauge was bonded to the inside of a cap. The cap was between the cap support and the Pelite disk. The normal force applied on the cap surface was measured from the diaphragm deflection. The pelite layer on top of the sensing surface was 2.80mm in thickness and was bonded to the outer surface of the cap by a thin layer of epoxy.

2.3.5. b Data Collection:

The data were collected after signal conditioning, using filters and amplifiers. Filter cut-off frequency was 1kHz. An amplifier gain of 4000 was used in walking trials. In pilot studies using this transducer, data collection was performed at 500Hz sampling rate, later a 125Hz sampling rate was set. The signal obtained had a bandwidth of 0-40Hz. A low-pass filter had to be used to filter out high frequency noise signals. In the initial design a strip-chart recorder performed data acquisition. Later an A/D converter was used and the data were fed to a personal computer for processing. The system was controlled using a program written in Quick basic.

2.3.5 c Positioning of Transducer in the socket:

The transducers were positioned in a mount (table 2.1) bonded to the outside of a socket such that the sensing surface was flush with the pelite lining the inside of the socket. The transducers were placed in low curvature locations of clinical interest, because of the concern that the transducer would distort the normal socket shape. Holes measuring 8.73mm in diameter were drilled perpendicular to the wall of the socket.

Site	Abbr.	Description of Location
Anterior lateral Proximal	**ALP**	at the level of the tibial tubercle, lateral side
Anterior Medial Proximal	**AMP**	at the level of the tibial tubercle, medial side
Anterior Lateral Distal	**ALD**	distal stump, anterior tibial border, lateral side
Anterior Medial Distal	**AMD**	distal stump, anterior tibial border, medial side
Lateral	**L**	femoral neck,~2cm distal to the fibular head
Posterior Proximal	**PP**	mid-calf, on the posterior longitudinal midline
Posterior Distal	**PD**	distal-calf, on the posterior longitudinal midline

Table.2.1 Position of transducer sites (Reproduced for Sanders and Daly, 1999)

2.3.6 Force Sensing Resistors:

Force sensing resistors have emerged as a result of development in technology. These are extremely thin sensors that are placed between the skin of the stump and the socket. All the techniques that were discussed earlier can measure pressure at discrete focal sites because of the large diameter of the sensing surface. However using force sensing resistors a sensor mat with an array of pressure cells can measure the distribution of pressure around the socket. Commercial systems using Force sensing resistors have been developed, namely the F-scan system and the Rincoe socket fitting system. Studies have been done with the F-scan system in trans-tibial amputees (Convery and Buis, 1998, Convery and Buis, 1999) and similarly the Rincoe Socket fitting system has also been used (Shem et al. 1998). However the accuracy of both systems have always been under debate and studies have been carried out comparing both the above mentioned systems (Polliack et al. 2000). Buis and Convery (1997) reported problems of calibrating the force sensing resistors.

(a)

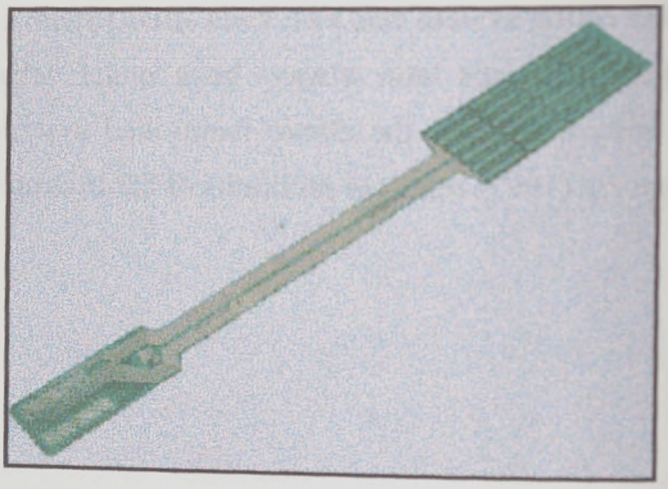

(b)

Figure 2.9 F-scan socket pressure measurement system

(Reproduced from Tekscan systems website)

2.3.6.a F-Scan System:

This is made up of pressure-sensitive, resistive, and conductive silver-based inks, embedded in a Mylar coating. Columns and rows intersect to form a tiny cell, and there are 96 such cells. Four such transducers were used, with a total of 350 cells (figure 2.9 a&b). They were attached to the inner wall of the prosthesis using a non-agressive spray adhesive. The transducers were attached to the anterior, medial, posterior and lateral walls. Every single cell continues as a wire embedded in the Mylar coating and terminates at the connector, this is then connected to a pre-amplifier. The resistance of each cell is inversely proportional to the pressure applied. Therefore, during walking as the pressure varies the resistance varies proportionally giving varied signals. These signals are relayed through the wire to the pre-amplifier and are conditioned and converted from analog to digital signals. The data are then taken by a co-axial cable to an expansion card situated in the CPU of a computer, where they are scanned electronically every 50-100 msec. The data arerecorded and stored.

The transducers are calibrated while attached to the inner walls of the socket. A pre-determined pressure is applied to the inner socket wall via a pressurised gel filled sheath. When subjected to repeated pressure application, there is an average variation in the applied pressure of +/-2% and a maximum of +/-10% for any individual cell in the sensor array (Buis and Convery 1997).

Before mounting the transducers onto the socket, a sensor reference grid is established using a socket axis locator. Four longitudinal lines are used to centre the transducers, and taking the bottom centre of the socket as a reference, circumferential lines are used to locate the transducers axially.

The data was collected at a sampling frequency of 150Hz, for approximately 0.8 seconds. In the given data collection parameters, the 350 pressure sensors collected about 42,000 pressure readings in a single step. This huge amount of data is then

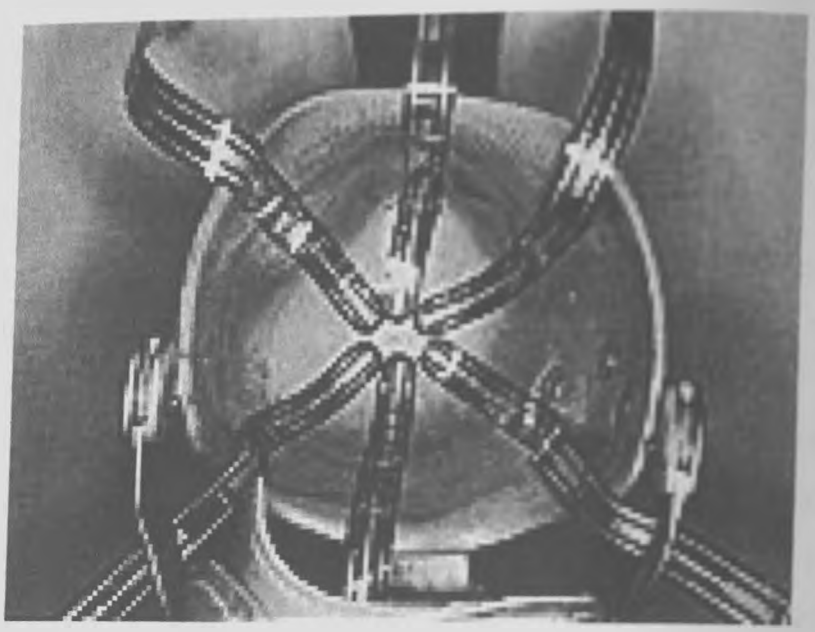

Figure 2.10 The Rincoe Socket fitting system

(Resproduced from Rincoe website)

processed in the computer using a special software provided by TEKSCAN®, who are the manufacturers of this transducer. The software displays two and three dimensional graphs or pressure distribution images. For statistical analysis the data may be stored in the form of an ASCII file. The software is user friendly.

2.3.6 b The Rincoe Socket Fitting System (SFS)

This transducer also uses force sensing resistors (fig 2.10). It is primarily used as a diagnositic tool by the prosthetist to improve the fit of the socket

The transducer is extremely thin, and is placed inside the socket, to measure the pressures inside them. The pressure measurements are done by up to 60 pressure sensors placed in six equally placed strip around the socket wall. Depending on the areas of pressure, the strips can be positioned accordingly. The transducer is attached to a 30ft long cable, which permits pressure readings to be taken for up to 60ft, and at any point of the gait cycle. The computer then processes the collected data and using the Socket fitting System (SFS)® graphics, the pressure distribution inside the socket can be visualised. A detailed description of the Rincoe socket fitting system can be found in section 3.1

2.3.7 Summary:

All the transducers discussed so far have both advantages and disadvantages, either in the design or on the working. However these have not been studied enough and validated. The F-Scan system can be used to study the interface pressures, because the instrumentation of the socket is quite easy. But a discrete method measurement although measuring only selected areas of the residual limb, gives a more accurate estimate of the stresses.

CHAPTER:3

INSTRUMENTATION AND DESIGN

3.1 Rincoe Socket Fitting System

3.1.1 Introduction

The shape and contour of a trans-tibial socket varies from amputee to amputee. To study the behaviour of the interface in these sockets the areas of high pressure need to be determined. In interface pressure measurement studies that were conducted earlier (Sanders and Daly 1999, Wandrum 2000) the transducers were mounted at anatomically predetermined points in the socket. However one of the objectives of the present study was to identify areas of high pressure and to monitor the pressure in these points during standing, walking with various indented positions of the patellar tendon bar. The Rincoe Socket Fitting System was used to detect areas of high pressure in the socket, and these later became the sites where the Entran pressure transducers were mounted

3.1.2 Selection of Rincoe System

The Rincoe Socket fitting system is a diagnostic tool used by prosthetists to assist in obtaining a good fit of the socket. But the Rincoe socket fitting system has also been used for scientific studies to determine interface pressures in trans-tibial amputees (Shem et al 1998). There are also studies which show the Rincoe socket fitting system to be less accurate in terms of the pressure measurements compared to other systems such as Tekscan (Polliack et al 2000, Hunter 1996). However it has been made clear by the above studies that these systems are adequate in indicating areas of high pressure at the stump socket interface, provided its limitations are taken into account. The sensor strips that are placed at the interface between the stump and the socket, being extremely thin do not elevate the pressures due to their presence. These reasons justified the selection of the Rincoe socket fitting system.

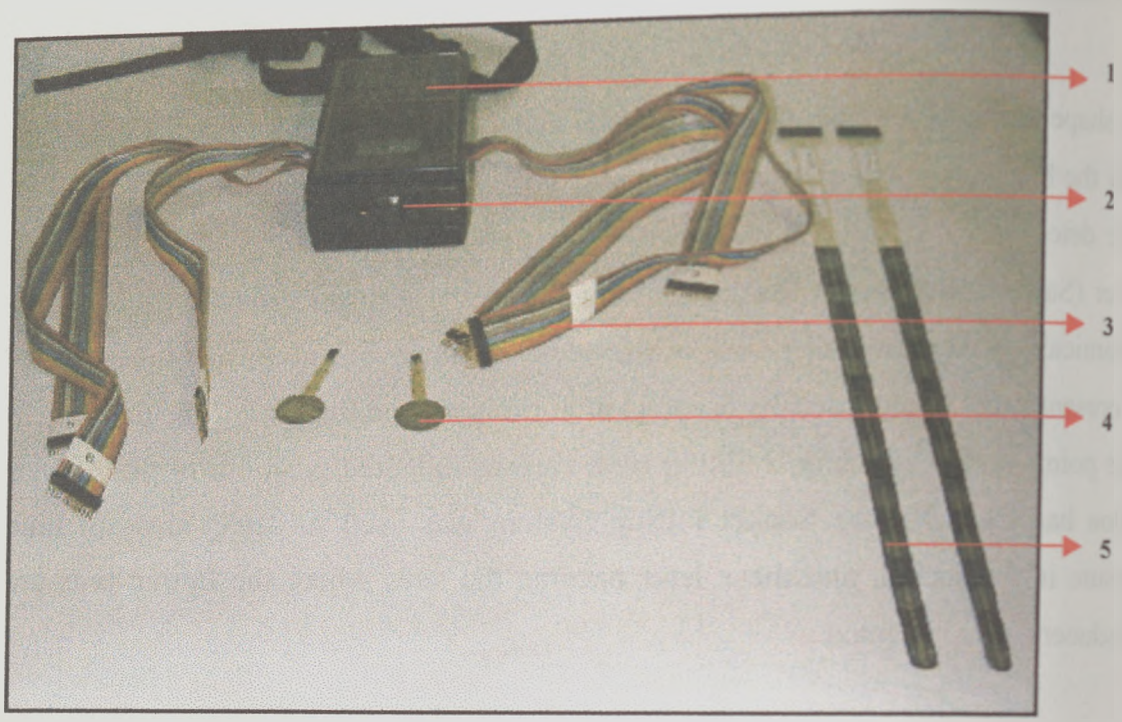

Figure 3.1 The Rincoe Socket Fitting System

Legend

1 – Hardware box

2 – Connection socket for communication cable.

3 - Integrated flat cables for the 6 sensor strips

4 – Foot switches

5 – Sensor strips

3.1.3 Features and components of the Rincoe system

As discussed earlier in the literature review (section 2.3.6 b), the Rincoe Socket Fitting System (SFS) utilises the Force Sensing Resistance (FSR) technology. The extremely thin calibrated SFS sensors can measure pressure within a socket. Readings can be taken while the amputee is standing still, walking, running, sitting and going up and down stairs. The system consists of the following components (Figure 3.1):

1. A hardware box, which is battery operated (9.6V). This collects the raw data from the sensors and then inputs to a computer for further processing. It also contains 6 flat integral cables, which connect to the 6 sensor strips.
2. Sensor strips (6 off), which are made up of 10 force sensing resistors in each. The sensors are embedded in polyvinilidyne fluoride strip which is 0.36mm in thickness. Each strip is 54.9cm long and has 10 sensor areas of 0.45cm^2 each. The 10 sensors in each strip are placed with a 2.3cm space between each of them. The sensors are attached to the inner side of the socket by means of double-sided adhesive tape.
3. Three foot switches (FSR's) which are used to detect heel strike, mid stance and toe-off phases of the gait cycle.
4. A 1.22 m long, 6 strand, sheathed cable which has a RJ 11-6 connector on one end. The other end has three cables coloured red, blue and green with 2 pin connector at each end which connect to the foot switches.
5. A 9.14 m foot long communications cable, with a RJ 11-4 connector at one end and a custom moulded DB25 connector at the other end. This connects the hardware box with the computer.
6. A floppy disk, which consists of the special DOS-based software which processes the information collected by the hardware box into pressures, and displays them graphically either in the form of strip graphs or circumference graphs. The software also allows storing data collected from various subjects in the form of a database. The floppy disk also

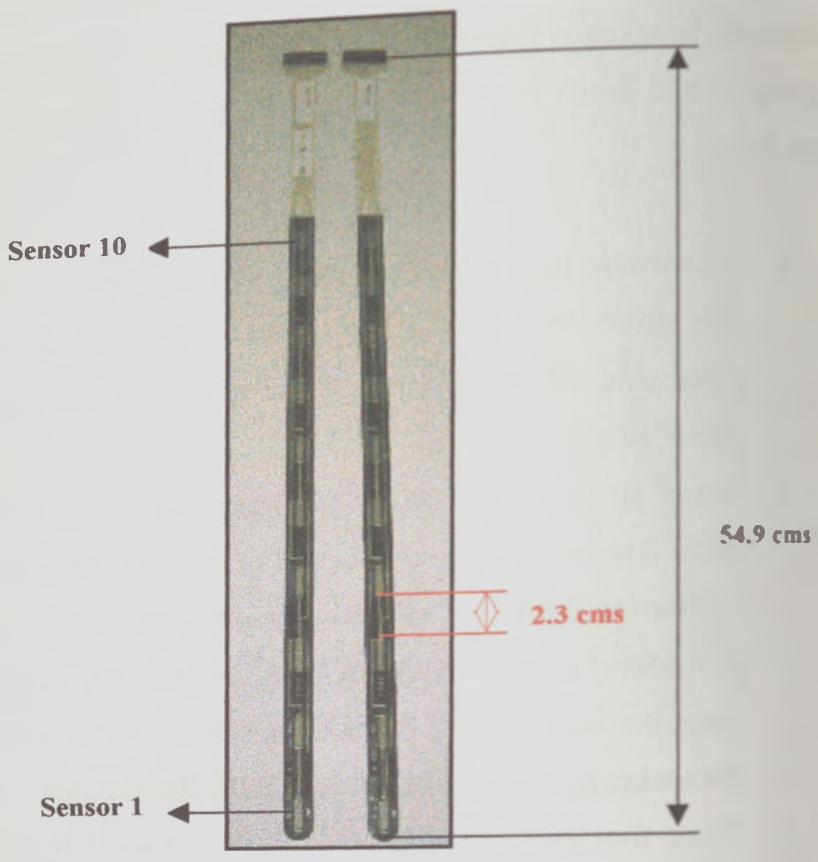

Figure 3.2 Rincoe sensor strips with its dimensions and distance between each sensor and the order of arrangement

contains the calibration data of each sensor. The 60 Sensors are calibrated by the manufacturer in the company itself.

7. The manufacturer also recommends the use of only 386 model computers for data collection, because this clock speed suits the hardware settings of the Rincoe system.

The Rincoe socket fitting system is powered by Rechargeable Ni-cad batteries which supply a P.D of 9.6V.

3.1.4 Characteristics of Data collection

The data from the 60 sensors are sampled at a sampling frequency of 100Hz. Both static and dynamic measurements can be taken. The software graphically displays the results in two forms. The strip graph presents the data strip wise showing the pressures recorded in each sensor of one particular strip. The other form of presentation is the circumference graph, which presents the data from a horizontal ring at a particular level incorporating all six sensor strips. A real-time display of variation of pressures in a socket can be displayed in the strip mode.

During dynamic pressure recording, only three consecutive frame recordings are possible i.e. Heel strike, midstance and toe-off. The pressures are displayed in psi. The system can measure pressures upto 12psi (82.68kPa). Between 1.5psi (10.335kPa) and 5psi(34.45kPa) the system has a resolution of 0.5psi(3.445kPa). From 5 psi to 12 psi the system has a resolution of 1psi (6.89kPa).

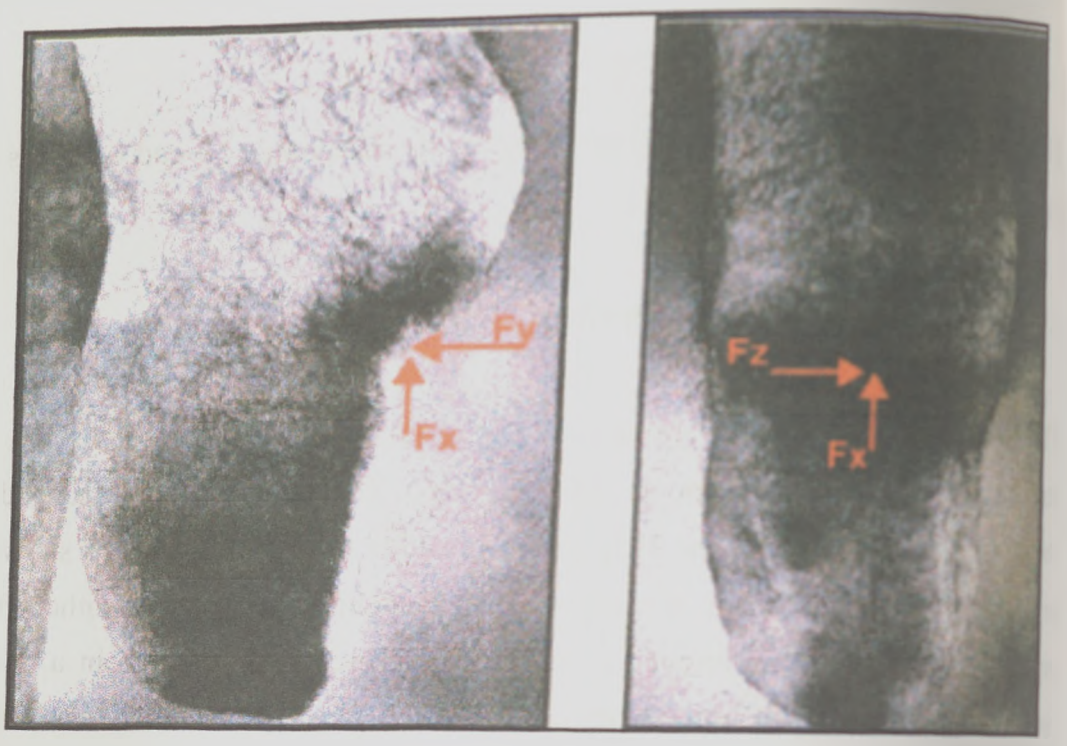

Figure 3.3 Directions of the three Orthogonal forces (Fx,Fy,Fz) at the patellar tendon region.
(Reproduced from Osman 1999)

3.2 Patellar tendon bar (PTB) Mark-II Transducer

3.2.1 Introduction

The main objective of this study was to measure the interface pressures in the trans-tibial socket for different horizontal displacements of the patellar tendon bar. This could possibly aid in understanding the variations of distribution of pressures around the socket by increasing the compression at the patellar tendon region. It was also of interest to monitor the pressure and shear stresses experienced at the patellar tendon region during this displacement of the patellar tendon bar. This necessitated the design of a special transducer which could advance the patellar tendon bar horizontally and at the same time measure the forces in the three orthogonal directions of Fy, Fx and Fz as shown in figure 3.3 . The normal pressure and the shear stresses at the interface can be computed from the three orthogonal forces respectively.

3.2.2 Earlier design of the PTB transducer

A custom made tri-axial pressure transducer, catering for the above-mentioned requirements was designed for a similar study (Osman 1999). The transducer measured both normal and shear forces using strain gauge technology. The device not only measured the loads acting on the patellar tendon bar, but was also capable of being moved $\pm$ 5mm in a linear fashion horizontally. The transducer was glued to the Patellar tendon bar, which was removed from the socket. This form of bonding of the patellar tendon bar to the transducer, posed difficulties when it had to be changed from one socket to another. The physical dimensions of the transducer were also felt to be cumbersome. This led to the designing of a similar transducer which took into account the above needs in its design criteria.

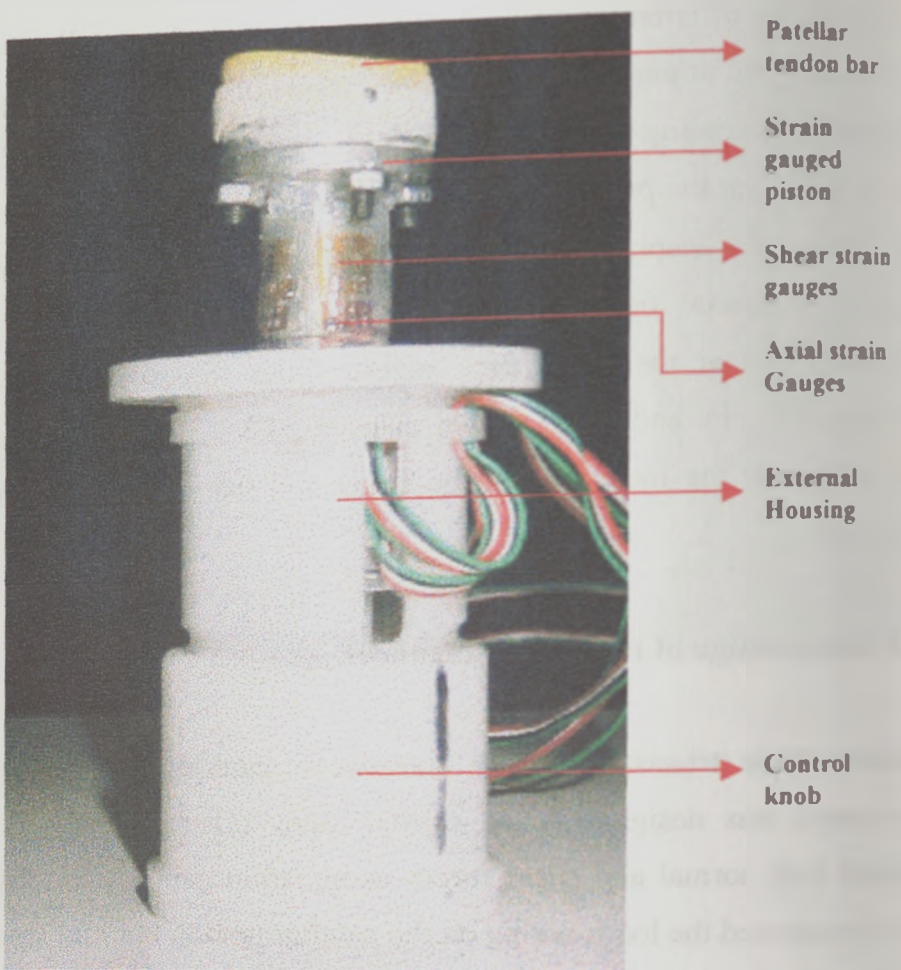

Figure 3.4 Patellar Tendon Bar (PTB) Mark-II Transducer and its parts

3.2.3 Design of the PTB mark-II transducer

The PTB mark-II transducer was designed using the same principles as its predecessor. Strain gauge technology was used in the design of this transducer, and it measures the forces in three orthogonal directions (Fx, Fy, and Fz). The PTB mark-II transducer consists of the following components.

- Strain gauged piston
- External Housing
- Housing extension
- Spacers(2 off)
- Control Knob
- Single row radial bearing

The assembly of the PTB mark-II transducer is shown in figure 3.4.

3.2.4 Description of individual components

The main component of the PTB mark-II transducer is the strain gauged piston (Drawing A4)*. This carries the strain gauges, which measures the normal and shear stresses. Like the strain gauge piston in the previous model, it was machined from a solid round bar of aluminium alloy commonly known as HE30. This was chosen due to its mechanical properties, which have been discussed in detail by Osman (1999). The main feature that was incorporated in this design was a flange that was machined at the end of the strain gauged piston. This flange was the means of attachment to the patellar tendon bar by four 3mm screws. A spacer made from the same material was sandwiched between the patellar tendon bar and the flange of the transducer.

The external housing (Drawing A2)*, the control knob (Drawing A3)* and the housing extension (Drawing A6)* where are all machined from acetal material.

* Drawings refer to appendix 1

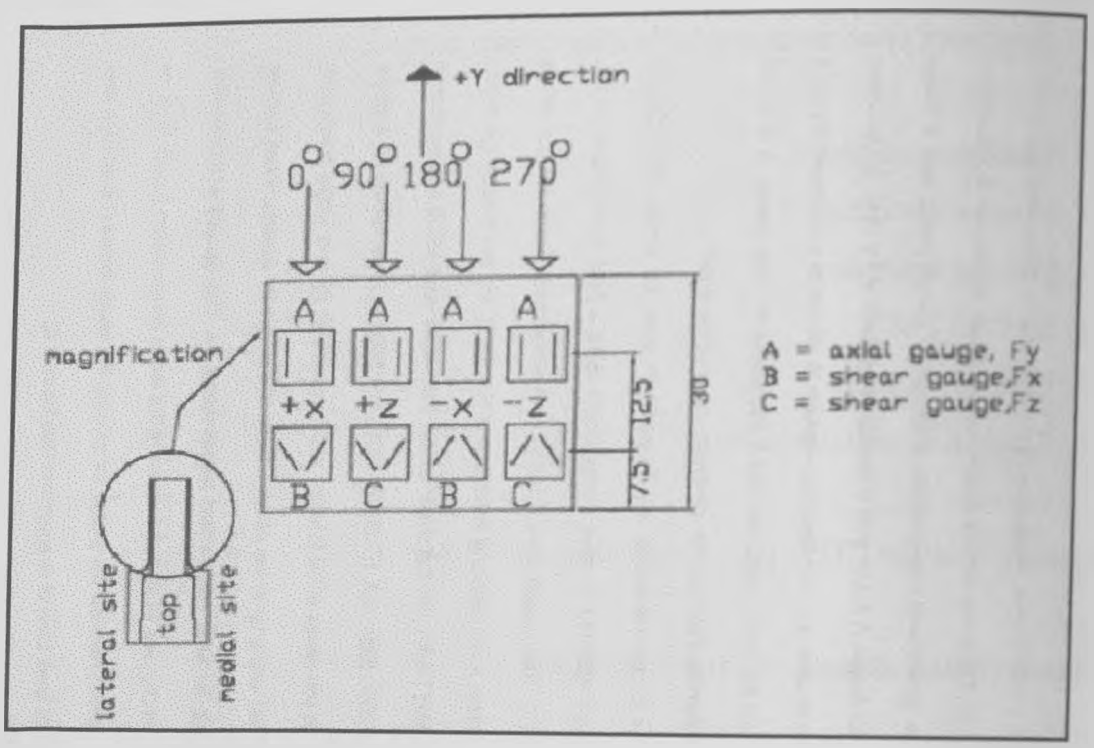

Figure 3.5 Arrangement of the axial and shear gauges on the strain gauge piston
(Reproduced from Osman (1999))

This was done to reduce the overall weight of the transducer. The new design was able to reduce the overall length of the transducer to about 6.5cms (excluding the housing extension). The housing extension was later incorporated into the design to get the patellar tendon bar flush with the inner surface of the socket. The PTB mark-II transducer can be advanced in the horizontal direction inwards by approximately 15mm from the flush position. This means that only the strain-gauged piston with its strain gauges would move with the Patellar tendon bar at its end, and that the rest of the components would remain fixed to the trans-tibial socket. This was achieved by the single row radial ball bearing (RHP 606) supplied by RS components Ltd, U.K. The threads on the control knob and External housing allows the advancement of the strain gauged piston, by rotation of the control knob, the ball bearing prevents the strain gauged piston from rotating along with it, thus maintaining the orientation of the strain gauges. The control knob rotated over the external housing by means of a thread with 1mm pitch. This 1mm pitch was created so that a single complete rotation of the control knob would advance the Strain gauged piston by 1mm. The whole assembly was attached to the socket by means of screws (discussed in detail in Instrumentation of socket).

3.2.5 Strain gauging of the PTB mark-II transducer

The strain gauging was done in the same way as the previous PTB transducer. Three full-bridge strain gauges made up the transducer and each gave the output for the three loads Fx, Fy and Fz respectively. The strain gauges where arranged in two rows as shown in the figure 3.5. The upper row consisted of strain gauges, which measured the axial load. They had a gauge factor of K=2.0555 and resistance of R=350Ω. There were two Rosettes (90^0) in each arm of the full bridge and were equi-spaced. The lower row consisted of strain gauges, which measured the shear load. They had a gauge factor of K=2.0 and resistance of R=120Ω. There were two rosettes in each arm of the full bridge and were equi-spaced. The rosettes for the shear gauges were inclined to each other by 45^0 in order to measure the shear loads. It was assumed that the strain gauges were adequately placed away from the ends to eliminate any end effects. The strain gauges both axial (type: EA-06-062TT-350)

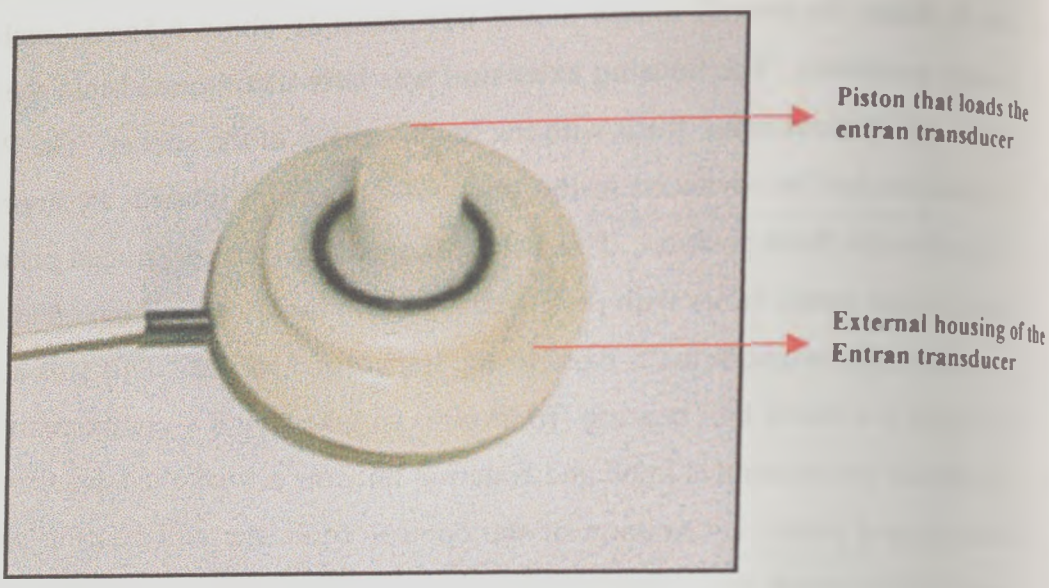

Figure 3.6 Entran transducer in its housing

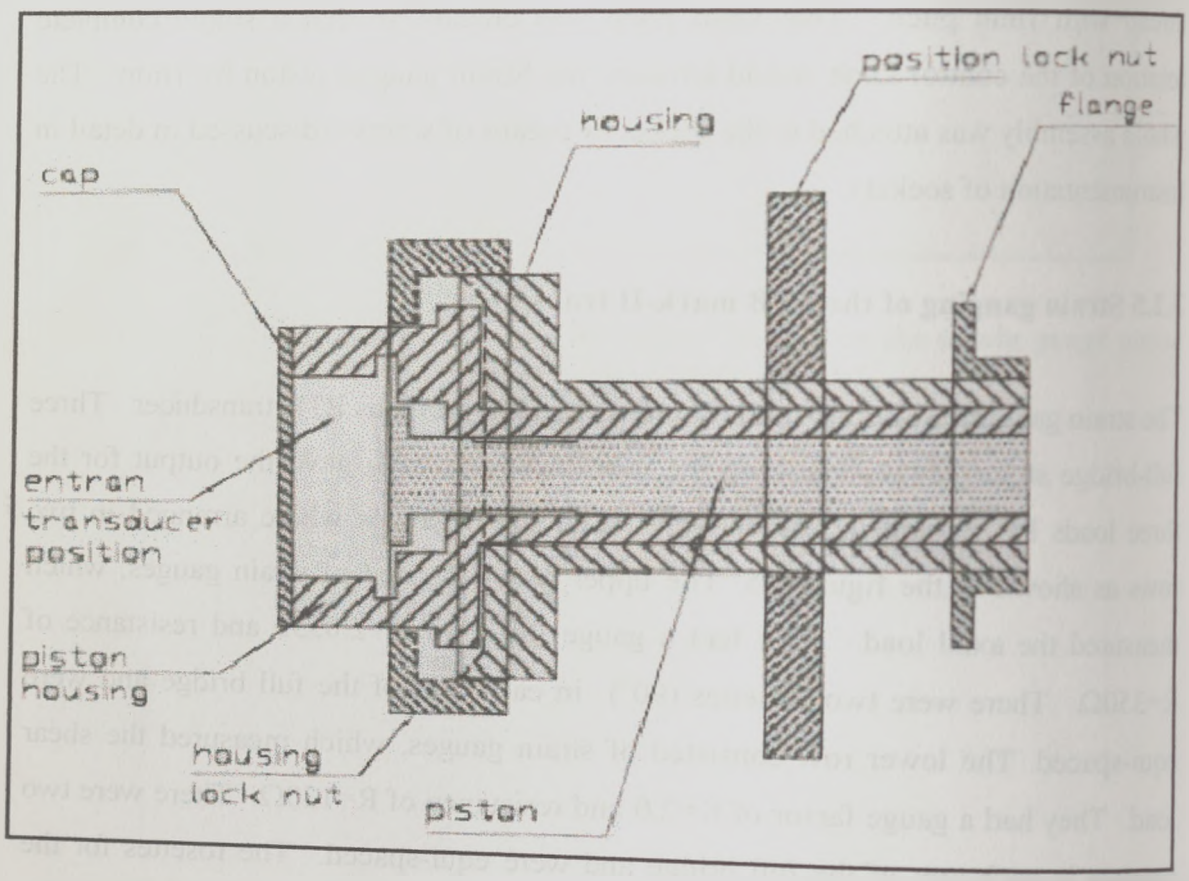

Figure 3.7 Complete assembly of Entran Transducer
(Reproduced from Osman 1999)

and the shear (type: EA-12-062Th-120) were supplied by Measurement group UK Ltd . The process of mounting these gauges onto the strain gauge piston was done with great precision. The surface on which the strain gauges had to be mounted was adequately cleaned and prepared. The strain-gauges were than attached to the piston by heat curing adhesive (M-bond 610). This process was carried out by the electronics technician with great care and accuracy. Following the mounting of the strain gauges it was wired and checked and then was completely covered by a protective layer of silicone rubber.

3.3 Entran Transducer

Apart from the patellar tendon area the pressures were monitored in six other areas of high pressures distributed around the socket. The Entran load cell (ELM-400-2)was used for this purpose. The Entran load cells (figure 3.6) were used in special housing (figure 3.7) which were originally designed by Torres-Moreno (1991) and later was re-designed by Osman 1999 for use in trans-tibial sockets. This is a resistive type of a transducer and works using a diaphragm deflection strain gauge. It measures the loads in only one direction and that is the axial load and therefore was used to measure the normal pressure. They have the characteristics as shown in table 3.1

Frequency range	0-900Hz
Hysteresis	$\pm$ 0.5% FSO
Non-linearity	$\pm$ 0.5% FSO
Full scale sensitivity	8mV
Load Range	0-2lbs (0-8.8995N)
Over Range	0-4lbs (0-17.799N)
Input impedence	600Ω
Output Impedence	600Ω
Thermal Sensitivity	$\pm$ 1%/55 ^{0}C
Operating Temperature Range	-40 to +120 ^{0}C

Table 3.1 Characteristics of Entran transducers

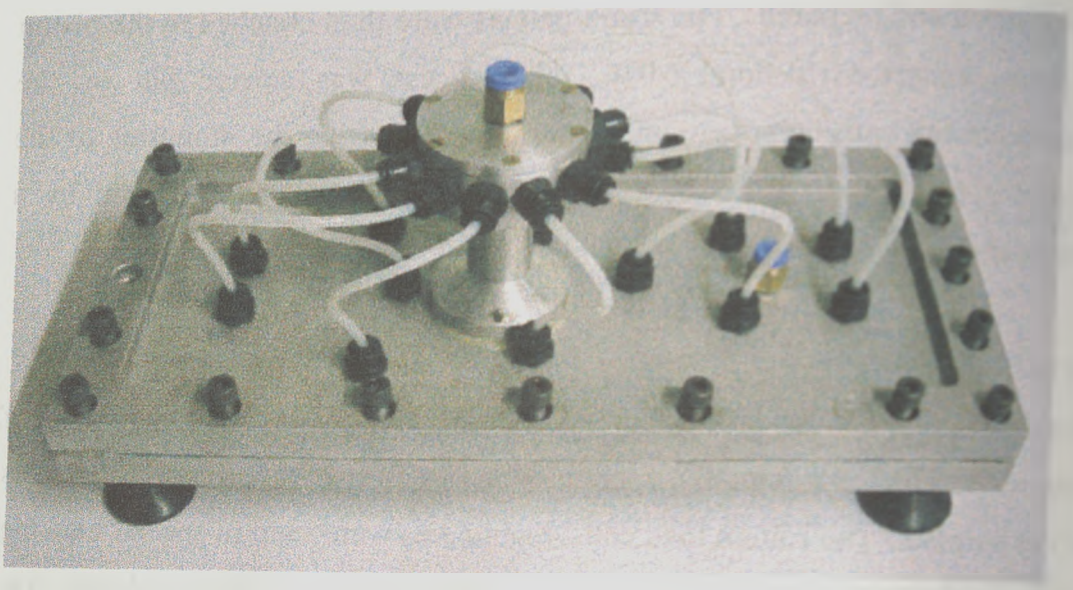

Figure 4.1 Exterior view of the pressure rig

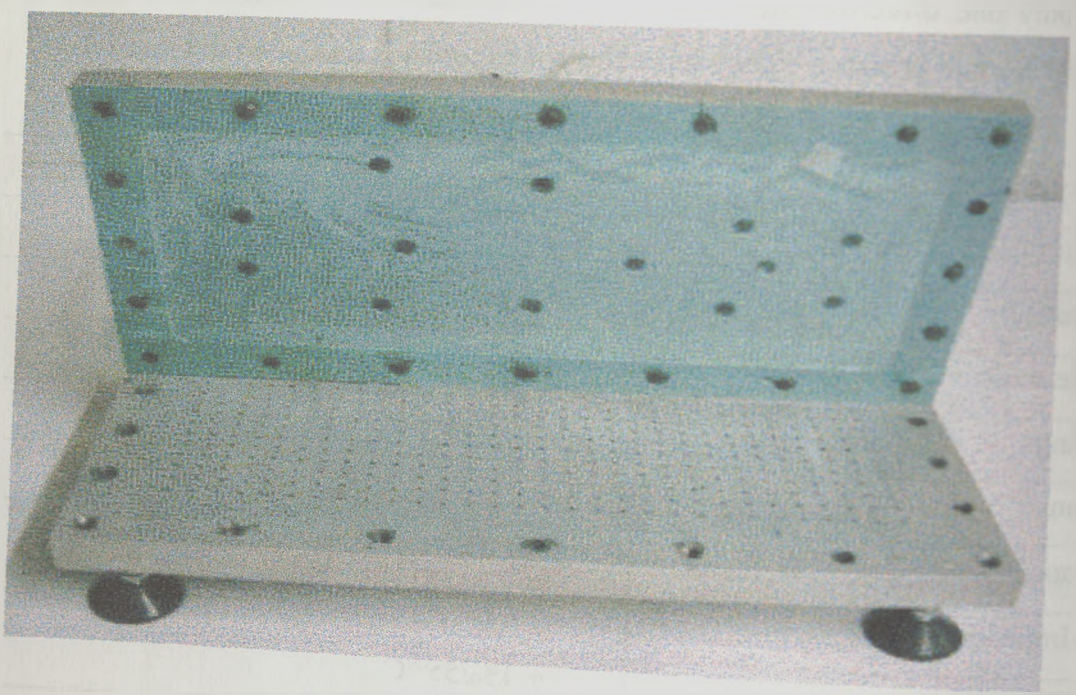

Figure 4.2 Interior view of the pressure rig

Chapter 4

Experimental Design and Methodology

4.1 Validation of the Rincoe Socket Fitting System

The Rincoe Socket fitting system measures the pressures at the stump socket interface by means of special DOS-based software which processes the information collected by the hardware box. The calibration data for each of the sensors of the six sensor strips are provided in a floppy disk. These calibration data are unique for each of the sensor strips and the manufacturer performs this calibration just before the strips are being shipped to the customer. In order to check the system for any significant errors the process of validation needs to be carried out. Validity of any measuring system can be defined as the accuracy of the system in relation to input and output (Buis, 1997).

4.1.1 Need for Validation

In the present study validation, of the Rincoe socket-fitting system was carried out in the first place to determine the errors due to linearity, hysteresis and accuracy errors. The sensor strips that were used in this study were new but they had been purchased from the manufacturer a few years back, so the author was concerned about the validity of the calibration data provided by the manufacturer at the time of purchase.

4.1.2 Pressure rig

The strips of the Rincoe socket fitting system were tested using a pressure rig (figure:4.1, 4.2) designed by Buis (1997), originally used for external calibration of the F-scan system. This pressure rig was used for static testing purpose. The complete set up of the pressure rig consisted of

- Pressure rig with mylar diaphragm
- Air flow regulator
- Digital Pressure monitor

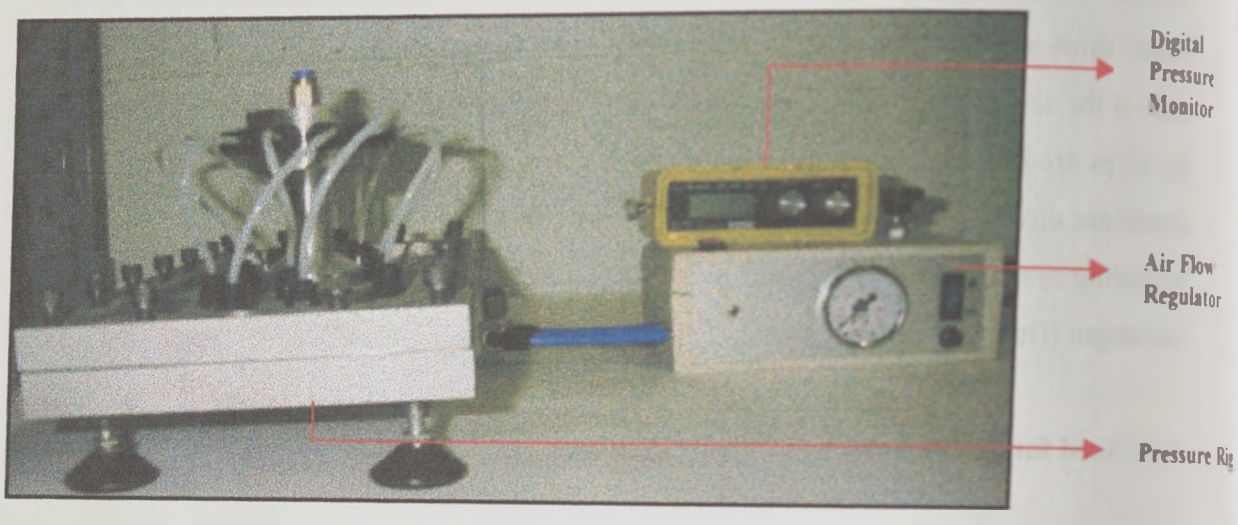

Figure 4.3 Equipment used for validation of the Rincoe System

The air flow regulator (Figure:4.3) had also been designed by Buis (1997) for regulating the pressurised air for both static and dynamic calibration. In this study the static mode of the air flow regulator was used. The digital pressure monitor is a product of RS components, and this provided the output in bars and measured up to 2 bars.

The pressure rig consists of an aluminium alloy base plate (30cmx17cm x10cm) perforated with 1mm holes, and spaced 10mm centre to centre. The pressure rig also consists of a top plate made of aluminium alloy (30cmx17cmx20cm). On the underside it incorporates a central milled chamber with dimensions of 24cmx12cmx 0.1cm. The chamber is covered and sealed with a mylar sheath 0.2mm in thickness. Ten air inlet holes of 5mm diameter each are connected to this central chamber.

4.1.3 Testing Procedure

The testing of the Rincoe socket fitting system was performed by loading the sensor cells in each strip with a known uniform pressure in the pressure rig and reading the output computed by the Rincoe's DOS-based data collection software. Only 4 sensor strips were tested at one time, and the procedure had to be repeated twice on the same strip because only 8 sensor cells fitted into the pressure rig at one instance. The sensor cells were numbered from 1-10 in each sensor strip, number one being the farthest from the connector of the strip. The details of placement of the six sensor strips are found in table4.1

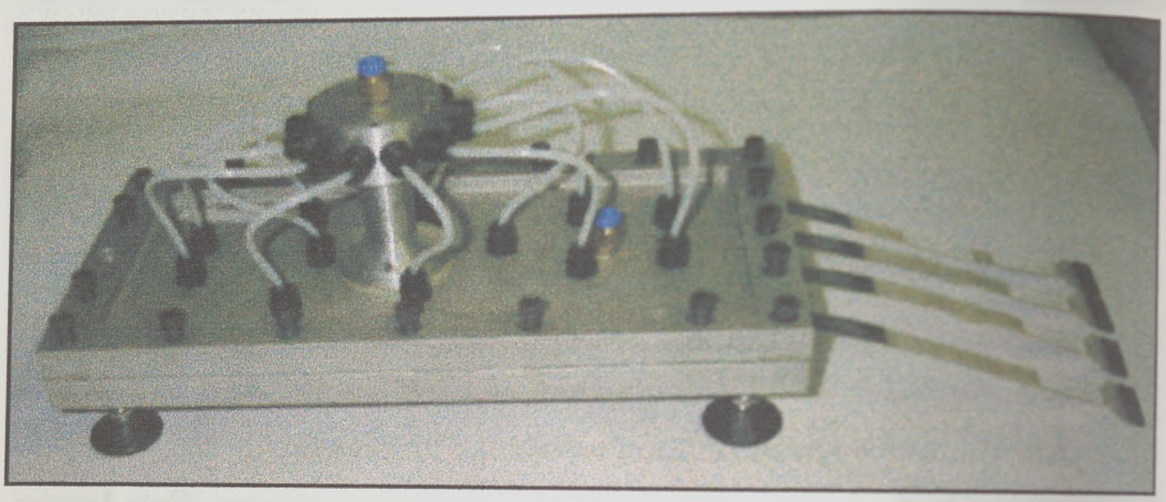

Figure 4.4 Placement of Rincoe strips in the pressure rig for validation tests

Strip	Final plancement of the strips in the socket
1	Anterior Medial
2	Anterior
3	Anterior Lateral
4	Posterior Lateral
5	Posterior
6	Posterior Medial

Table 4.1 Placement of Rincoe strips in the socket

The air pressure regulator was connected to the compressed air output from the wall socket. The pressure obtained from the wall socket was approximately 800 kPa. Since the Rincoe system could tolerate only pressures up to 12 psi (82.74 kPa), the pressure regulator was manually adjusted to give an output pressure of less than 12psi. The output from the air pressure regulator was connected to the pressure rig.

The Rincoe sensor strips were placed in between the base plate and the top plate of the pressure rig (figure 4.4), in such a way that it was well within the area of the central milled chamber. The plates of the pressure rig were then secured to each other by means of 24 cap screws. The screws had to be secured tightly to prevent any air leak from the chamber. The pressure inside the chamber was measured through an output hole on the top plate connected to a digital pressure monitor. This was done to eliminate any loss of air pressure as it travelled from the air regulator to the pressure rig.

The sensor strips were then connected to the corresponding cables of the hardware box. The two sensor strips that could not be tested in the first instance were simply connected but no readings were taken from them. The output from the hardware box was connected to a serial port of a PC (Processor model: 386). The special DOS-based Rincoe software was used to collect data. Before the tests were run the

calibration table for each strip was individually loaded in order to read the output pressures from them.

The pressures read by the sensor strips were monitored using the strip graph mode that shows the variations in pressure in real time. The pressures were increased from 0 to10 psi using the air pressure regulator and the pressure in the pressure rig was verified using the digital pressure monitor. The pressure read by the sensor strips at various known input pressures were recorded manually from the strip graph i.e. output pressures given by the Rincoe system at pressure levels of 0,2,4,6,8,10 psi. After the input pressures reached 10psi the pressure was reduced in the same fashion as it was increased and the output pressures displayed by the Rincoe system in the strip graph were manually recorded. The remaining two sensor cells outside the pressure rig were positioned inside the pressure rig and tested similarly. The whole procedure was repeated for the remaining two sensor strips 5 and 6.

From the output values obtained for different pressure levels the accuracy error and hysteresis error of each sensor cell was determined using the following formula

$$\text{Accuracy Error} = \left| \frac{\text{Input Pressure} - \text{Output pressure}}{\text{Input Pressure}} \right| \times 100 \quad \text{----------Equation 4.1}$$

$$\text{Hystereis Error} = \left| \frac{Si - Sd}{Sd} \right| \times 100 \quad \text{----------Equation 4. 2}$$

Where

Si = Sensor response while increasing the pressure

Sd = Sensor response while decreasing the pressure

4.2 Calibration of the PTB mark-II transducer

4.2.1 Theory of Calibration

The patellar tendon bar mark-II transducer as discussed in chapter:3 uses the strain gauge technology, with strain gauges connected in a full wheatstone bridge configuration. Application of force on to the transducers causes the strain gauges to undergo strain depending upon the direction of the forces. This causes a change in their resistance, which in turn changes the output of the whole circuit. However this change in the potential difference is usually in the order of milli volts and requires to be amplified. Finally the output or signal obtained is in volts, and this in turn is converted to forces by using a calibration factor. Calibration is the process whereby an accepted standard is compared against an unknown quantity and used to determine its value.

The PTB mark-II transducer has three channels and hence has three output signals, Si (i=1,2,3). This output signal is obtained due to three different inputs which are forces Fi (i=1,2,3). However these three forces are often applied in a combination and hence can give different outputs in the three different channels. So the outputs and signals are related to each other through a constant calibration coefficient which can be mathematically expressed as

$$Si = \sum_{i=1}^{3} Mij\ Fij \qquad \text{---------- Equation 4.3}$$

This can also be expressed in a matrix form as

$$[S] = [M]\,[F] \qquad \text{---------- Equation 4.4}$$

Where

$$[S] = \begin{vmatrix} SFx \\ SFy \\ SFz \end{vmatrix}$$ = Output signals from channels Fx,Fy,Fz.

$$[M] = \begin{vmatrix} M_{11} & M_{12} & M_{13} \\ M_{21} & M_{22} & M_{23} \\ M_{31} & M_{32} & M_{33} \end{vmatrix}$$

$$[F] = \begin{vmatrix} Fx \\ Fy \\ Fz \end{vmatrix}$$

From equation 4.4 if matrix [M] and [F] where to be multiplied to give matrix [S] it can be expressed as

$$SFx = M_{11}Fx + M_{12}Fy + M_{13}Fz$$

$$SFy = M_{21}Fx + M_{22}Fy + M_{23}Fz$$

$$SFz = M_{31}Fx + M_{23}Fx + M_{33}Fx$$

Through the calibration process matrix [M] can be computed. During the calibration process a known force is applied in all the three channels individually and the output signal is recorded for each known force that is applied. The only unknown quantity is the calibration coefficient, which is expressed as a 3x3 matrix as [M]. This is expressed in the form of a matrix in order to eliminate any cross talk effect that can result from the other channels on loading a single channel.

During the experiment to find out the interface pressures, equation 4.4 has to be now rearranged in order to obtain unknown forces from the known signals that are recorded as channel output and the calibration matrix that has been computed through the process of calibration. This relationship can be expressed as in equation 4.5

$[F] = [M]^{-1} [S]$ ----------Equation4. 5

Where $[M]^{-1}$ is the inverse calibration matrix.

This is the theory behind calibration.

4.2.2 Calibration Procedure

The three channels of the patellar tendon bar mark-II transducer were connected to the strain gauge amplifier. The strain gauge amplifier has six input channels, which can be amplified simultaneously. However, while calibrating the PTB mark-II transducer only three channels would be used, the other three channels are connected to dummy gauges. The amplifiers were then switched on and the bridge voltages and gains were set. The bridge voltages for the Fx and Fz channels were set at 3 volts and the Fy channel was set at 6 Volts. The gain was set at 500 for all three channels. The channel outputs were zeroed using a digital voltmeter, which read the channel output individually. The strain gauge amplifiers were switched on 30 minutes before the actual calibration was commenced in order to obtain stable outputs from the output channels of the amplifier.

4.2.3 Data Collection Hardware

A Pentium-I computer (Hewlett Packard) was utilised for data collection from the channel outputs from the strain gauge amplifier. This computer was specially fitted with a data collection PCI card supplied by National instruments (PCI-6023E). This data collection card is run by software called Ni-daq, which is supplied in a CD-ROM on purchase from the manufacturer. The Ni-daq software once installed in the computer helps the card to be configured to receive inputs from 16 channels simultaneously. The channels can be named and in these experiments the first three channels where named Fx, Fy, and Fz. The channels were also configured to read

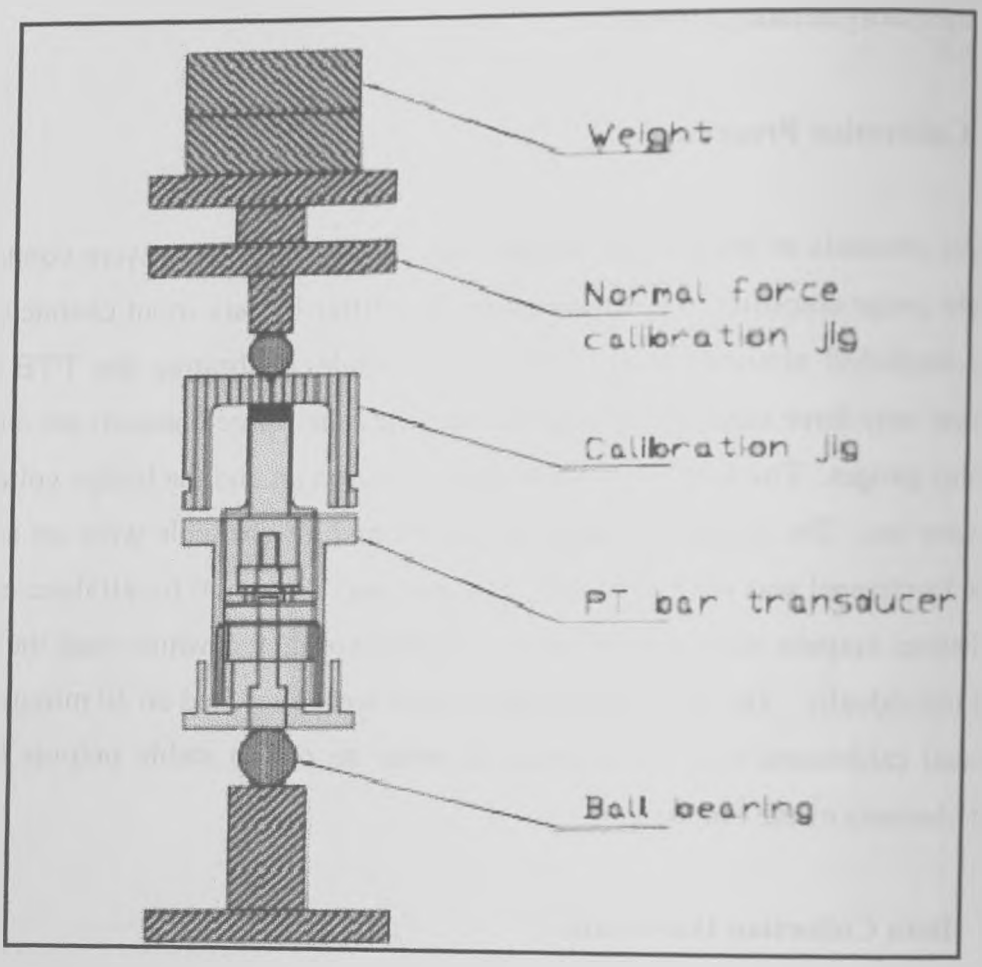

Figure 4.5 The set up of the axial loader used for axial calibration of the patellar tendon bar mark-II transducer
(Reproduced from Osman 1999)

the outputs from the strain gauge amplifiers in volts and had a resolution of 0.1 mV. The scan rate of each channel was 1000 scans/second.

4.2.3 Data collection Software

The data that was scanned from the outputs of the strain gauge amplifiers need to be collected and stored for analysis. This was done by a special programme (appendix:2) written in Labview (version 5.0). The programme was written in such a way that data were collected simultaneously from all 3 channels (Fx, Fy and Fz). The software then processed the collected data. The actual process involved was that the software collected 100 samples and then discarded the first 10 samples and the last 10 samples and then gave the mean of the remaining 90 samples. This mean of all the 3 channels was directly written to an excel worksheet (Excel 97, MS-office). The reason for eliminating the first and the last 10 samples was to obtain the steady output from the channels just after it had been loaded with dead weights.

4.2.4 Axial Force Calibration

To calibrate the axial force (Fy) the patellar tendon bar mark-II transducer was fixed to a calibration jig and placed in a special device called the axial loader as shown in figure 4.5. This device enabled the axial channel to be loaded accurately. In order to achieve point loading, steel ball bearings were used at the interface of the patellar tendon bar mark-II transducer and the axial loader. The transducer was loaded only in the compressive direction, since tensile forces are not expected to occur in the Fy direction when the transducer is used to measure interface pressures. On setting up the transducer in the axial loader the outputs from the strain gauge amplifier were zeroed. The software, recorded the outputs from the three channels. Known loads were then added to the top of the axial loader and the simultaneously the corresponding channel outputs were recorded at each instance of loading. The transducer was loaded up to 94.52 N. This was decided from the previous results of Osman (1999) and Wandrum (2000). The transducer was then unloaded by removing the known loads in the same sequence as they were loaded, and the

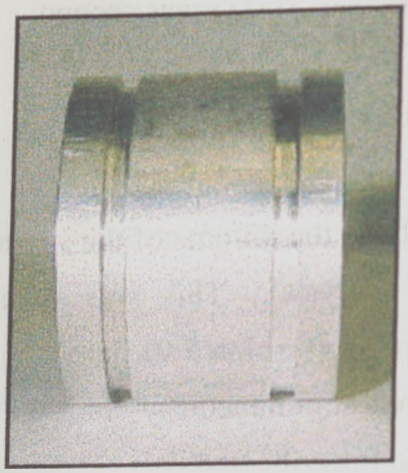

Figure 4.6 External view of calibration jig used for shear calibration

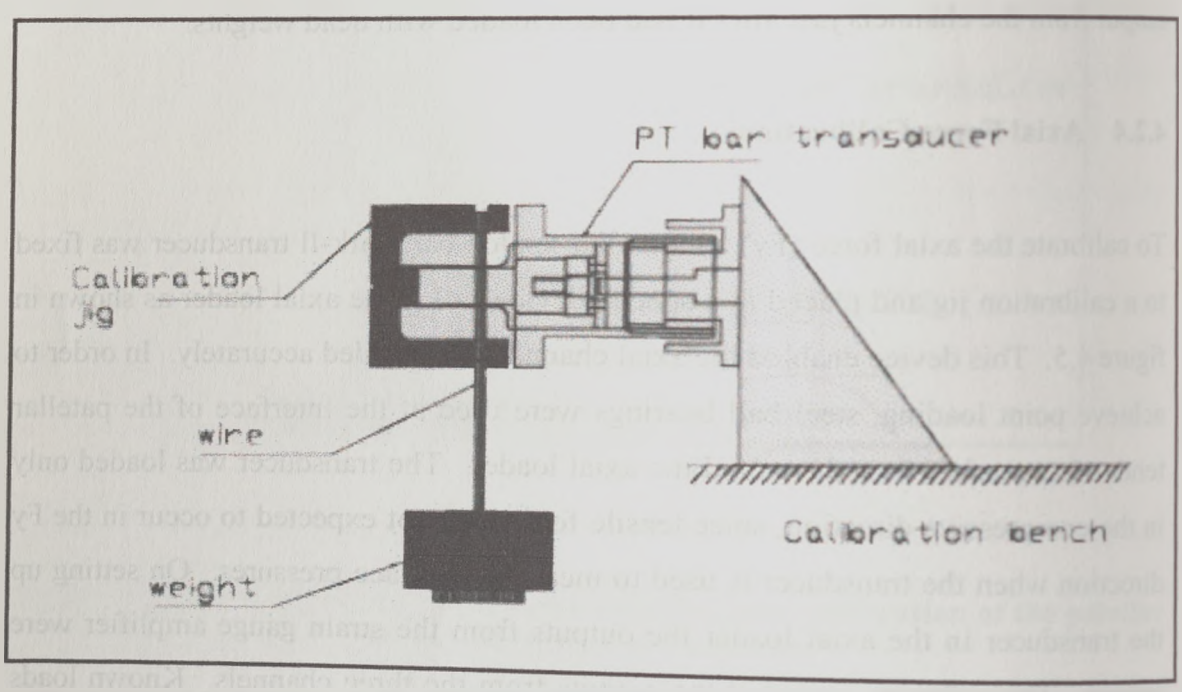

Figure 4.7 Calibration set-up for shear channels (Fx,Fz)
(Reproduced from Osman,1999)

corresponding channel output was recorded. This process of loading and unloading was done 5 times and the output was recorded by the software directly onto an excel sheet. The average outputs of all three channels from the five cycles of loading and unloading was computed using the Excel 97 (MS-office) program, and was plotted as a graph by the same program.

4.2.5 Calibration of Shear Force

To calibrate the shear forces Fx and Fz a calibration jig as shown in Fig.4.6 was used. This was designed by (Osman, 1999). The PTB mark-II transducer was attached to the calibration bench by means of a cap screw, which fits into the bottom of the control knob of the transducer assembly. The calibration jig is designed in such a way that the central metal projection (Drawing B1 appendix :1) fitted into the strain gauged piston and thus attached to the PTB mark-II transducer as shown in figure 4.7. A groove was also incorporated on the outer surface of the calibration jig, so that the forces could be applied directly over the lower row of strain gauges in the PTB mark-II transducer's strain gauged piston. This sort of a set up would eliminate any bending moment that the strain gauged piston would have experienced if the weights would have been suspended at the end of it.

The calibration procedure was similar to that of the axial force calibration procedure. The data were also collected using the same data acquisition software and program. A pure shear stress was first produced in the Fx direction by suspending known weights on the calibration jig as shown in figure 4.7. The load was increased from 0 to 71.76N and outputs from all three channels were recorded. The transducer was then unloaded back to 0 during which the outputs from all three channels were recorded. This process was repeated 5 times. On completion the transducer was rotated by 90 degrees to the right and the shear force Fz was calibrated in the same manner as channel Fx. On completion of Fz channel the transducer was rotated another 90 degrees to the right and the negative Fx force was calibrated and on rotation of another 90 degrees the negative Fz channel was calibrated. The data from all the four different directions of loading was then analysed using Excel 97 (MS-

office). The means of all the 5 loading and unloading cycles were calculated and the data were plotted. The initial results obtained in the shear channels showed a large cross talk from the Fy channel during shear force calibration.

For reasons discussed in section 6.3 the central metal projection of the calibration jig was removed. The PTB mark-II transducer was then attached to the calibration jig by attaching the flange on top of the strain gauged piston to the bottom on the inside of the calibration jig by means of four 3 mm screws. The calibration procedure was repeated in the same procedure as outlined above and data the obtained were processed using Excel 97 and then data were plotted as graphs.

From the data obtained from both the axial and shear calibrations the calibration matrix [M] was calculated as shown in the example in appendix:4. The inverse of this calibration matrix was then used in the actual experiments to convert all the data obtained in volts into forces. Knowing the sensing surface area of each transducer the interface stresses were computed.

4.3 Calibration of the Entran Transducer

The Entran transducer measures the axial pressures. And was calibrated in the modified housing that was designed by Osman (1999). The calibration set up that was used is shown in figure 4.8. The set up consisted of a beam with one end resting over a knife-edge and the other end was placed over the piston of the modified housing of the Entran transducer. The piston transmitted the force applied to it on to the Entran transducer inside the housing. To obtain point loading a ball bearing was attached to the underside of the beam, at the spot where it came in contact with the piston. Known weights were suspended from the beam and this created a moment about the knife edge and so pressing the transducer end of the beam over the ball bearing and there by onto the piston which in turn loaded the Entran transducer. The load applied to the Entran transducer was calculated by assuming that all clockwise moments equalled anti-clockwise moments. The six Entran transducers were attached to the six channels of the strain gauge amplifier, and the amplifier was

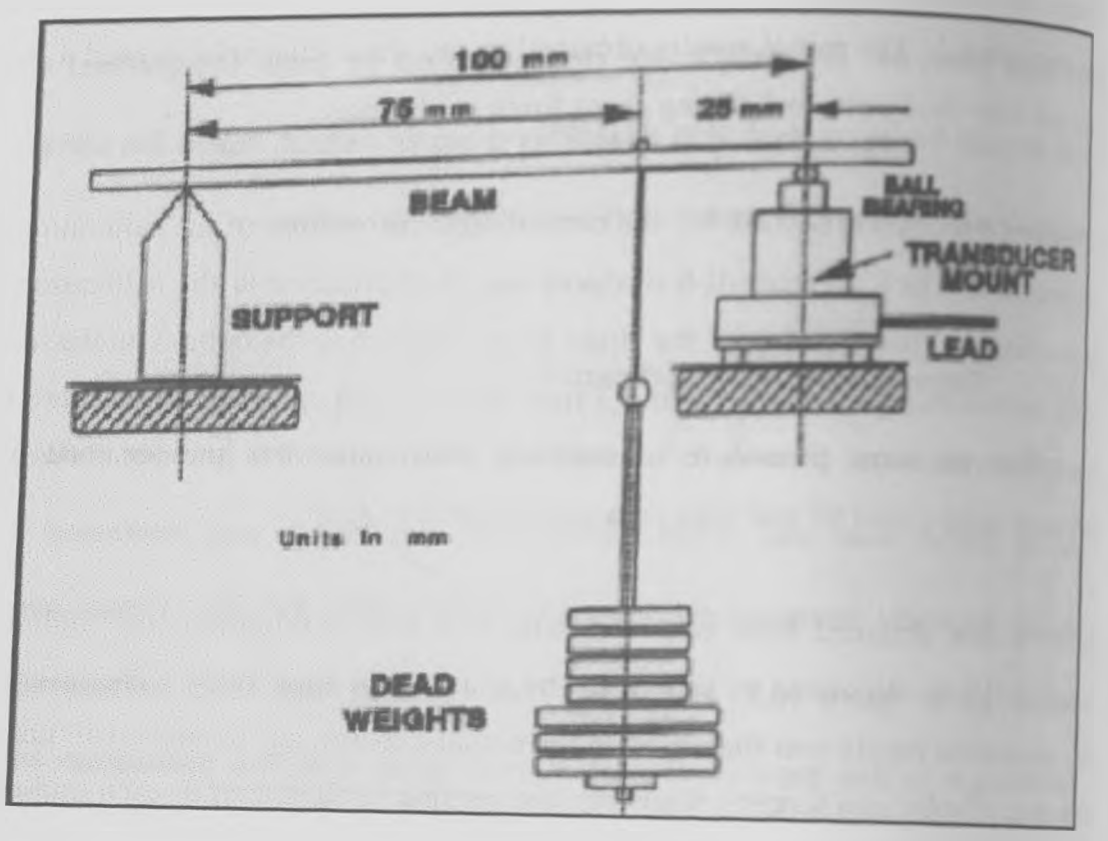

Figure 4.8 Set-up used for Entran Transducer calibration

(Reproduced from Osman,1999)

switched on 30 minutes before the calibration tests in order to obtain a steady output. The bridge voltage for the entran transducer was set at 5V and the gain was set at 500. Although all the six transducers were connected to the strain gauge amplifier only one transducer could be calibrated at a time.

The Entran transducer to be calibrated was firmly attached to the calibration bench by means of adhesive tape to prevent any movement. The beam was then set up as described. The channel output was then zeroed. The weights were then suspended starting with the weight holder, and the output from the strain gauge amplifier was recorded manually using a digital voltmeter. A time gap of 10 seconds was given between the actual loading of the transducer and the recording of the output. This time gap was found adequate to overcome any initial drift in the output immediately after loading the transducer.

The transducer was loaded up to a maximum of 3.6 N and then unloaded back to zero. The channel output from the strain gauges was recorded manually. Five cycles of loading and unloading were performed. And the above procedure was carried out on all 6 Entran transducers.

The recorded data of the channel outputs were then manually entered into an Excel97 worksheet. The Excel 97 program was then used to calculate the mean of all the 5 cycles of loading and unloading and the result was plotted as graphs. The calibration coefficients were then calculated using the slope of the line that was obtained from plotting the graph.

4.4 Subject Testing

One of the main objectives of this study was to carry out interface pressure measurement studies on more than one subject. It was planned initially to have 3 subjects, but in the course of the study only two subjects were tested mainly due to the constraints and also due to non-availability of suitable subjects for the tests. The two male subjects who were chosen for the tests were both right-sided trans-tibial amputees leading a very active life. Both have been using Patellar tendon bearing

prosthesis for a considerable period of time. Subject one had taken part in studies earlier conducted in the Bioengineering Unit (Osman 1999, Wandrum 2000).

4.4.1 Subject:1

Subject 1 was 80 years old and had undergone a trans-tibial amputation of his right lower limb in 1944 due to gangrene following a motor bike crash. He had also developed a hip fracture on his left side. In 1985 he had undergone a total hip replacement and is presently awaiting a replacement of that hip and had mild pain in the left hip during the time of testing, but this did not significantly affect his activities of daily living.

His stump did not have any skin break down or ulcers. On examination before the test his stump showed mild redness over the anterior tibial crest. No adherent scars were seen and healed suture wounds were found at the bottom of the stump. On sensory examination he had loss of touch at the end of stump, which possibly could be due to desensitisation following constant use of prostheses. His muscle power was normal and the range of motion of the knee joint was within normal limits. His stump dimensions are shown in table 4.2

4.4.2 Subject:2

Subject:2 was 70 years of age and had undergone trans-tibial amputation of his right lower limb in 1995 following thrombosis of right lower limb due to elevated levels of cholestrol. Following the amputation he had undergone regular rehabilitation for 3 months following which he had been able to walk using a patellar tendon bearing prosthesis. On examination he was found to have a bony stump and all bony prominences were easily palpable. He also had mild redness over the distal end of the fibula. The skin was intact all over the stump. On sensory evaluation he was found to have diminished sensation at the anterior distal end of the stump. He does not however have any associated medical complications such as diabetes mellitus and peripheral vascular disease. His muscle power on his amputated limb was found

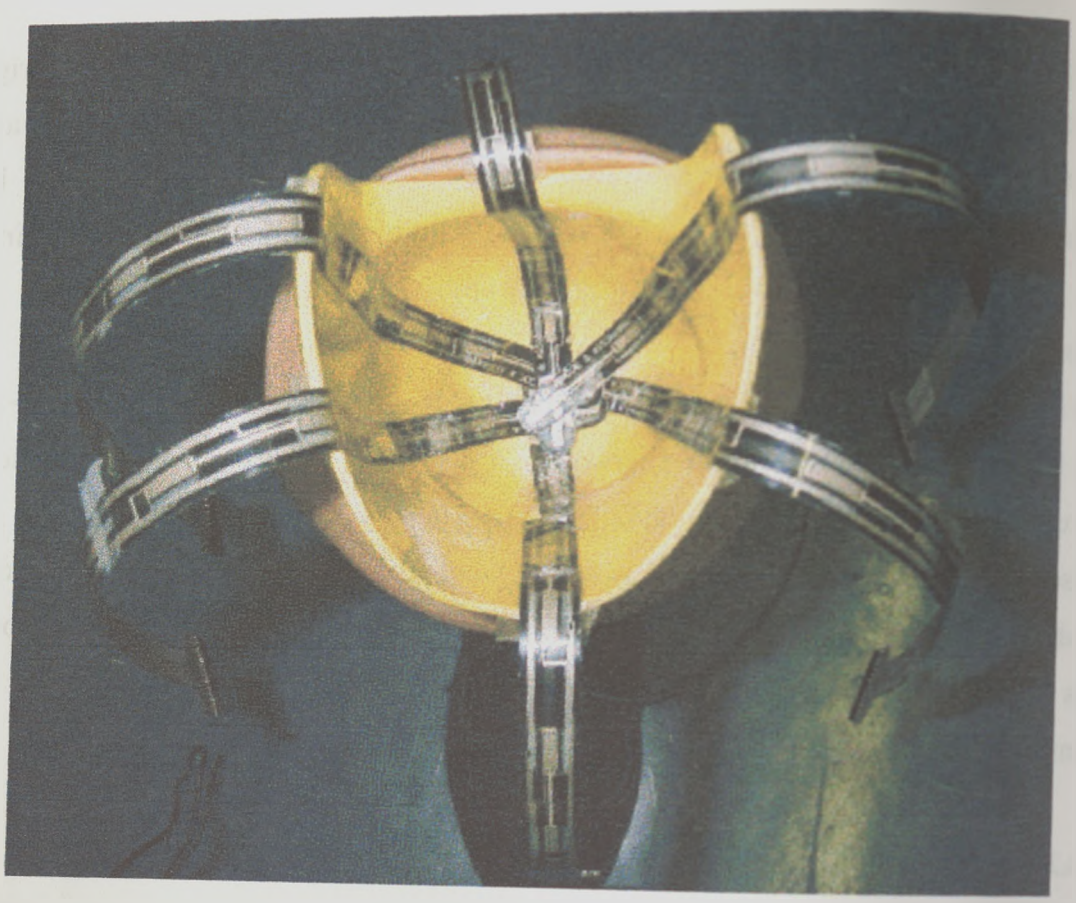

Figure 4.9 Positioning of the Rincoe sensor strips in the socket

to be normal and his range of motion of his knee joint was within normal limits. His stump dimensions are shown in table:4.2

Stump dimensions	Subject:1	Subject:2
Length (From tibial plateau to the end of the stump)	22.5 cms	16 cms
Proximal circumference (level of tibial plateau)	34.5 cms	33 cms
Distal circumference	17 cms	20cms

Table 4.2 Stump dimensions of subjects 1&2

4.5 Subject testing using the Rincoe Socket fitting system

A preliminary test was performed on both subjects using Rincoe socket fitting system to detect areas of high pressure in order to position the Entran pressure transducers. Test sockets (hydrocast socket) were made for both subjects with sleeve suspension. The prosthesis was assembled using Otto-bock, Gmbh, Germany, modular components. The tests were carried out at the biomechanics laboratory of the Bioengineering Unit, University of Strathclyde. Each subject was tested separately.

At the start the test procedure was explained to the subject. The subjects were then asked to try the test prosthesis. Since no liner was used, the subjects had to don a few additional stump socks to obtain the correct fit. The subjects were then asked to walk with the test prosthesis and dynamic alignment was corrected out by the prosthetist. After the patients had reported that they were comfortable in using the test socket, it was removed. The six Rincoe sensor strips were then attached to the inner wall of the test socket as shown in the figure 4.9 using double-sided adhesive tape (Advance Tapes UK). The strips were arranged in the order as mentioned in Table 4.1. In each sensor strip, sensor: 1 was placed at the bottom of the socket, and all the sensors were positioned in the same level (eg. Sensor:3 of all the strips were at

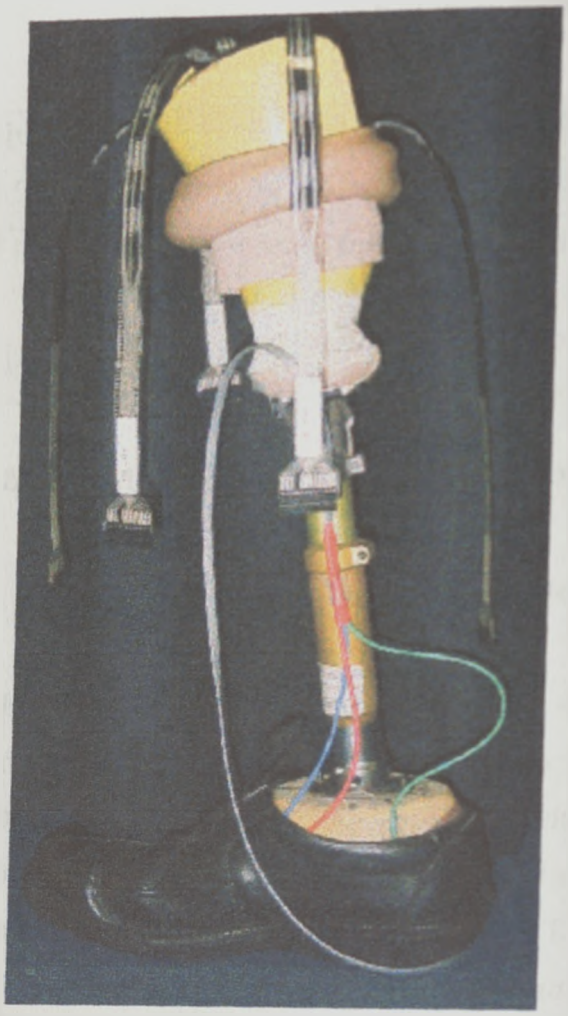

Figure 4.10 The complete set up for the Rincoe test.

the same level around the socket in order to obtain circumference graphs. As the adhesive tapes were slightly broader than then sensor strips they tend to stick to the subjects stump sock. In order to prevent this talcum powder (Johnson & Johnson) was sprinkled inside the socket. The three foot switches were attached to the subjects shoe using double sided adhesive tape (figure 4.10). The communication cable for the foot switches had 3 coloured cables. The green cable was attached to the footswitch at the heel of the subject's shoe, the blue cable was attached to the foot switch under the ball of the foot, and the red cable was attached to the footswitch under the toe.

The subject was then asked to wear the socket and the sleeve suspension was applied over the socket. The sensor strips were then connected to the hardware box of the Rincoe System. The hardware box was worn by the subject around the waist (figure 4.11). The data collected by the hardware box were transmitted to the computer (model : 386), via a 9 metre long cable attached to its serial port. The DOS-based Rincoe software was used for data collection. The calibration tables provided by the manufacturer were then loaded for each strip.

A preliminary check was performed to check the outputs from all the six strips. This was done by asking the subject to stand and a real time monitoring of outputs from all six strips was performed using the strip graph mode. The subjects were also instructed to perform a few preliminary walking trials in order to become accustomed to the set up attached to the socket. After the subjects had felt comfortable to the new socket environment the actual testing and data collection began. Both static and dyanamic tests were performed on both subjects. During the static test the subjects were asked to stand normally distributing weight equally between their amputated and normal leg. The data were then collected using the static mode and the collected data were displayed as circumference graphs.

The dynamic test was performed by asking the subject to walk. The dynamic mode was turned on after the subject started walking. The footswitches located under the subjects shoe, detected the heel strike, mid-stance and toe-off, and data were

Figure 4.11 Subject wearing the instrumented prosthesis for the Rincoe test

collected during these phases of the gait cycle. The collected data were then displayed as circumference graphs, and were then saved. Two trials of both static and dynamic tests were carried out on each subject. The subjects were then asked to remove the test sockets and the Rincoe strips were repositioned by shifting each strip to the right (clcokwise), in order to obtain data from almost every area of the socket. The same test procedure as explained above was carried out.

The collected data were then stored and later were printed out by using a dot matrix printer (Canon). The collected data were manually analysed by comparing it with the data obtained from the validation of the Rincoe socket fitting system. The points of high pressure were determined by considering the accuracy error of each sensor. Before fixing a particular area as an area of high pressure, the surrounding sensor positions were thoroughly checked for the pressures recorded and their accuracy errors.

These areas of high pressure once obtained were later used as areas for mounting the six Entran pressure transducer.

4.6 Subject Testing using the PTB Mark-II and Entran Transducers

4.6.1 Instrumentation of the socket

The testing of the subjects were carried out once the mounting of the transducers on the socket wall of the prosthesis completed. First of all the areas of high pressure determined from the Rincoe test were marked clearly on the inside of the socket. Holes were then drilled through these marked positions. Specially designed supports made from aluminium alloy, used in previous studies (Torres-Moreno, 1991, Osman, 1999, Wandrum 2000) were fixed to the socket walls in these holes using epoxy adhesive resin (Otto-bock, GmbH, Germany). The transducer mounts were then mounted onto these aluminium rings. The aluminium rings were designed in such a way that the sensing surface of the transducer i.e. the piston surface, came flush with the inner surface of the socket wall (figure 4.12)

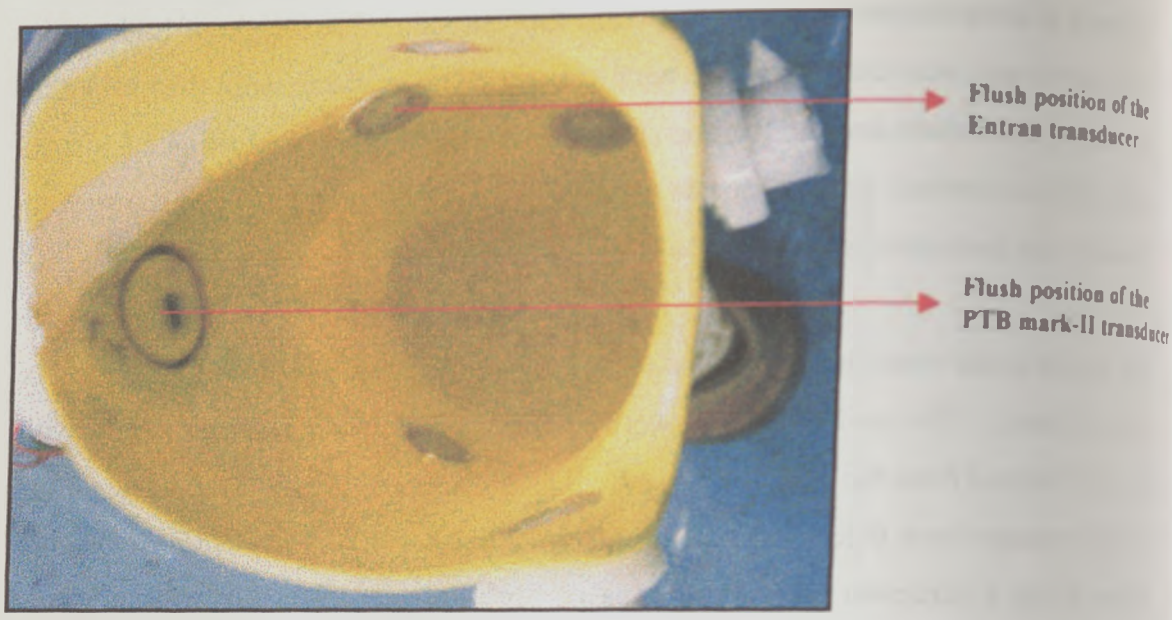

Figure 4.12 Internal view of the instrumented subject

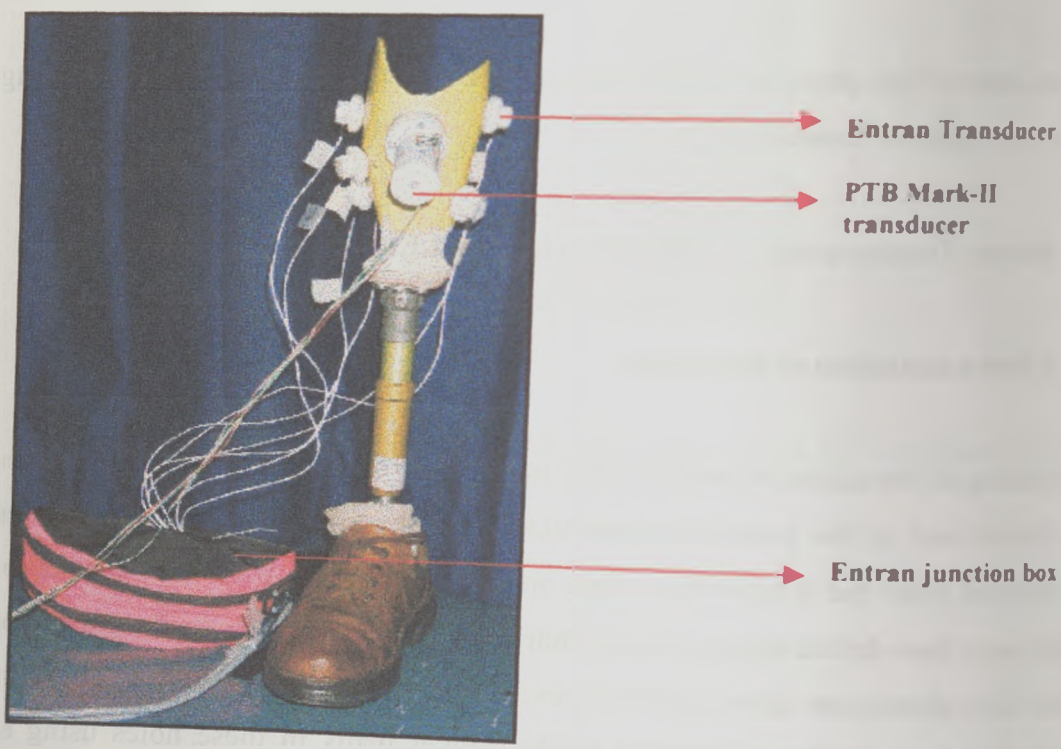

Figure 4.13 External view of the instrumented socket

The Patellar tendon bar area was then marked out on the socket. And a circle measuring 25mm in diameter was cut out from this area. On the outer surface of the cut patellar tendon bar, four 3mm screws were embedded in fast curing putty (Akemi putty , Otto-bock, GmbH, Germany) with their threads facing away from the surface. The patellar tendon bar was then attached to the Strain gauged piston of the PTB mark-II transducer by means of the four 3mm screws. A spacer made of aluminium alloy was sandwiched between the patellar-tendon bar and the flange of the strain-gauged piston. On the outer surface of the socket around the hole drilled in the patellar tendon area a specially designed aluminium ring was fixed using two screws counter sunk on the socket wall. This specially designed aluminium ring had six holes of which two were used to fix it on to outer side of the socket as described earlier. It also had a central large hole with a diameter of 28mm to allow the travel of the strain-gauged piston into the socket. Because of the contour of the socket the aluminium ring did not sit flat on the outer surface of the socket, but had a gap, which varied according to the contour. This gap was filled with fast curing putty (Akemi putty, Otto-bock, GmbH, Germany). This procedure ensured that the PTB mark-II transducer would be perpendicular to the stump surface. The PTB mark-II transducer was fixed to the socket via a spacer (Drawing A6 appndix:1) between the aluminium ring and itself.

The instrumented socket (figure 4.13) was now ready for testing.

4.6.2 Data Acquisition

The three channels from the PTB mark-II transducer and the six Entran transducers were connected to a bank of two strain gauge amplifiers. The output from the strain gauges were then connected to a special data acquisition card (Ni-Daq card – PCI6023E3) which is was installed in a computer (Hewlett Packard Pentium-I) (figure 4.14). This data acquisition card works using special software provided by the manufacturer. This helps to configure the 9 channels obtained from the strain gauge amplifiers. An additional channel was taken directly from the Kistler force plate's Fy channel (vertical load) and connected to the data acquisition card along

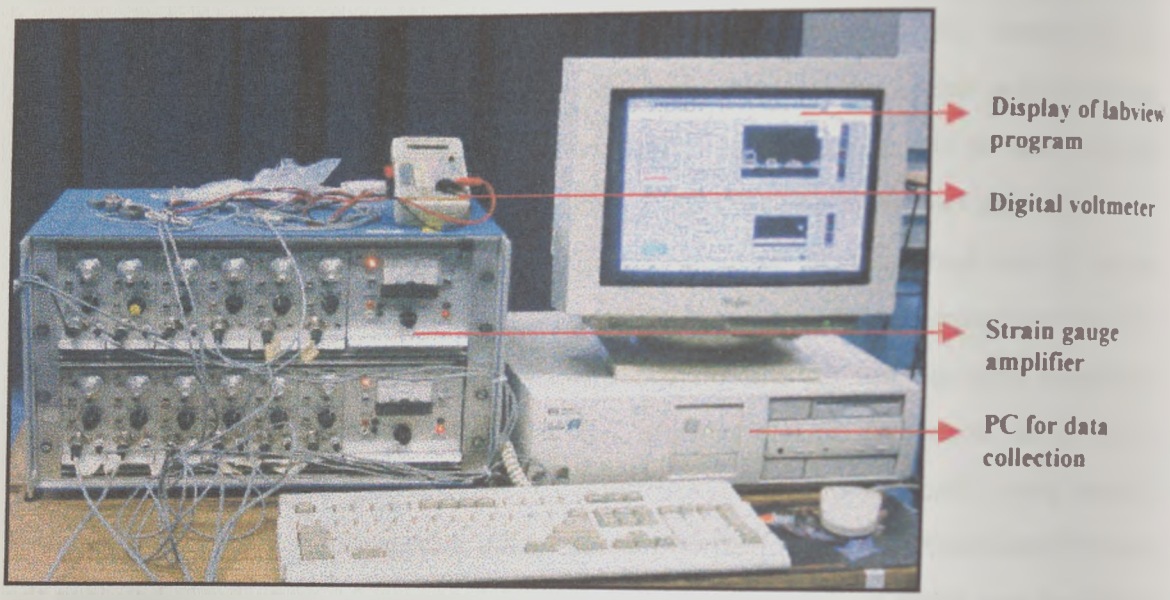

Figure 4.14 Data collection equipment used during subject testing

with the other 9 channels. The vertical load on the force plate was monitored to detect heel strike, midstance and foot flat during dynamic testing. Data were therefore acquired simultaneously from all10 channels during the testing procedure.

The special program called 'Acquire' was used for data collection and processing from all 10 channels. This program was written by Sherrif (1999) using Labview (version 5). This program made it possible to collect data simultaneously from all 10 channels at a sampling frequency of 100 – 300 Hz. The sampled data were then converted into an array and were stored in an Excel 97 (MS-office) worksheet. The data were measured in volts and it had a resolution of 0.1mV

4.6.3 Subject testing protocol

After the sockets were instrumented both subjects were tested separately. The testing was conducted in the Biomechanics laboratory, Bioengineering unit, University of Strathclyde. Before the start of the test a short assessment of the subject was carried out using a evaluation form as shown in appendix: 5. The procedures involved were then clearly explained to the subjects. The subjects were then asked to sign a consent form as shown in appendix:6. Meanwhile the PTB mark-II transducer and the Entran transducers were connected to the strain gauge amplifiers and the system was switched on 30 minutes prior to testing in order to stabilise the output from the strain gauges. The bridge voltages in both Fx and Fz channels of the PTB mark-II transducer was set at 3V, and in the Fy channel it was set at 6V. In all six Entran transducers the bridge voltages were set at 5V. The gain for all the 9 channels was set at 500. Before mounting the transducers onto the socket each of them were individually checked for consistent output. The PTB mark-II transducer was then attached to the socket. The sensing surface of the strain gauged piston i.e. the patellar tendon bar was placed approximately in a flush position with the socket wall. The subject was then asked to wear the same number of stump socks as worn during the Rincoe testing and they were then asked to don the test socket. During this time the subject was asked to be standing. The patellar tendon bar was then moved forward or backward using the control knob, until it gave an output of zero i.e that it was

Figure 4.15 Subject wearing the instrumented socket.

flush with the inner wall of the socket and just touching the stump. The six Entran transducers were then mounted onto the six areas determined by the Rincoe test. A single output from the Fy channel (vertical load) of the Kistler force plate was directly connected to the data acquisition card in the computer.

The set up being complete (figure 4.15) an initial data collection was performed to check the output in all channels. The subject was then asked to stand and to take a few trial walks, and report any discomfort to the prosthetist. Subject:2 while testing wanted a few changes in his alignment at this point and this was performed by the prosthetist. After all the checks were completed both the subjects underwent four different tests.

TEST-I – The subject was asked to stand only on his 'good' leg (socket unload)
TEST-II – The subject was asked to stand only on his prosthesis (single support)
Test-III- The subject was asked to stand normally with weight equally distributed on both legs (double support)
Test-IV – The subject was asked to walk along a 7 m long walkway with the force plates in the middle (dynamic gait).

During the first three tests data were collected for 10 seconds and two trials were done. The sampling frequency was set to 100Hz in order to detect the peak pressures. During the fourth test data were collected during the time the patient took his first step and to the time he had just crossed the force plates in the centre of the walkway. Further trials were done if the patient missed the force plates, and only the two with complete force plate data were taken for analysis. After all the four tests were performed the Patellar tendon bar was advanced by 1mm i.e. one full rotation of the control knob. The four tests were then carried out again, in this sequence the patellar tendon bar was advanced by 10mm in subject:1 and 9mm in subject:2. The tests were stopped at 9mm in subject:2 as he complained of mild discomfort. The test was immediately stopped and the stump was examined, no adverse effects were found.

The data collected from all the trials in the four different tests in both subjects were converted into forces by using the calibration matrix in the case of the PTB mark-II transducer and the calibration co-efficient in the case of the Entran transducers. The sensing areas were measured in all the transducers and knowing the areas the pressures were computed for both the Patellar tendon area and the other selected areas around the socket. The diameter of the sensing surface of the Entran transducer was found to 5.6mm and the diameter of the PTB mark-II transducer was found to be 25mm.

A few simple statistical methods were applied to the collected data such as mean and standard deviation. The difference between the mean and the peak pressures were also computed. The results were plotted using the SPSS statistical program (Delta graph version 5.0)

Chapter:5

Experimental Results

5.1 Introduction

The results of all the tests that were carried out throughout the course of this project have been presented in this chapter. The order in which these results have been presented are the same in which their methodologies have been presented. Most of the data are presented in both graphical and numerical form so that they can be easily compared with one another. Additional information has also been provided in the appropriate appendix in order to give a concise and clear picture of the outcome of the study.

5.2 Validation of the Rincoe Socket fitting system

This test was mainly carried out to ascertain the errors involved in the Rincoe system. Previous investigators who have used the Rincoe system (Hunter, 1996, Polliack et al., 2000), have clearly explained that this system is adequate in indicating areas of high pressure at the stump socket interface, but requires to be used with caution. Therefore in order to obtain as accurate as possible a picture of areas of high pressure the validation process was carried out. The two errors calculated were the hysteresis error and the accuracy error. Results of the same are presented. The Rincoe socket system as explained in section 3.1.4 record pressure up to 12 psi. Therefore pressures up to 10 psi were used for the tests. However some sensors, due to accuracy error, saturated and returned a pressure reading of 99.9 psi even when 10 psi was applied as input pressure. While applying statistical methods and calculations this saturated value of 99.9 psi showed large deviations, so in order to analyse it more realistically the value of 99.9 psi was taken as 12.1 psi. This value thus means that the sensor is indicating a value more than 12 psi, and since it is not within its range, it shows a value of 99.9psi, which for the ease of our calculations have been, assigned an arbitrary value of 12.1psi.

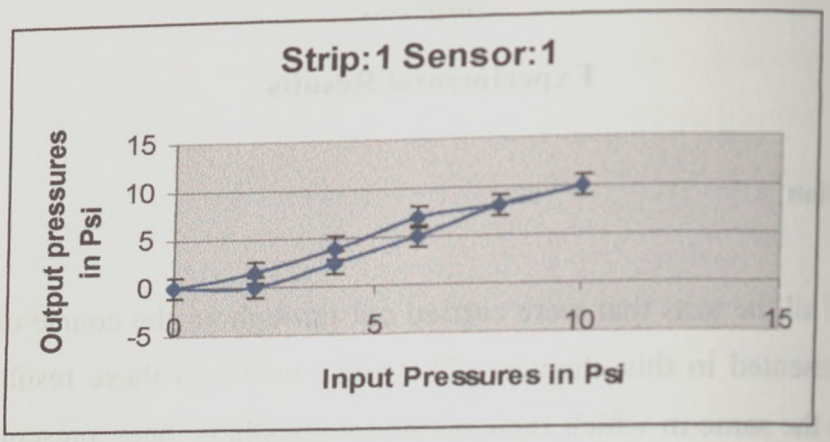

(a)

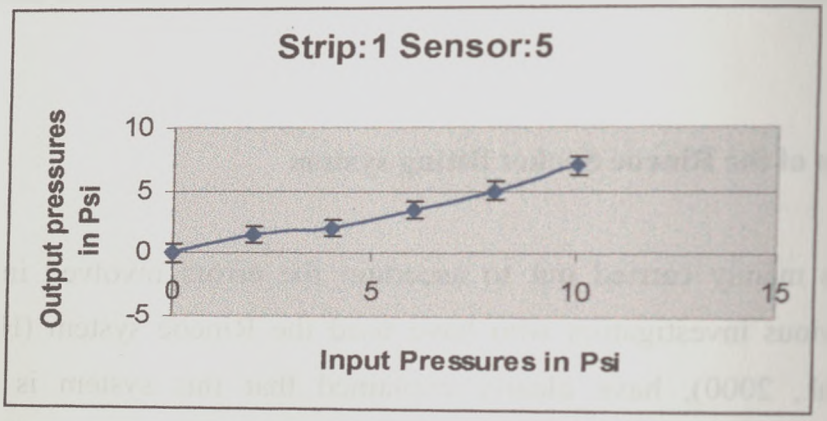

(b)

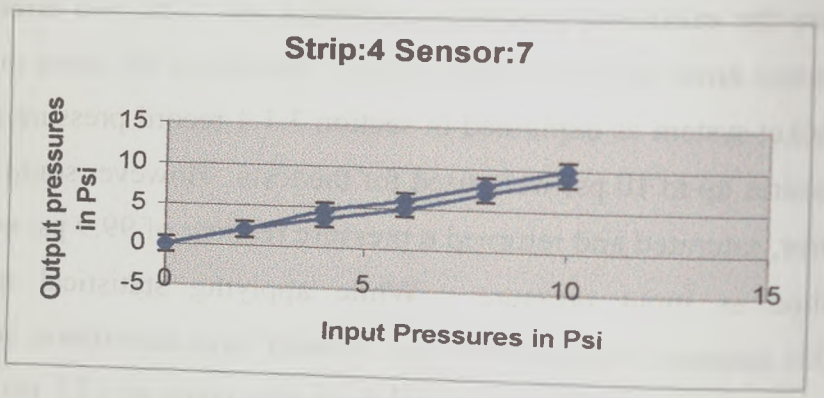

(c)

5.1 a,b,c Sample graphs obtained from Rincoe system validation

Sensor	One	Two	Thee	Four	Five	Six	Seven	Eight	Nine	Ten
Strip 1										
Accu. Error	19.58	45.25	35.17	42.92	36.83	33.50	30.25	38.42	10.17	16.67
Hyst. Error	33.21	6.50	10.50	2.86	0.00	9.83	6.50	6.86	10.33	11.19
Strip 2										
Accu. Error	12.67	10.92	22.02	12.50	16.33	13.17	22.53	9.25	15.17	22.17
Hyst. Error	4.00	10.75	2.39	10.36	10.67	3.33	0.00	7.89	12.23	8.52
Strip 3										
Accu. Error	7.92	13.42	6.25	7.00	12.83	12.08	9.92	10.92	12.67	20.33
Hyst. Error	5.08	7.08	2.50	8.44	4.00	2.22	9.56	15.19	14.36	2.22
Strip 4										
Accu. Error	1.25	6.17	11.83	15.33	7.42	20.16	6.42	10.25	7.67	8.92
Hyst. Error	2.50	8.33	19.98	5.00	5.83	16.70	12.28	6.50	13.12	11.08
Strip 5										
Accu. Error	15.08	19.25	18.50	17.58	8.92	13.92	6.42	18.50	8.92	17.17
Hyst. Error	10.08	14.08	7.83	5.08	12.83	11.86	11.83	0.00	17.65	14.94
Strip 6										
Accu. Error	7.67	3.50	10.75	12.67	10.17	13.92	3.92	15.42	9.33	10.58
Hyst. Error	13.87	6.82	7.86	14.36	14.51	11.86	7.83	4.86	7.00	8.04

Table 5.1 Summary of errors in all sensors in the 6 sensor strips used

All values are given in percentage.

The over all errors of the system were calculated as

Accuracy Error = 15.27 ± 5.33 %

And the hysteresis error was calculated as

Hysteresis Error = 9.05 ± 1.34 %

Load (N)	Fx (V)	Fy(V)	Fz(V)
0	0.0002	0.0045	-0.00156
9.04	0.00032	-0.02492	-0.00396
18.09	0.0003	-0.05478	-0.00456
27.12	0.00026	-0.0847	-0.00484
37.19	0.00028	-0.11722	-0.00488
47.14	0.00002	-0.15004	-0.00518
57.16	0.0002	-0.18356	-0.0058
66.22	0.00018	-0.21292	-0.006
76.39	0.00052	-0.2468	-0.00724
85.46	0.00012	-0.2761	-0.00724
94.52	-0.00006	-0.30554	-0.00776
85.46	0.00018	-0.27648	-0.00796
76.39	0.0007	-0.2465	-0.00742
66.22	0.00042	-0.21254	-0.00606
57.16	0.00046	-0.18174	-0.00564
47.14	0.00038	-0.14912	-0.005
37.19	0.00034	-0.11676	-0.00488
27.12	0.00038	-0.08344	-0.00484
18.09	0.00022	-0.05396	-0.00466
9.04	0.00012	-0.02374	-0.0045
0	0.0002	0.00616	-0.00216

Table 5.2 Calibration Data : -Fy Channel

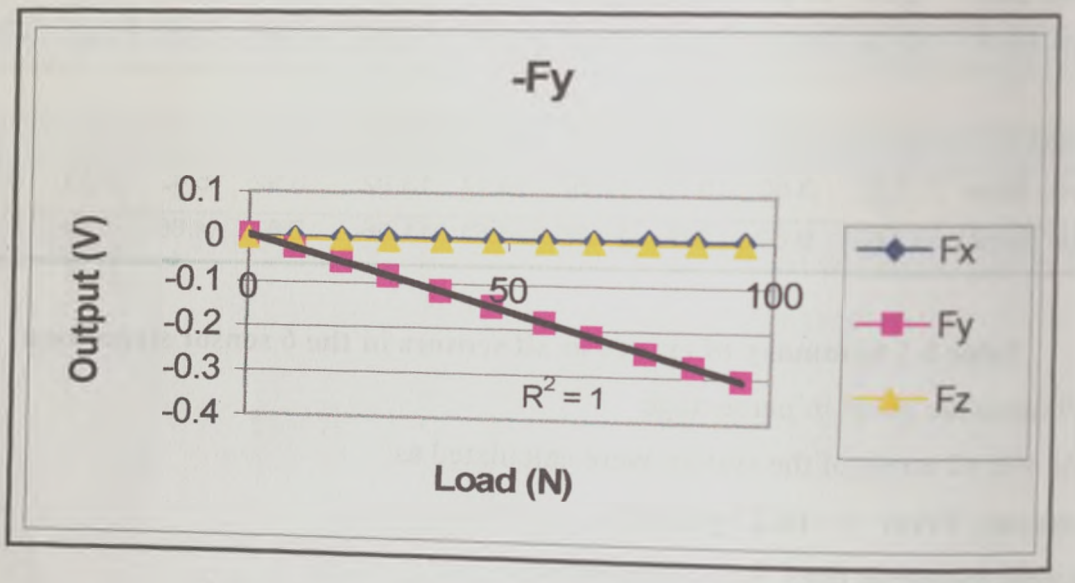

Figure 5.2 Calibration graph of channel -Fy

5.3 Calibration of the PTB mark-II transducer

In this section the calibration results of the PTB mark-II transducer have been presented. The first calibration that was done showed significant cross talk from the Fy channel during the calibration of the shear channels and hence was with some design modifications were made to the calibration jig. This modification has already been mentioned in section 4.2.5. Looking at the cross talk from the first calibration test it was believed that this could have taken place due to the central metal projection of the calibration jig directly applying a bending moment on the Fy gauges from the inside of the strain gauged piston. So this was removed and the flange of the strain gauged piston was directly attached to the bottom of the calibration rig with screws. The calibration that was performed with this kind of a set up did not show any significant cross talk from the Fy channel. The results of the same are presented in tables 5.2 to 5.6 and in a graphical form in figures 5.2 to 5.6. However the results obtained from the first calibration test can be viewed in appendix:3 .

The results presented are the mean of five cycles of loading and unloading in each channel, with outputs recorded from the principal channel and the other channels.

Load(N)	Fx(V)	Fy(V)	Fz(V)
0	0.00242	0.0046	-0.00026
5.54	0.03658	0.00468	-0.00224
14.58	0.08686	0.00526	-0.00396
23.63	0.13704	0.0061	-0.00662
32.66	0.18692	0.00726	-0.00614
42.73	0.24286	0.00882	-0.01034
52.68	0.2979	0.01056	-0.01164
62.7	0.35304	0.0125	-0.0142
71.76	0.40308	0.01508	-0.01358
62.7	0.35324	0.01342	-0.01202
52.68	0.2984	0.01074	-0.01136
42.73	0.24318	0.00878	-0.0103
32.66	0.18706	0.00728	-0.00824
23.63	0.13684	0.00588	-0.0067
14.58	0.08698	0.00524	-0.00486
5.54	0.03708	0.00538	-0.00316
0	0.00328	0.0064	-0.00068

Table 5.3 Calibration Data: Fx channel

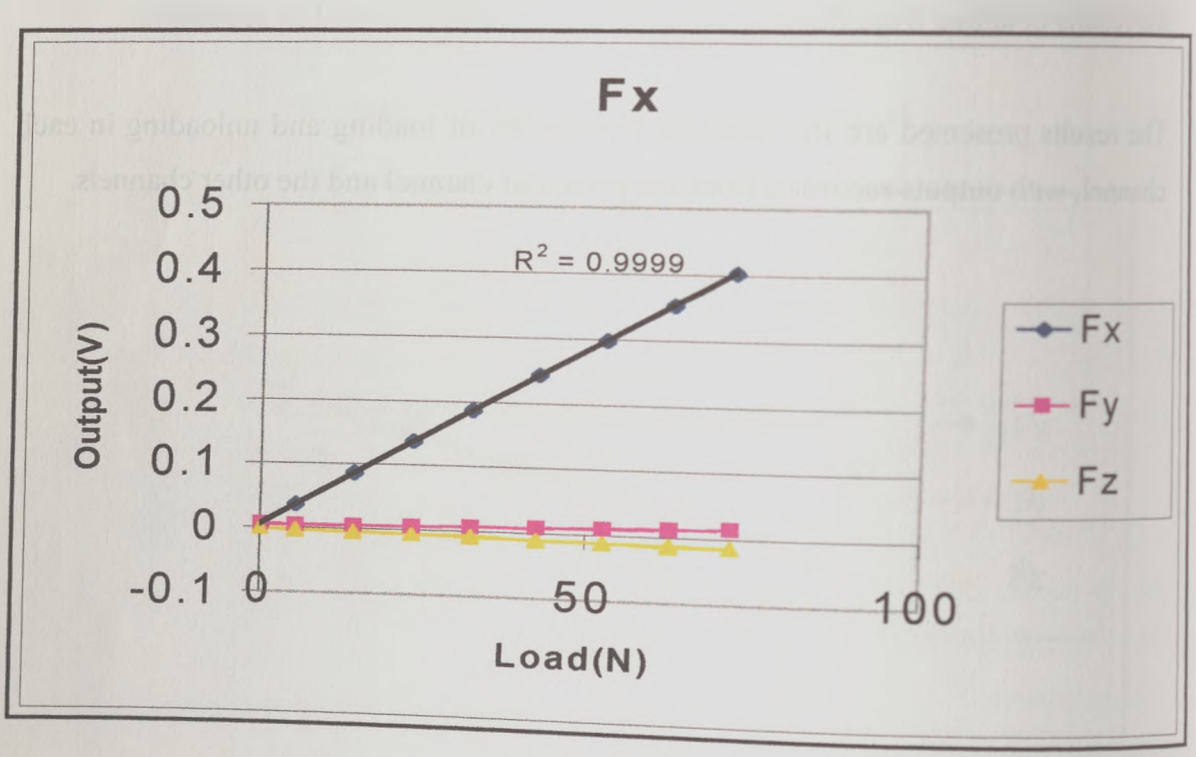

Figure 5.3 Calibration graph of channel Fx

Load(N)	Fx(V)	Fy(V)	Fz(V)
0	-0.00554	0.001	-0.00492
5.54	-0.03984	0.00072	-0.0049
14.58	-0.09042	0.00156	-0.00252
23.63	-0.14118	0.00304	-0.00054
32.66	-0.19138	0.00512	0.00234
42.73	-0.24808	0.00782	0.0041
52.68	-0.30304	0.01102	0.00708
62.7	-0.35898	0.01406	0.00514
71.76	-0.41032	0.018	0.0126
62.7	-0.35982	0.01476	0.01058
52.68	-0.3045	0.01136	0.00832
42.73	-0.2492	0.00754	0.00532
32.66	-0.19284	0.00442	0.00344
23.63	-0.14232	0.00226	0.00084
14.58	-0.09168	0.00102	-0.00214
5.54	-0.04098	0.0009	-0.0045
0	-0.00602	0.0018	-0.00494

Table 5.4Calibration data: channel -Fx

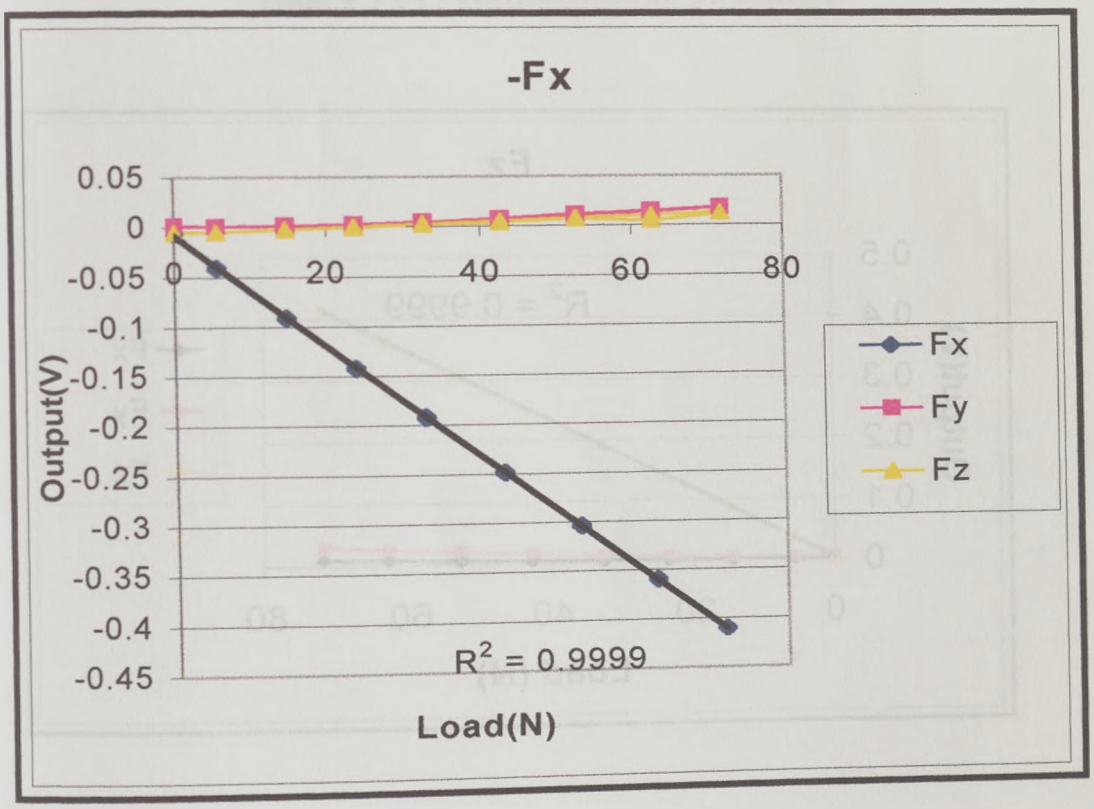

Figure 5.4 Calibration graph of channel -Fx

Load(N)	Fx(V)	Fy(V)	Fz(V)
0	0.00064	0.0028	0.00028
5.54	0.00142	0.00392	0.03608
14.58	0.00184	0.00588	0.0879
23.63	0.00258	0.00892	0.1409
32.66	0.0023	0.01268	0.19058
42.73	0.00412	0.01622	0.249
52.68	0.0051	0.02122	0.3073
62.7	0.00798	0.02568	0.3621
71.76	0.00936	0.03016	0.415
62.7	0.0081	0.02584	0.36234
52.68	0.00704	0.02052	0.30754
42.73	0.00566	0.01598	0.24904
32.66	0.00426	0.0118	0.1909
23.63	0.00324	0.0087	0.14134
14.58	0.0024	0.00606	0.08794
5.54	0.00156	0.0042	0.0373
0	0.00078	0.00372	0.00042

Table 5.5 Calibration Data : Fz Channel

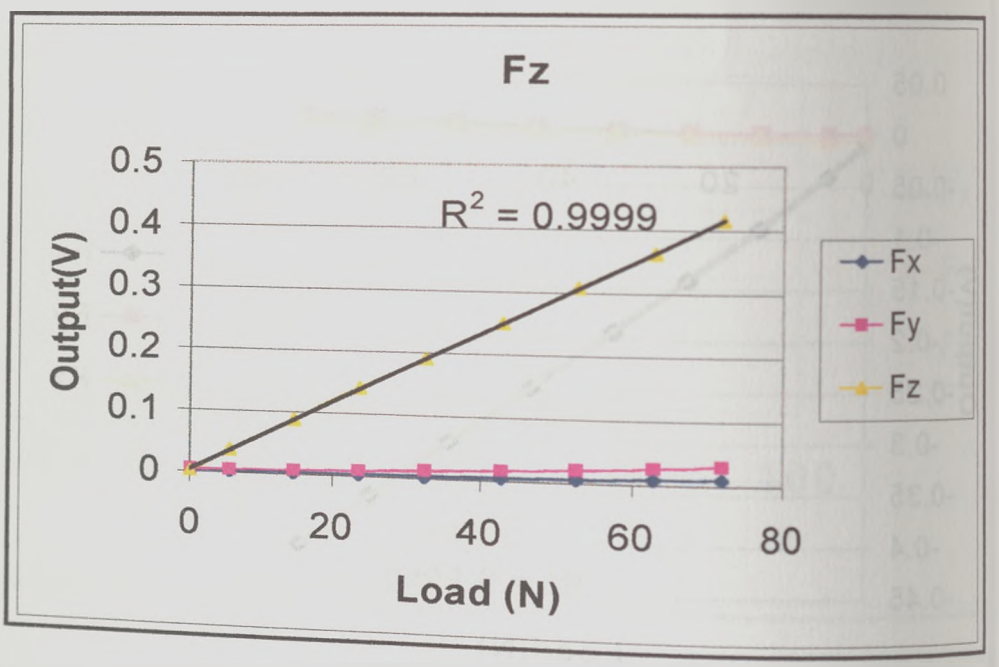

Figure 5.5 Calibration graph of Channel Fz

load(N)	Fx(V)	Fy(V)	Fz(V)
0	0.0017	0.0036	-0.00042
5.54	0.00194	0.00224	-0.03764
14.58	0.0016	0.0015	-0.09094
23.63	0.00066	0.00122	-0.1444
32.66	-0.00158	0.00012	-0.19786
42.73	-0.00104	-0.00056	-0.25738
52.68	-0.00254	-0.00028	-0.31514
62.7	-0.00284	0.0001	-0.37394
71.76	0.00342	-0.00032	-0.42658
62.7	0.00254	-0.00184	-0.37552
52.68	0.00012	-0.00288	-0.31724
42.73	0.0021	-0.00274	-0.25902
32.66	0.00226	-0.00258	-0.20016
23.63	0.00248	-0.00196	-0.14658
14.58	0.00232	-0.00086	-0.0929
5.54	0.00246	0.00082	-0.03896
0	0.00256	0.00394	-0.00072

Table 5.6 Calibration Data: Channel -Fz

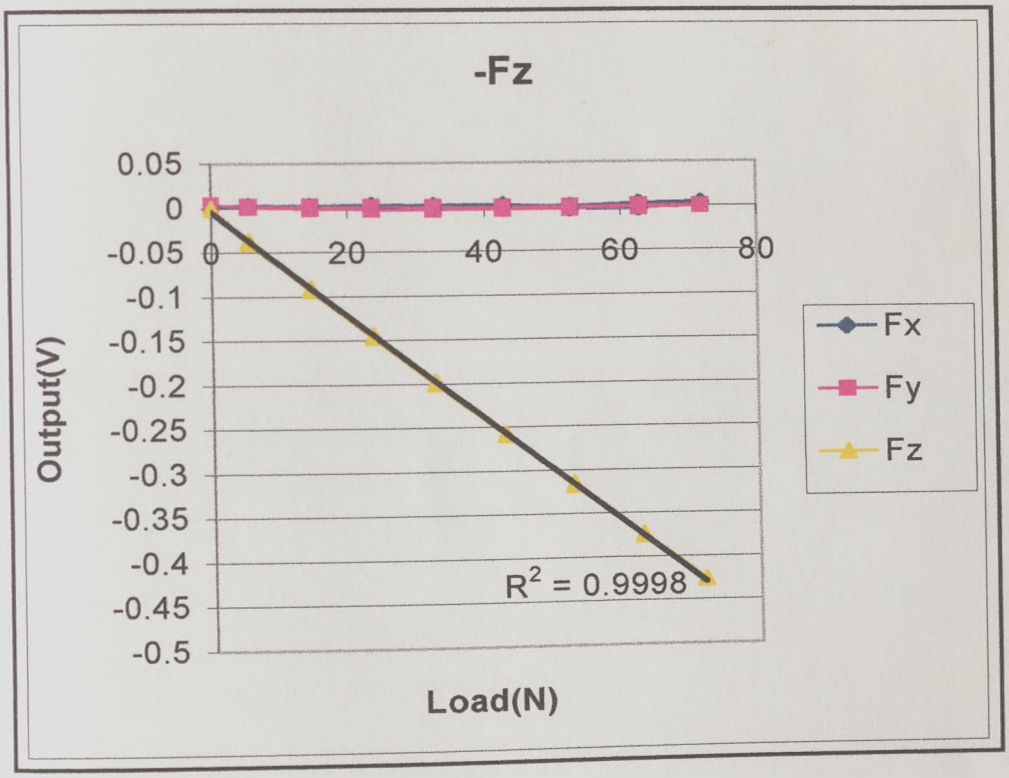

Figure 5.6 Calibration graph of channel -Fz

5.3.1 Calibration matrix of the PTB mark-II transducer

From the calibration data the calibration co-efficients for the principal channel and the two cross talk channels were determined. This was calculated as shown in the model calculation outlined in appendix:4.

The calibration matrix [M] of the PTB mark-II transducer was as follows

$$\begin{vmatrix} 0.005599 & -0.0000027 & 0.000069225 \\ 0.000185 & -0.003288 & 0.00021585 \\ -0.00021 & -0.000063 & 0.0058575 \end{vmatrix} \text{ N/V}$$

In order to calculate the forces from the signals the inverse of matrix [M] needs to be used. This inverse matrix was calculated using Excel 97 (MS-Office).

$$[M]^{-1} = \begin{vmatrix} 178.53 & -0.11 & -2.11 \\ 10.45 & -304.36 & 11.09 \\ 6.63 & -3.28 & 170.76 \end{vmatrix} \text{ V/N}$$

This inverse matrix was later used for all calculations to convert the signals in volts to forces.

Calibration graphs of Entran transducers

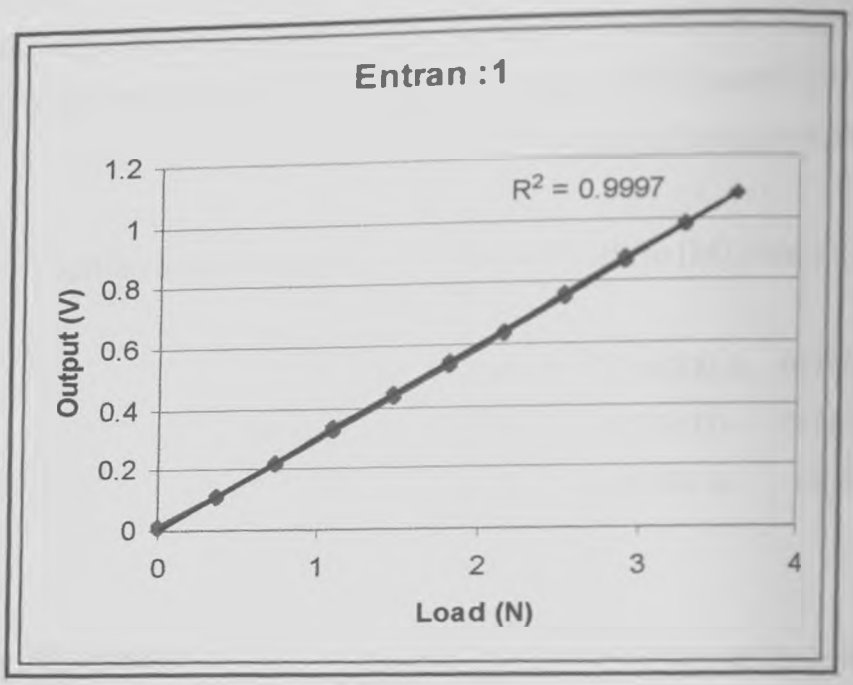

Figure 5.7 Calibration graph of Entran transducer 1

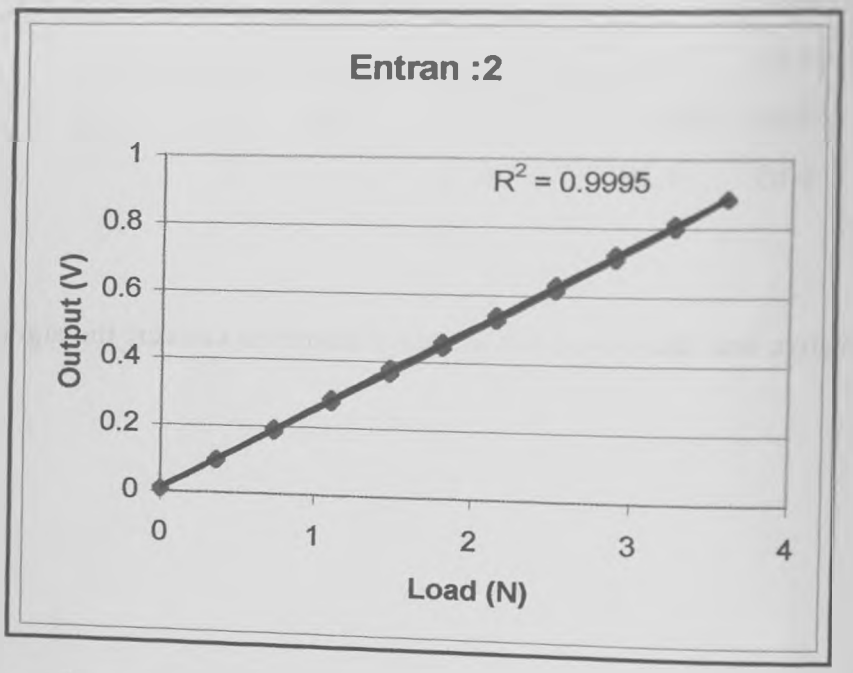

Figure 5.8 Calibration graph of Entran transducer 2

5.3.1 Calibration matrix of the PTB mark-II transducer

From the calibration data the calibration co-efficients for the principal channel and the two cross talk channels were determined. This was calculated as shown in the model calculation outlined in appendix:4.

The calibration matrix [M] of the PTB mark-II transducer was as follows

$$\begin{vmatrix} 0.005599 & -0.0000027 & 0.000069225 \\ 0.000185 & -0.003288 & 0.00021585 \\ -0.00021 & -0.000063 & 0.0058575 \end{vmatrix} \text{ N/V}$$

In order to calculate the forces from the signals the inverse of matrix [M] needs to be used. This inverse matrix was calculated using Excel 97 (MS-Office).

$$[M]^{-1} = \begin{vmatrix} 178.53 & -0.11 & -2.11 \\ 10.45 & -304.36 & 11.09 \\ 6.63 & -3.28 & 170.76 \end{vmatrix} \text{ V/N}$$

This inverse matrix was later used for all calculations to convert the signals in volts to forces.

Calibration graphs of Entran transducers

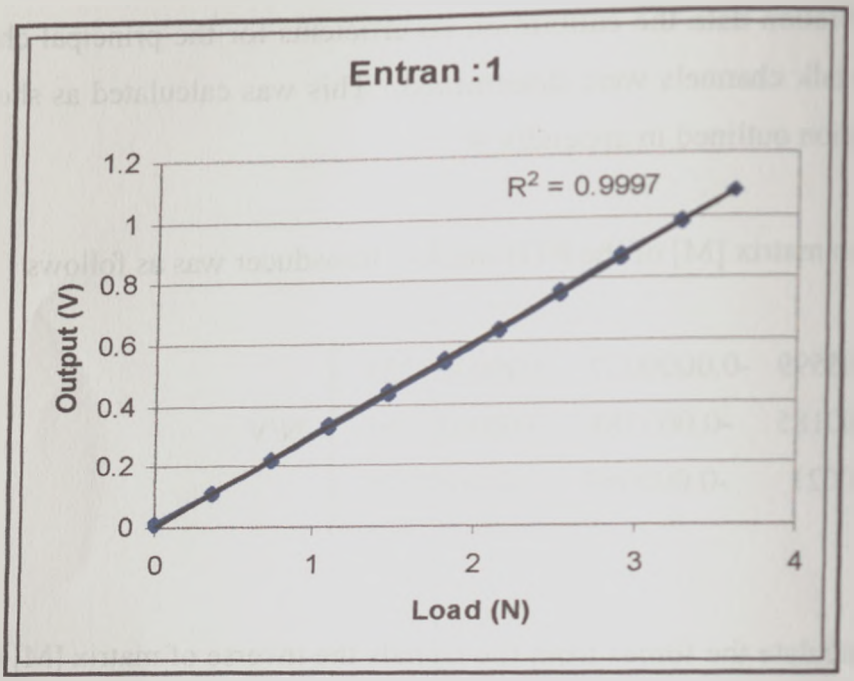

Figure 5.7 Calibration graph of Entran transducer 1

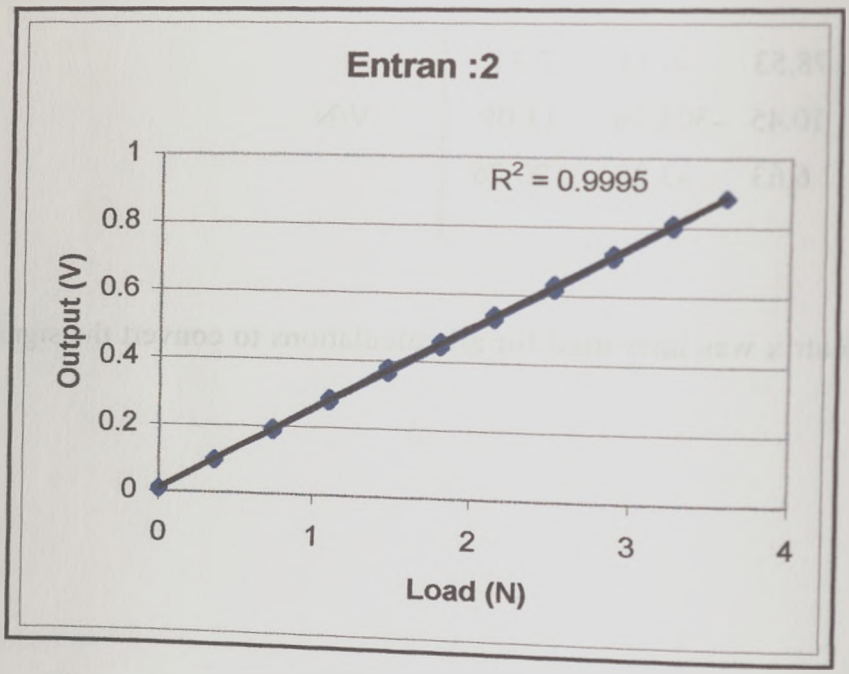

Figure 5.8 Calibration graph of Entran transducer 2

5.4 Calibration of Entran Transducers

The Entran transducers were calibrated as described in the methodology. The six Entran transducers were calibrated separately and data were collected manually using a digital voltmeter. The results presented in table 5.7 are a mean output in volts of 5 cycles of loading and unloading. The calibration graphs for Entran transducer 1-6 are given in figures 5.7-5.12

Load(N)	Entran1 (V)	Entran2 (V)	Entran3 (V)	Entran4 (V)	Entran5 (V)	Entran6 (V)
0	0.0086	0.00604	0.00136	0.01542	0.00856	0.00236
0.365	0.111	0.096	0.1032	0.1048	0.081	0.0966
0.737	0.2158	0.187	0.2084	0.2086	0.159	0.1938
1.104	0.3236	0.2756	0.3124	0.3126	0.2378	0.2918
1.475	0.4332	0.364	0.4178	0.4252	0.3172	0.3892
1.808	0.535	0.445	0.5124	0.5298	0.3892	0.4788
2.146	0.6364	0.5268	0.609	0.6382	0.4618	0.5682
2.515	0.748	0.617	0.7146	0.7386	0.5406	0.6662
2.884	0.8644	0.7082	0.8192	0.8576	0.6204	0.7646
3.253	0.978	0.801	0.924	0.9656	0.7008	0.8642
3.586	1.0814	0.8858	1.0192	1.0782	0.7738	0.9542
3.253	0.9824	0.8126	0.9272	0.9812	0.7052	0.8674
2.884	0.8758	0.722	0.8254	0.8616	0.6274	0.77
2.515	0.7586	0.6324	0.7194	0.7548	0.5486	0.6714
2.146	0.6434	0.5408	0.6144	0.6426	0.4698	0.5734
1.808	0.543	0.4588	0.5176	0.5358	0.3968	0.482
1.475	0.4428	0.3786	0.423	0.4342	0.3252	0.394
1.104	0.3352	0.2858	0.3172	0.3246	0.246	0.296
0.737	0.2212	0.1928	0.2122	0.2132	0.1662	0.191
0.365	0.1124	0.0984	0.1058	0.106	0.086	0.06272
0	0.0112	0.0086	0.0026	0.0208	0.0116	0.0038

Table 5.7 Mean outputs obtained during calibration

From the data in table 5.7 the calibration co-efficient for each of the six entran transducer was determined and displayed in table 5.8

Transducer	Co-ef V/N	Inv N/V
1	0.299	3.345
2	0.245	4.081
3	0.284	3.521
4	0.296	3.378
5	0.213	4.695
6	0.265	3.774

Table 5.8 Calibration co-efficients and their inverse for the six Entran Transducers

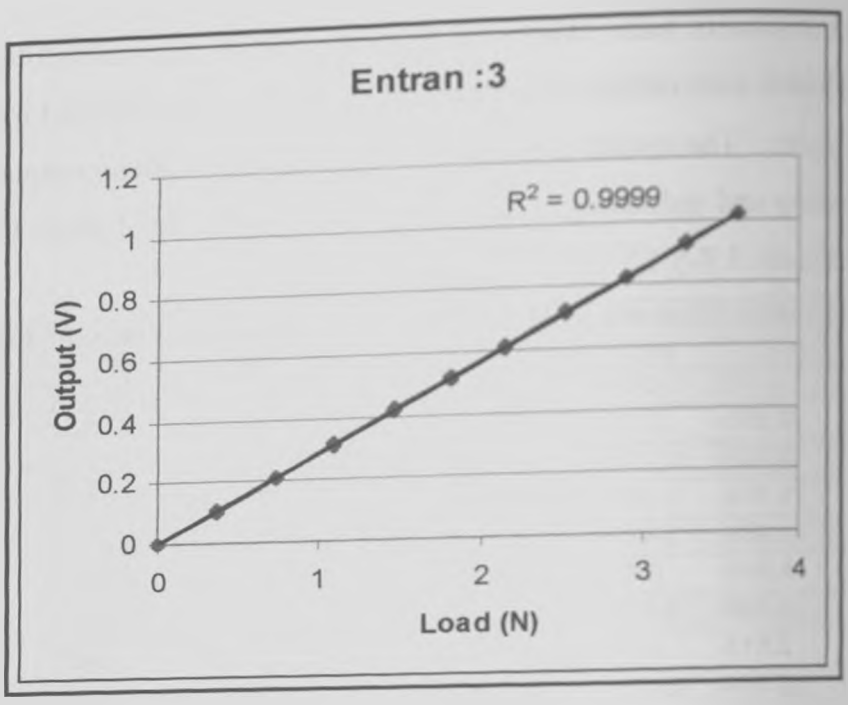

Figure 5.9 Calibration graph of Entran transducer 3

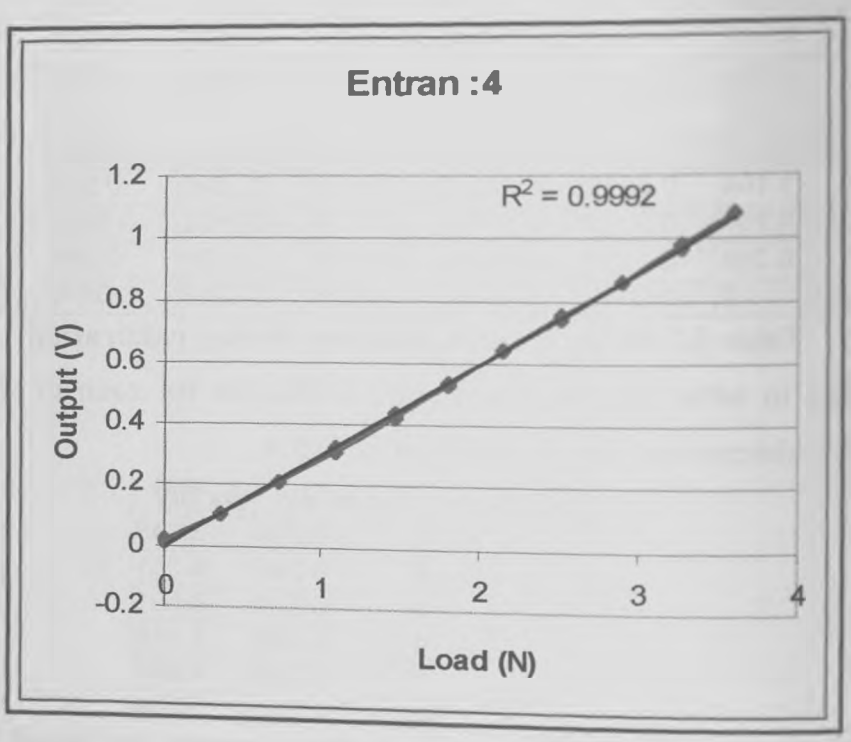

Figure 5.10 Calibration graph of Entran transducer 4

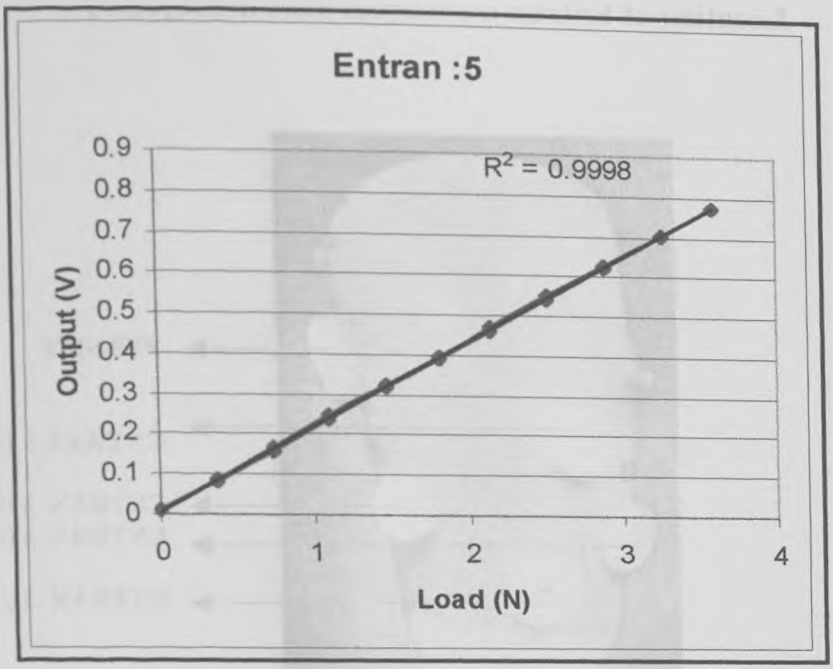

Figure 5.11 Calibration graph for Entran transducer 5

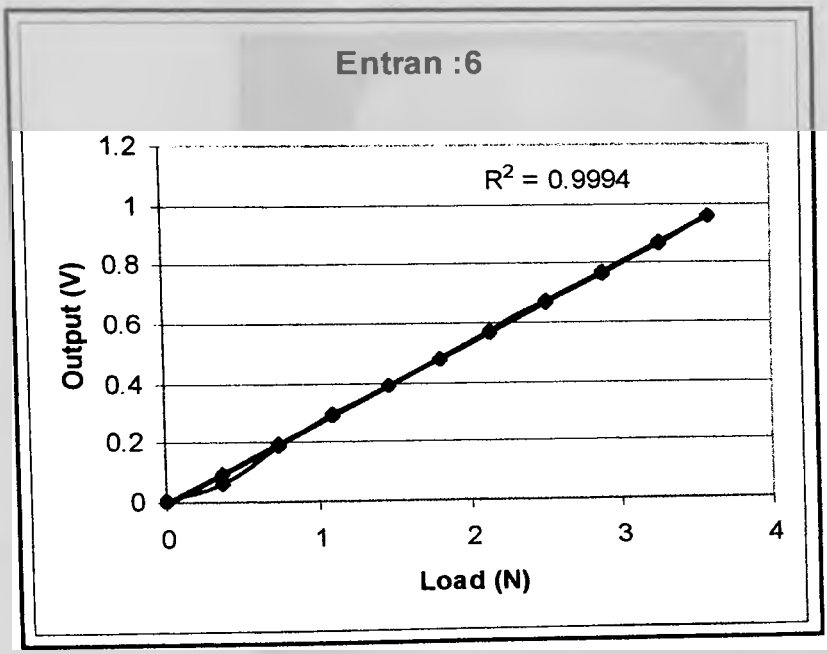

Figure 5.12 Calibration graph for Entran transducer 6

Location of Entran transducer sites in subject: 1

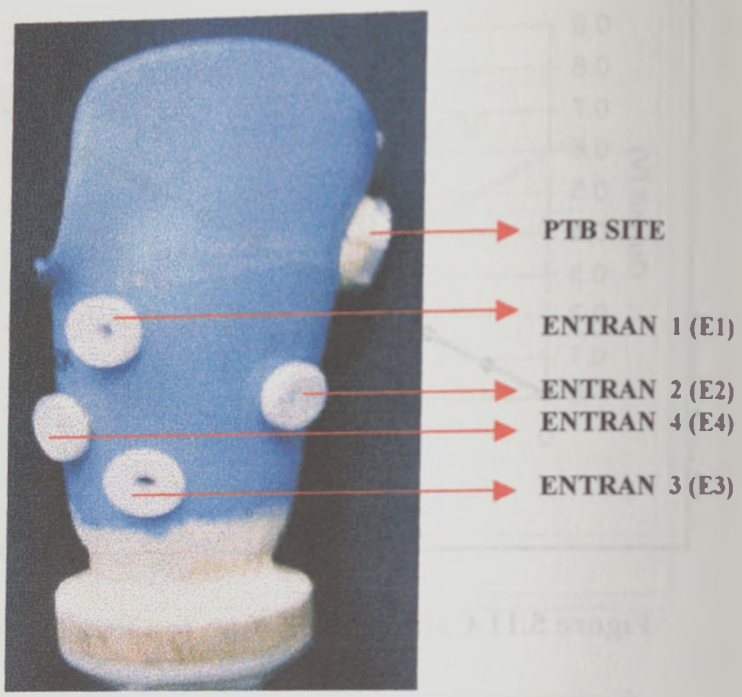

Figure 5.13 Lateral view of the socket in Subject: 1

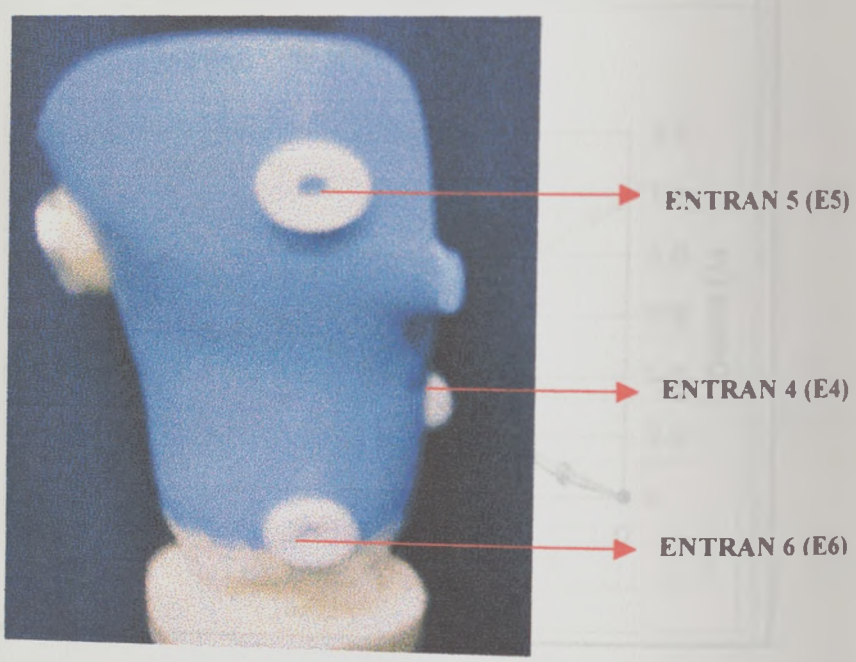

Figure 5.14 Medial view of the socket in Subject:1

5.5 Results of Rincoe test

This test was conducted to identify the areas of high pressure in the socket in order to mount the Entran transducers and monitor the pressures around the socket. The methodology of this test has been discussed in detail in section 4.5.

5.5.1 Subject: 1

During the test it was noted that all the 10 sensors in each sensor strips did not fit into the socket due to the size of the socket and varied around the socket. The data was collected from sensors 1-8 as these were the total number of sensors that fitted from the bottom to the brim of the socket in each strip. When the sensors saturated and read 99.9 psi it was assumed for calculation as 12.1 psi.

The pressure recorded in each of the six sites that were selected for mounting the Entran transducers are given in table 5.9 along with the accuracy and hysteresis error of the sensor that recorded it. The pressures quoted are the mean pressures of both static and dynamic tests.

Entran Transducer site number	Pressure recorded by Rincoe system (Psi)	Accuracy error of the recording sensor (%)	Hysteresis error of the recording sensor (%)
1	5.50	7.42	5.83
2	7.51	12.50	10.36
3	5.38	6.25	2.50
4	5.75	15.33	5.00
5	3.88	3.92	7.83
6	4.75	10.75	7.86

Table 5.9 Pressures recorded in subject:1 by the Rincoe system along with the accuracy and hysteresis error

Location of Entran Transducer sites in Subject: 2

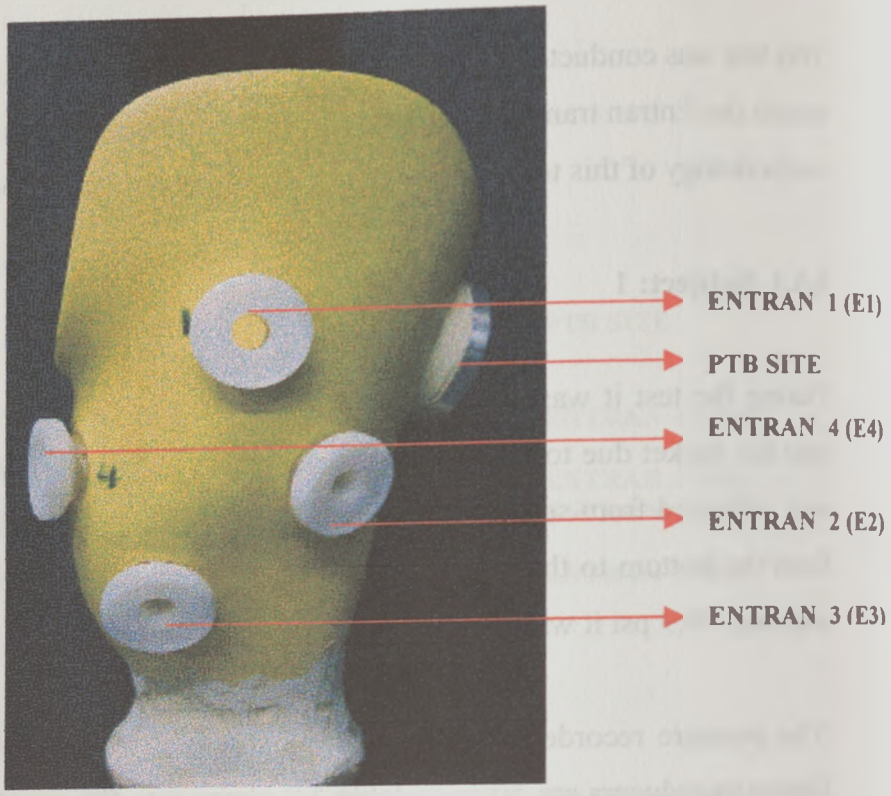

Figure 5.15 Lateral View of the socket in Subject: 2

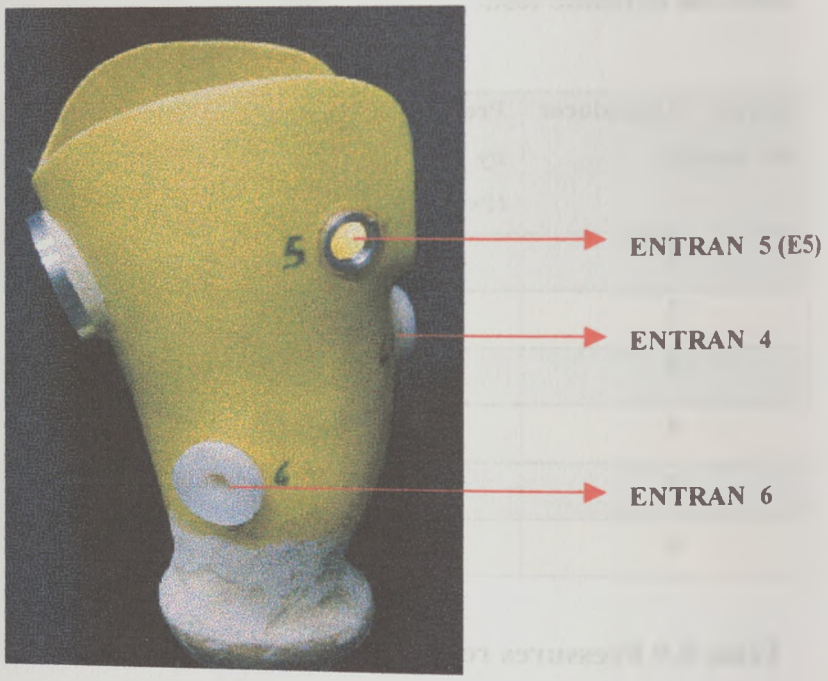

Figure 5.16 Medial view of the socket in Subject: 2

5.5.2 Subject: 2

During the test it was noted that only sensors 1-6 in each sensor strip did fit into the socket due to the smaller size of the socket..

The pressure recorded in each of the six sites are given in table 5.10 along with the accuracy and hysteresis error of the sensor that recorded it. The pressures quoted are the mean pressure of both static and dynamic tests.

Entran Transducer site number	Pressure recorded by Rincoe system (Psi)	Accuracy error of the recording sensor (%)	Hysteresis error of the recording sensor (%)
1	5.19	12.83	4.00
2	8.15	7.00	8.44
3	4.00	11.83	19.98
4	8.38	15.33	5.00
5	10.80	10.17	14.51
6	5.25	35.17	10.50

Table 5.10 Pressures recorded in subject:2 by the Rincoe system along with the accuracy and hysteresis error

When the sensors saturated and read 99.9 psi it was assumed for calculation as 12.1psi.

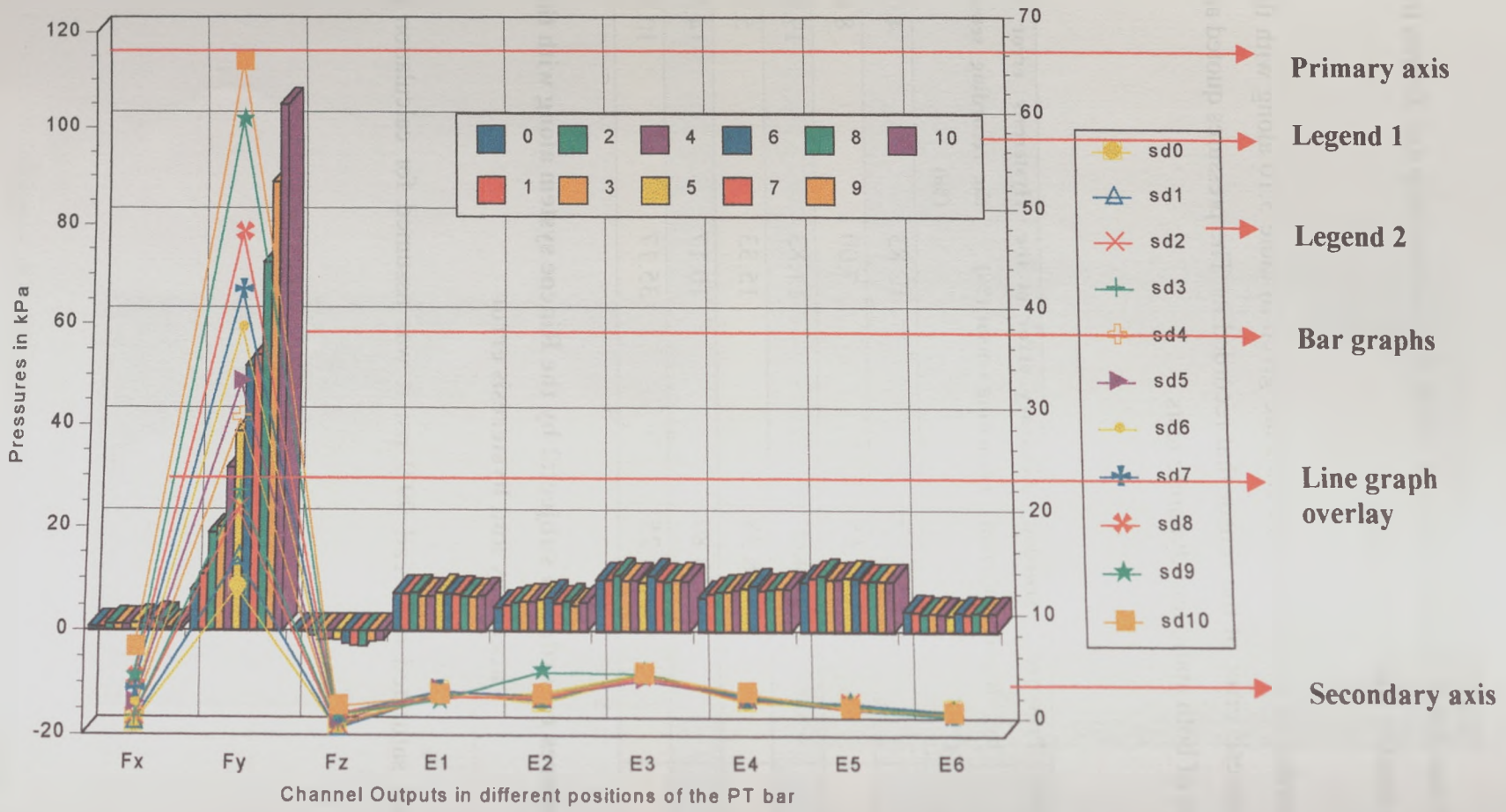

Figure 5.17 SAMPLE CHART

5.6 Results of subject testing using PTB mark-II and Entran Transducers

5.6.1 Introduction

The data collected from all four different tests i.e. socket unload (Test –I), single-leg stance (Test-II), double support (Test-III) and dynamic gait (Test-IV), have been presented separately for each of the subjects. The data as explained in the methodology were analysed using Excel 97 (MS-office) software and plotted using SPSS delta graph Version 5.0. The data collected during gait were plotted against time using Excel '97.

Statistical methods such as the mean and standard deviation for each of the tests have been computed and have also been plotted in the graph.

5.6.2 Parts of Delta graph (ver 5.0)

The explanation of the labelled sample delta graph shown in figure 5.17 is given below

- **Primary axis :** This shows pressures in kPa, and the mean or peak pressures are plotted against it as bar graph
- **Secondary axis:** This shows pressures in kPa and the standard deviation and difference between mean and peak pressure are plotted against it as line graphs
- **Legend:1** : This is the legend for the bar graphs and shows the position of the Patellar tendon bar in mm i.e. 0-10 mm
- **Legend:2 :** This is the legend for the line graphs and shows the standard deviation and difference between peak and mean pressures for different displacement of the PTB bar in mm (e.g. standard deviation at 3mm of displacement is sd 3 and the difference between peak and mean pressure is diff3)
- **Bar graph:** These graph show the mean and peak pressures during different displacements of PTB bar
- **Overlay line graph:** This shows the standard deviation and difference in peak and mean pressures at different displacements of the PTB bar.

The data are plotted separately for the 9 different channels i.e. Fx, Fy ,Fz,
E 1(Entran-1) to E 6(Entran-6) etc.

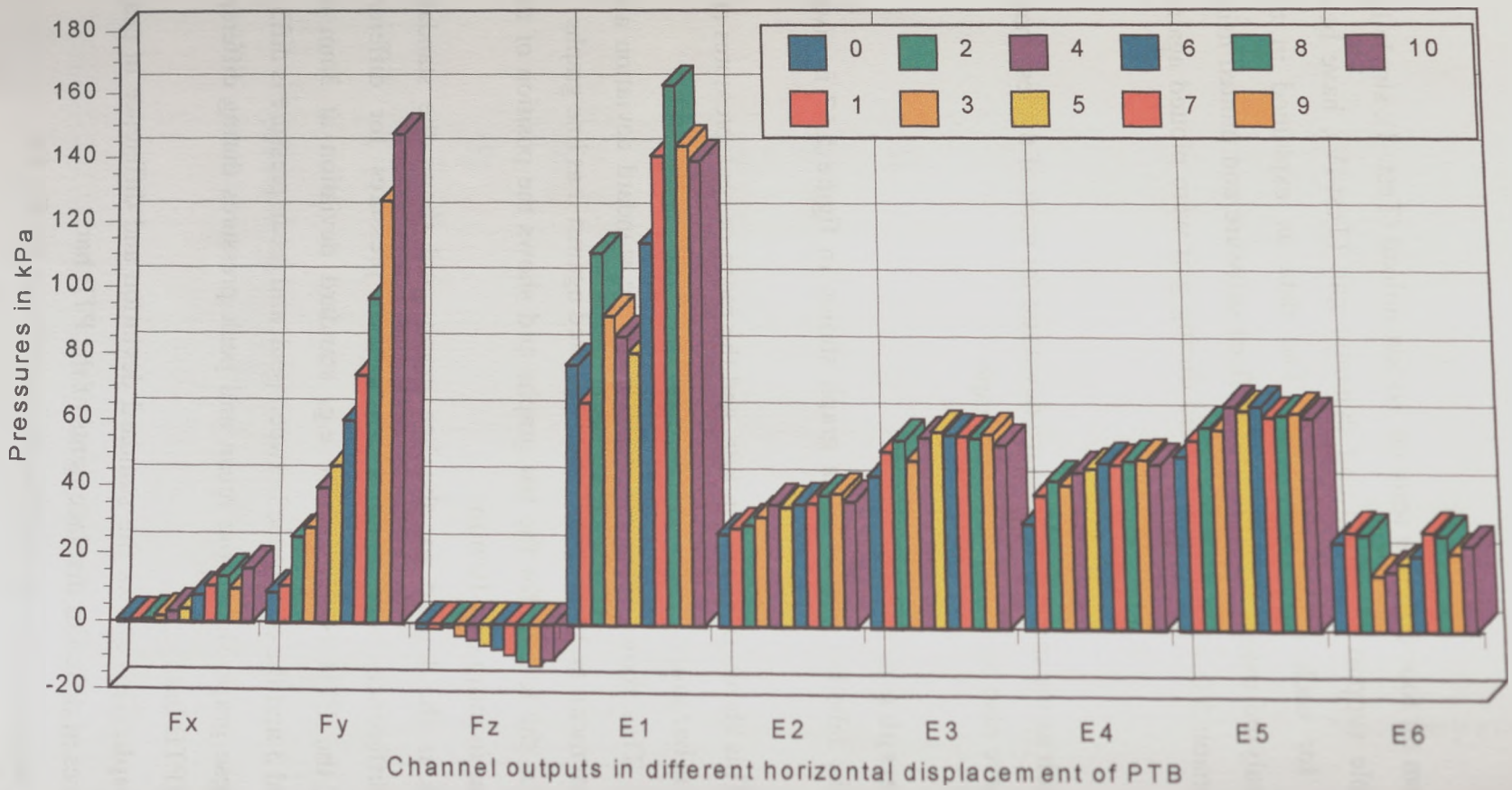

Figure 5.18 Subject:1 Summary of mean pressures during Single-leg stance on prosthetic side – Static Test (Test-II)

Legend – Refer section 5.6.2

5.6.3 Results of subject:1

A summary of all the results are given in both graphical (figures 5.18 to 5.30) and numerical form (table 5.11 to 5.23), for easy understanding and interpretation.

Chn	0mm (kPa)	1mm (kPa)	2mm (kPa)	3mm (kPa)	4mm (kPa)	5mm (kPa)	6mm (kPa)	7mm (kPa)	8mm (kPa)	9mm (kPa)	10mm (kPa)
Fx	0.46	0.49	0.78	1.66	3.14	3.76	7.98	10.48	13.43	9.77	15.83
Fy	8.65	10.69	25.15	27.91	39.76	46.22	59.87	73.75	96.78	126.87	147.64
Fz	-1.25	-1.24	-0.88	-3.23	-4.63	-6.12	-7.31	-8.65	-10.60	-11.84	-10.15
E1	77.13	65.80	110.88	91.86	85.51	80.63	114.00	141.00	162.71	144.12	139.37
E2	26.80	28.59	29.65	32.03	35.71	35.12	35.99	36.16	38.53	39.07	36.94
E3	44.41	51.66	55.31	49.14	55.97	57.85	56.90	56.59	55.96	57.29	53.97
E4	30.77	39.24	43.40	42.06	45.91	46.97	48.68	48.26	49.52	49.87	48.55
E5	50.70	55.54	59.58	58.89	65.94	64.51	65.88	62.67	63.20	64.06	62.54
E6	25.69	28.91	28.28	16.30	17.46	19.62	22.02	28.98	28.16	22.85	25.06

Table 5.11 Summary of mean pressures during single leg stance on prosthetic side – static test (Test –II)

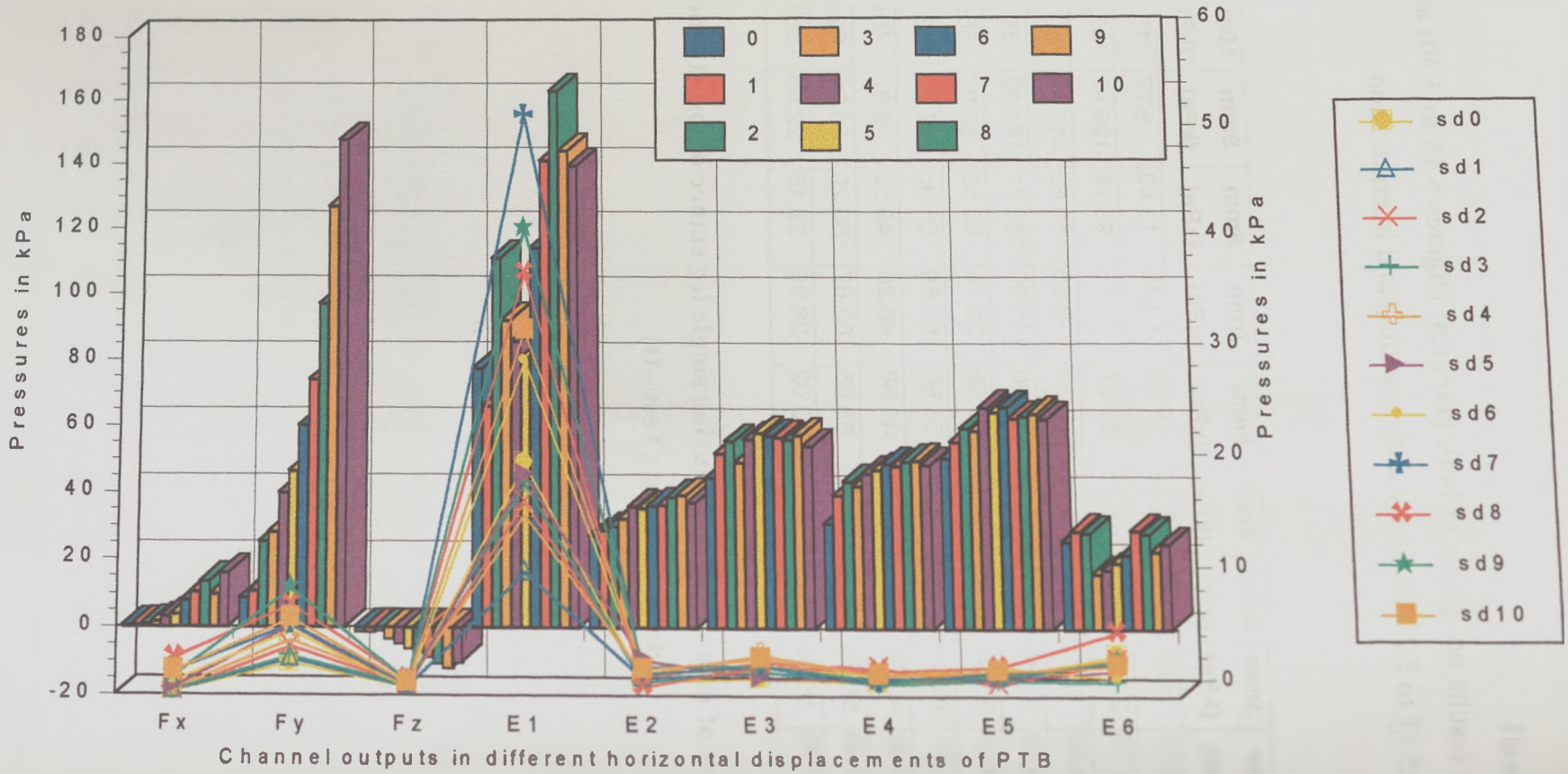

Figure 5.19 Subject:1 Summary of mean Pressures and Standard Deviations in Single-leg Stance on prosthetic side – Static Test (Test-II)

Legend – Refer section 5.6.2

	0mm (kPa)	1mm (kPa)	2mm (kPa)	3mm (kPa)	4mm (kPa)	5mm (kPa)	6mm (kPa)	7mm (kPa)	8mm (kPa)	9mm (kPa)	10mm (kPa)
Fx	0.35	0.34	0.25	0.43	0.53	0.67	1.14	2.11	3.20	1.67	2.03
Fy	2.78	3.18	4.24	3.42	4.84	6.10	5.68	6.18	7.93	9.43	6.74
Fz	0.73	0.74	0.89	0.93	1.05	0.68	0.63	0.93	1.36	1.22	1.06
E1	20.50	10.82	17.06	18.74	15.91	19.43	29.80	52.54	37.87	41.95	32.58
E2	1.22	1.51	1.65	1.16	1.92	3.14	1.88	1.96	0.76	2.58	2.31
E3	1.52	2.09	2.92	2.17	3.59	1.55	2.49	2.61	2.63	2.68	3.28
E4	1.21	1.63	2.47	1.06	1.91	1.43	1.92	1.23	2.24	1.40	1.88
E5	1.74	1.68	1.05	1.40	1.97	1.58	2.60	2.14	2.58	1.76	2.22
E6	3.59	2.94	3.19	1.26	3.23	2.29	1.58	2.80	5.69	3.17	2.69

Table 5.12 Summary of Standard deviations during single leg stance on prosthetic side – static test (Test-II)

Figure 5.20 Subject:1 Summary of Peak Pressures and their differences with their mean in Single-leg Stance on prosthetic side – Static Test (Test-II)

Legend – Refer section 5.6.2

	0mm (kPa)	1mm (kPa)	2mm (kPa)	3mm (kPa)	4mm (kPa)	5mm (kPa)	6mm (kPa)	7mm (kPa)	8mm (kPa)	9mm (kPa)	10mm (kPa)
Fx	1.87	1.87	1.92	2.65	4.58	5.59	10.71	14.38	19.90	13.74	18.82
Fy	14.78	19.75	37.53	38.81	52.04	68.07	78.82	89.47	119.99	149.94	171.46
Fz	-3.26	-3.20	-6.49	-6.45	-14.60	-7.42	-8.86	-10.35	-13.31	-14.95	-12.79
E1	119.63	91.12	148.56	129.68	121.94	137.56	216.46	227.45	220.53	214.55	195.00
E2	31.48	34.46	34.46	35.12	40.92	42.08	40.42	40.09	40.92	43.24	40.92
E3	49.60	57.89	61.03	53.03	62.75	63.46	61.75	62.18	61.03	61.75	59.32
E4	33.87	44.57	48.82	45.25	49.51	51.84	52.93	50.88	53.62	53.21	51.84
E5	53.94	59.47	62.33	61.37	68.81	67.09	68.81	66.14	66.52	67.09	65.18
E6	37.38	41.83	34.47	20.99	31.87	26.20	25.13	34.78	35.85	32.48	30.64

Table 5.13 Summary of Peak Pressures during single leg stance on prosthetic side – static test (Test-II)

	0mm (kPa)	1mm (kPa)	2mm (kPa)	3mm (kPa)	4mm (kPa)	5mm (kPa)	6mm (kPa)	7mm (kPa)	8mm (kPa)	9mm (kPa)	10mm (kPa)
Fx	1.41	1.38	1.14	0.99	1.44	1.83	2.73	3.90	6.47	3.97	3.00
Fy	6.13	9.05	12.37	10.91	12.28	21.85	18.94	15.72	23.20	23.06	23.81
Fz	2.01	1.96	5.61	3.22	9.97	1.30	1.56	1.71	2.71	3.11	2.64
E1	42.50	25.31	37.68	37.83	36.44	56.93	102.46	86.46	57.82	70.43	55.63
E2	4.68	5.87	4.81	3.10	5.21	6.96	4.43	3.93	2.39	4.17	3.98
E3	5.19	6.23	5.72	3.89	6.78	5.61	4.85	5.59	5.08	4.46	5.35
E4	3.10	5.33	5.42	3.19	3.60	4.86	4.25	2.61	4.10	3.34	3.28
E5	3.24	3.93	2.74	2.49	2.86	2.58	2.92	3.46	3.32	3.03	2.64
E6	11.69	12.91	6.19	4.69	14.41	6.57	3.11	5.79	7.69	9.63	5.58

Table 5.14 Difference between Peak pressure and mean pressures during single-leg stance on prosthetic side – static test (Test-II)

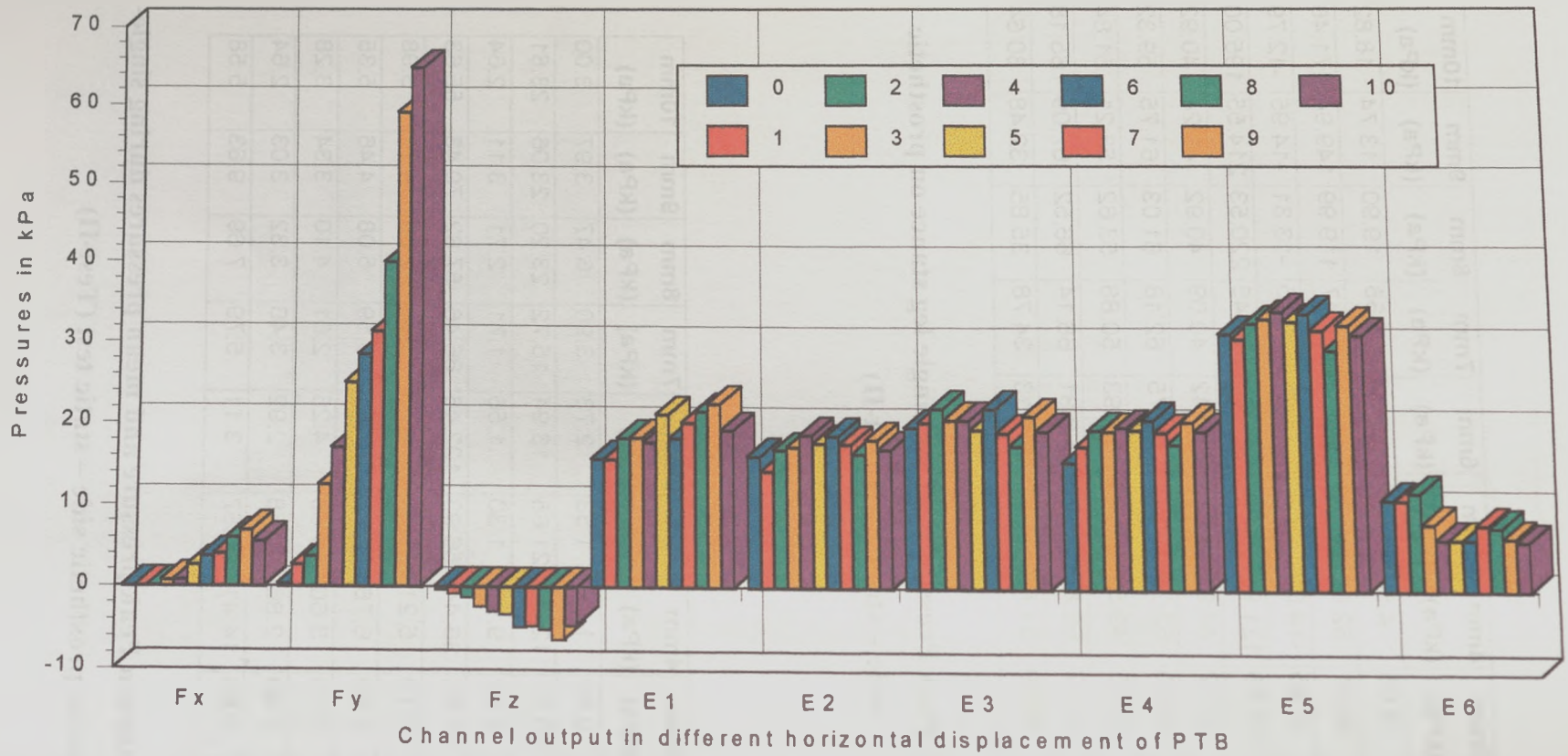

Figure 5.21 Subject:1 Summary of mean pressures during double support – Static test (Test-III)
Legend – Refer section 5.6.2

	0mm (kPa)	1mm (kPa)	2mm (kPa)	3mm (kPa)	4mm (kPa)	5mm (kPa)	6mm (kPa)	7mm (kPa)	8mm (kPa)	9mm (kPa)	10mm (kPa)
Fx	0.01	-0.02	0.02	0.70	0.75	2.55	3.64	4.01	5.96	6.85	5.49
Fy	0.32	2.63	3.68	12.39	17.00	25.07	28.46	31.35	39.99	59.06	64.78
Fz	-0.37	-0.79	-1.26	-2.29	-2.91	-3.25	-4.77	-4.63	-5.02	-6.24	-4.59
E1	15.70	15.64	18.26	18.35	17.79	21.26	18.29	20.24	21.69	22.62	19.33
E2	16.10	14.28	16.88	17.30	18.78	17.82	18.71	17.70	16.53	18.18	17.07
E3	19.78	20.43	22.24	20.78	20.77	19.58	22.19	19.21	17.59	21.28	19.42
E4	15.55	17.57	19.57	19.52	19.94	19.64	20.87	19.35	17.94	20.66	19.49
E5	31.46	30.87	32.72	33.37	34.25	33.02	34.01	31.95	29.45	32.60	31.34
E6	11.16	11.09	12.00	8.19	6.32	6.29	6.28	8.08	7.83	6.45	6.07

Table 5.15 Summary of mean pressures during double support – static test (Test-III)

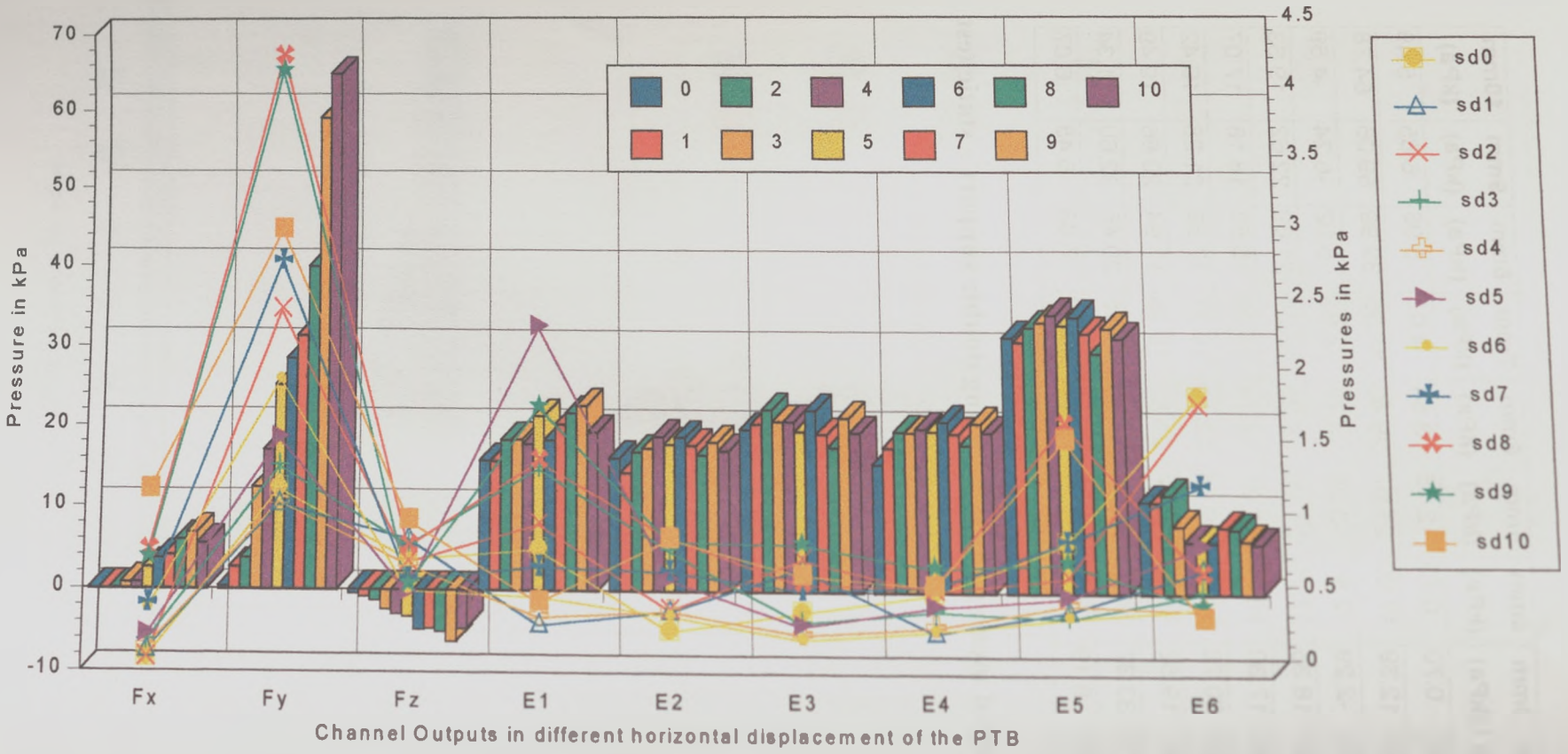

Figure 5.22 Subject:1 Summary of mean Pressures and Standard Deviations during double support – Static test (Test-III)

Legend – Refer section 5.6.2

	0mm (kPa)	1mm (kPa)	2mm (kPa)	3mm (kPa)	4mm (kPa)	5mm (kPa)	6mm (kPa)	7mm (kPa)	8mm (kPa)	9mm (kPa)	10mm (kPa)
Fx	0.08	0.14	0.08	0.20	0.15	0.24	0.42	0.45	0.81	0.76	1.23
Fy	1.25	1.14	2.50	1.40	1.15	1.60	2.01	2.84	4.33	4.22	3.07
Fz	0.76	0.90	0.74	0.86	0.73	0.54	0.55	0.63	0.85	0.59	1.03
E1	0.83	0.32	1.01	1.39	0.37	2.39	0.51	0.72	1.44	1.82	0.48
E2	0.28	0.42	0.43	0.83	0.42	0.63	0.39	0.69	0.91	0.89	0.91
E3	0.41	0.72	0.77	0.35	0.26	0.32	0.23	0.56	0.61	0.88	0.67
E4	0.54	0.28	0.56	0.43	0.32	0.46	0.29	0.60	0.60	0.72	0.60
E5	0.89	0.43	0.66	0.39	0.48	0.52	0.39	0.90	1.72	0.76	1.61
E6	1.91	0.72	1.84	0.56	0.44	0.88	0.46	1.30	0.69	0.47	0.39

Table 5.16 Summary of standard deviation of pressures during double support static test (Test-III)

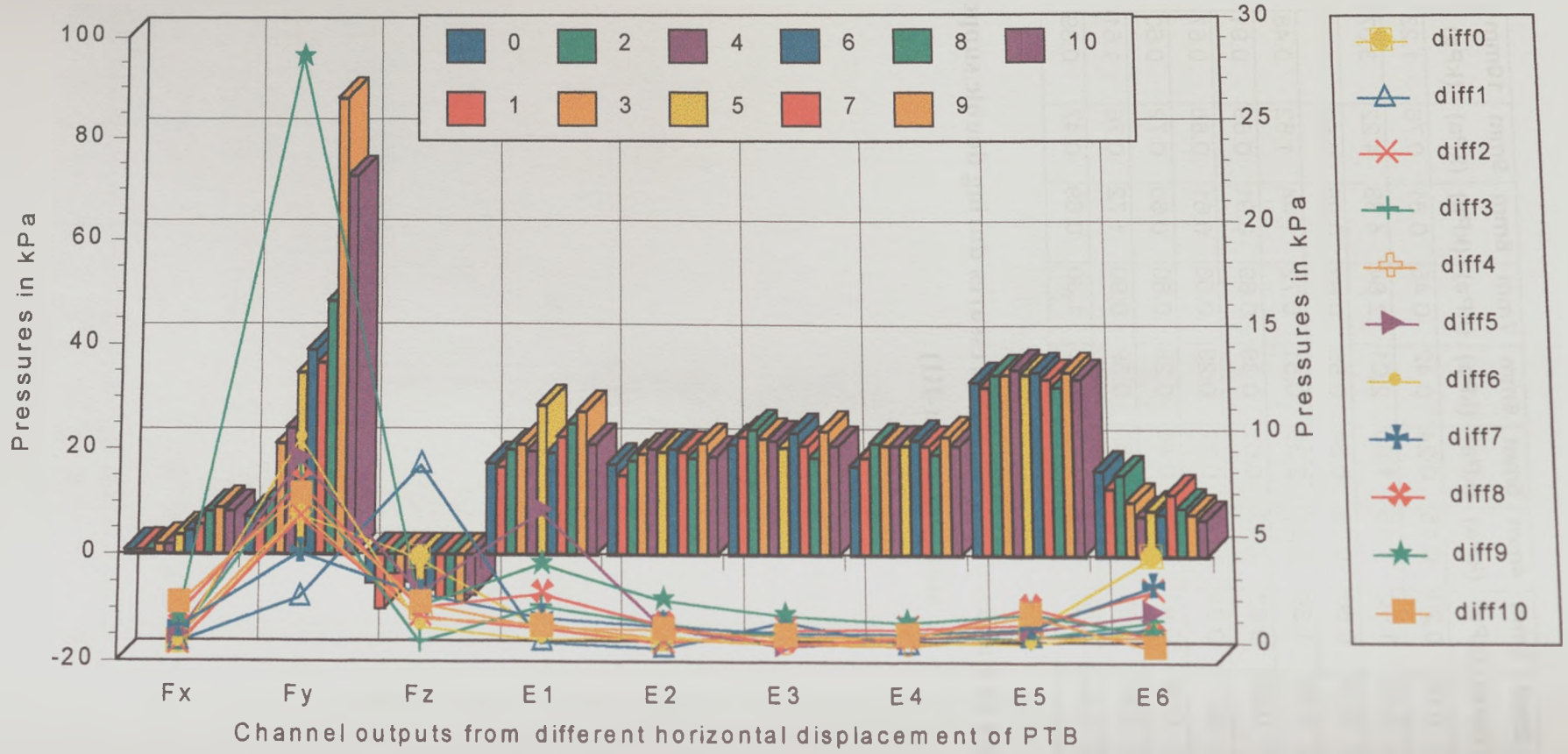

Figure 5.23 Subject:1 Summary of Peak Pressures and their differences with their mean during double support – Static test (Test-III)

Legend – Refer section 5.6.2

	0mm (kPa)	1mm (kPa)	2mm (kPa)	3mm (kPa)	4mm (kPa)	5mm (kPa)	6mm (kPa)	7mm (kPa)	8mm (kPa)	9mm (kPa)	10mm (kPa)
Fx	0.80	0.86	0.78	1.87	1.89	3.74	4.47	5.58	8.13	8.90	8.14
Fy	7.15	5.60	10.37	20.99	23.98	34.53	38.92	36.41	48.36	88.02	72.57
Fz	-5.12	-10.01	-3.34	-3.19	-4.90	-6.46	-6.38	-7.76	-7.54	-8.83	-7.28
E1	17.25	16.57	19.83	20.91	19.55	28.25	19.28	22.27	24.85	27.16	20.91
E2	17.06	14.91	17.73	19.05	19.88	19.38	19.88	19.38	18.22	21.04	18.56
E3	20.87	22.30	23.73	22.01	21.58	20.30	23.01	20.58	18.44	23.44	20.58
E4	16.73	18.38	21.12	20.71	20.71	20.71	21.80	20.71	19.06	22.49	20.71
E5	32.97	32.02	34.50	34.50	35.45	34.50	34.88	33.55	32.02	34.88	33.55
E6	16.09	12.72	15.32	10.11	7.51	8.58	7.81	11.64	9.04	7.81	6.74

Table 5.17 Summary of peak pressures during double support- static test (Test-III)

	0mm (kPa)	1mm (kPa)	2mm (kPa)	3mm (kPa)	4mm (kPa)	5mm (kPa)	6mm (kPa)	7mm (kPa)	8mm (kPa)	9mm (kPa)	10mm (kPa)
Fx	0.79	0.88	0.75	1.17	1.14	1.19	0.83	1.57	2.18	2.05	2.65
Fy	6.83	2.97	6.69	8.60	6.98	9.46	10.46	5.06	8.37	28.96	7.79
Fz	4.75	9.22	2.09	0.90	1.98	3.21	1.62	3.14	2.52	2.59	2.69
E1	1.55	0.92	1.56	2.56	1.77	6.98	1.00	2.03	3.16	4.54	1.59
E2	0.97	0.63	0.84	1.76	1.10	1.57	1.17	1.68	1.69	2.86	1.48
E3	1.09	1.87	1.49	1.23	0.82	0.71	0.82	1.37	0.85	2.17	1.17
E4	1.18	0.81	1.55	1.19	0.77	1.07	0.94	1.36	1.12	1.83	1.22
E5	1.52	1.15	1.77	1.13	1.20	1.48	0.87	1.59	2.57	2.28	2.20
E6	4.93	1.62	3.32	1.92	1.19	2.29	1.53	3.56	1.21	1.36	0.67

Table 5.18 Summary of the difference between mean and peak pressures during double support -static test (Test-III)

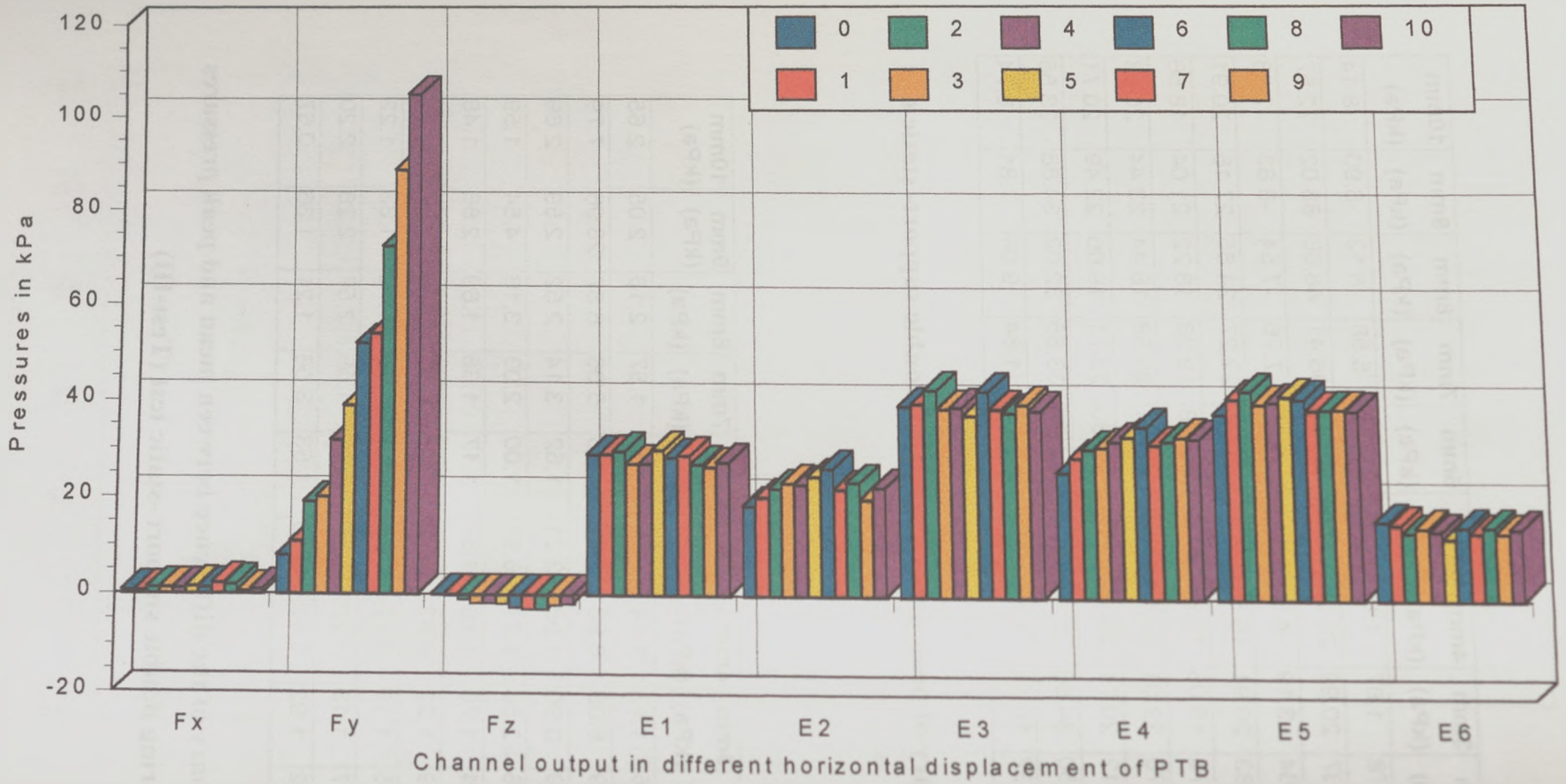

Figure 5.24 Subject:1 Summary of mean pressures during dynamic Gait – Stance phase (Test-IV)
Legend – Refer section 5.6.2

	0mm (kPa)	1mm (kPa)	2mm (kPa)	3mm (kPa)	4mm (kPa)	5mm (kPa)	6mm (kPa)	7mm (kPa)	8mm (kPa)	9mm (kPa)	10mm (kPa)
Fx	0.64	0.62	1.17	1.15	1.09	1.47	1.18	2.14	1.94	0.48	1.03
Fy	7.86	10.84	18.92	20.03	31.66	38.84	51.78	53.90	72.37	88.76	104.93
Fz	0.00	-0.11	-0.84	-1.58	-1.54	-1.65	-2.32	-2.72	-2.76	-1.93	-1.69
E1	114.79	115.25	117.69	107.07	107.29	118.81	112.69	114.14	107.11	105.28	109.14
E2	73.14	80.29	87.50	91.93	91.16	97.44	104.16	87.32	92.62	79.13	88.70
E3	156.46	158.31	170.10	154.34	155.64	149.12	169.15	154.20	151.38	158.25	153.16
E4	102.14	114.23	121.38	123.26	128.11	132.03	140.38	125.51	128.44	131.96	130.73
E5	150.99	163.96	170.11	159.43	161.06	165.70	163.88	154.91	155.15	155.51	154.43
E6	63.37	60.96	54.63	58.55	55.59	49.87	58.99	54.89	59.22	54.69	58.22

Table 5.19 Summary of mean pressures during dynamic gait- Stance phase (Test-IV)

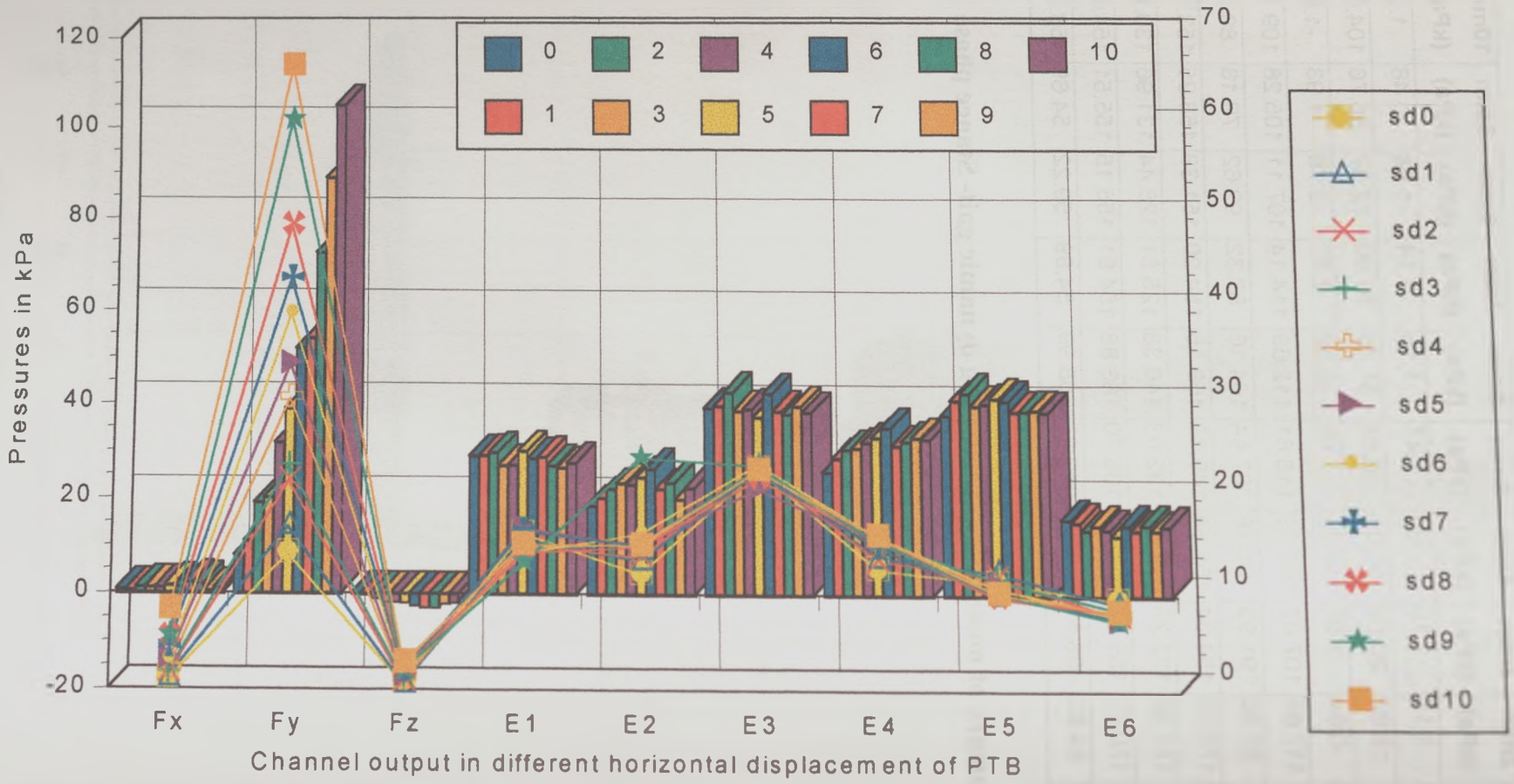

Figure 5.25 Subject:1 Summary of Mean Pressures and Standard Deviations during dynamic gait – Stance phase (Test-IV)

Legend – Refer section 5.6.2

	0mm (kPa)	1mm (kPa)	2mm (kPa)	3mm (kPa)	4mm (kPa)	5mm (kPa)	6mm (kPa)	7mm (kPa)	8mm (kPa)	9mm (kPa)	10mm (kPa)
Fx	0.96	1.14	1.58	1.60	1.97	2.87	2.89	4.27	5.23	5.42	8.20
Fy	-14.07	-16.98	-21.69	-23.34	-30.52	-34.17	-39.54	-43.33	-49.09	-60.74	-66.75
Fz	0.64	0.60	0.82	1.05	1.10	1.29	1.64	1.92	2.10	1.94	2.70
E1	64.54	61.96	60.16	57.90	58.52	66.81	56.09	65.74	56.43	52.43	60.02
E2	48.06	53.55	54.84	60.71	60.78	59.64	64.68	59.50	59.19	96.27	59.68
E3	92.19	91.64	93.10	92.11	90.79	83.67	94.12	91.04	87.95	93.63	91.43
E4	50.33	55.25	53.96	62.08	61.21	61.43	64.19	59.28	62.26	61.70	64.12
E5	45.02	49.30	47.37	46.22	42.92	43.44	42.69	40.28	38.89	40.67	40.59
E6	37.78	36.31	31.20	33.88	31.87	29.18	31.24	30.15	32.81	28.97	32.90

Table 5.20 Summary of standard deviation of pressures during dynamic gait - Stance phase(Test-IV)

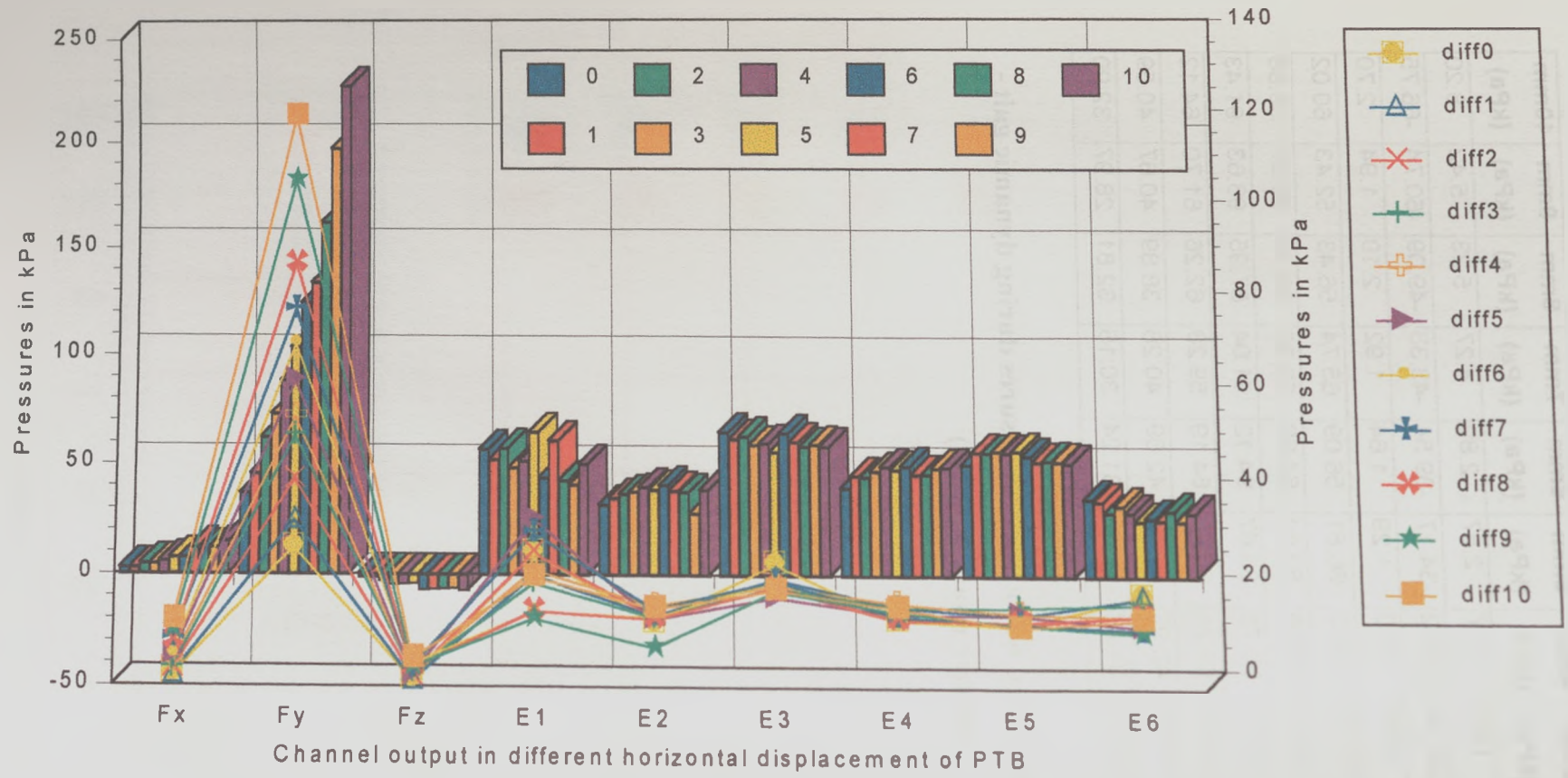

Figure 5.26 Subject:1 Summary of Peak Pressures and their differences with their mean in dynamic gait – Stance phase (Test-IV)

Legend – Refer section 5.6.2

	0mm (kPa)	1mm (kPa)	2mm (kPa)	3mm (kPa)	4mm (kPa)	5mm (kPa)	6mm (kPa)	7mm (kPa)	8mm (kPa)	9mm (kPa)	10mm (kPa)
Fx	2.58	2.59	4.44	4.46	5.56	7.38	7.43	11.80	10.72	11.83	14.41
Fy	36.67	45.36	62.12	72.56	88.15	103.15	124.06	133.63	162.13	196.96	227.42
Fz	-1.25	-1.16	-2.65	-4.28	-4.07	-3.85	-6.75	-6.49	-6.22	-5.81	-7.13
E1	225.37	207.00	228.07	192.40	203.21	257.26	174.03	241.58	168.62	161.06	199.43
E2	125.28	138.47	145.06	148.36	157.59	152.98	160.89	151.00	148.36	110.78	152.98
E3	258.28	247.47	251.45	236.09	238.94	222.44	257.14	241.78	233.25	237.23	233.25
E4	157.19	180.11	178.47	189.39	197.03	192.12	198.67	183.93	183.93	194.30	195.94
E5	201.78	223.78	222.26	226.06	222.26	226.06	216.95	207.09	209.37	207.09	204.06
E6	139.64	135.37	114.64	128.05	114.64	100.00	105.49	102.44	118.91	100.00	114.64

Table 5.21 Summary of peak pressures during dynamic gait – Stance phase (Test-IV)

	0mm (kPa)	1mm (kPa)	2mm (kPa)	3mm (kPa)	4mm (kPa)	5mm (kPa)	6mm (kPa)	7mm (kPa)	8mm (kPa)	9mm (kPa)	10mm (kPa)
Fx	1.95	1.96	3.27	3.31	4.47	5.92	6.25	9.67	8.78	11.35	13.38
Fy	28.81	34.52	43.20	52.53	56.48	64.32	72.28	79.73	89.75	108.21	122.49
Fz	1.25	1.05	1.81	2.70	2.53	2.20	4.43	3.77	3.47	3.88	5.44
E1	110.58	91.75	110.39	85.33	95.92	138.45	61.34	127.45	61.51	55.77	90.28
E2	52.14	58.18	57.56	56.43	66.43	55.54	56.73	63.68	55.74	31.65	64.27
E3	101.82	89.16	81.36	81.75	83.29	73.32	87.99	87.58	81.87	78.98	80.09
E4	55.05	65.88	57.09	66.13	68.92	60.09	58.29	58.42	55.49	62.34	65.21
E5	50.79	59.83	52.16	66.63	61.20	60.36	53.07	52.18	54.22	51.58	49.63
E6	76.26	74.41	60.01	69.50	59.04	50.13	46.50	47.56	59.68	45.32	56.41

Table 5.22 Summary of difference between mean and peak pressures during dynamic gait (Test-IV)

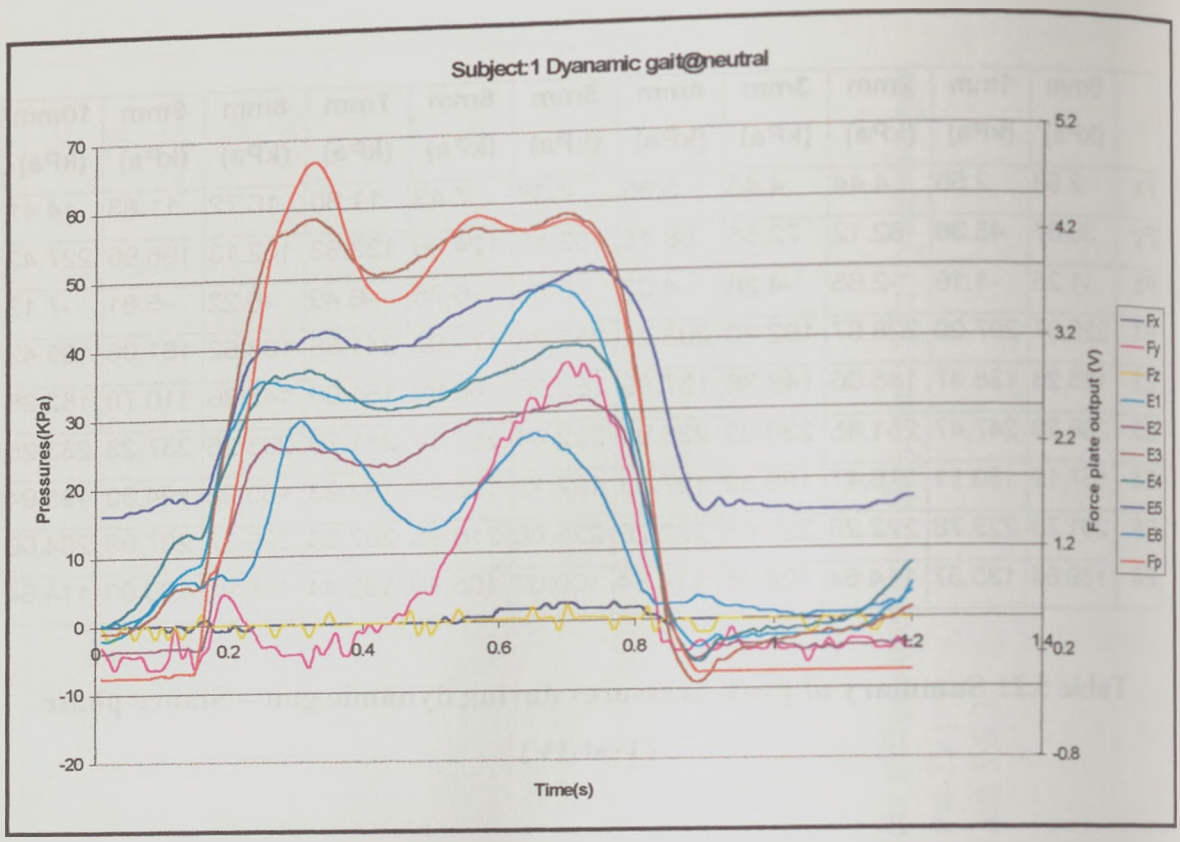

Figure 5.27 Pressure variation around the socket during dynamic gait with the patellar tendon bar flush with the socket wall

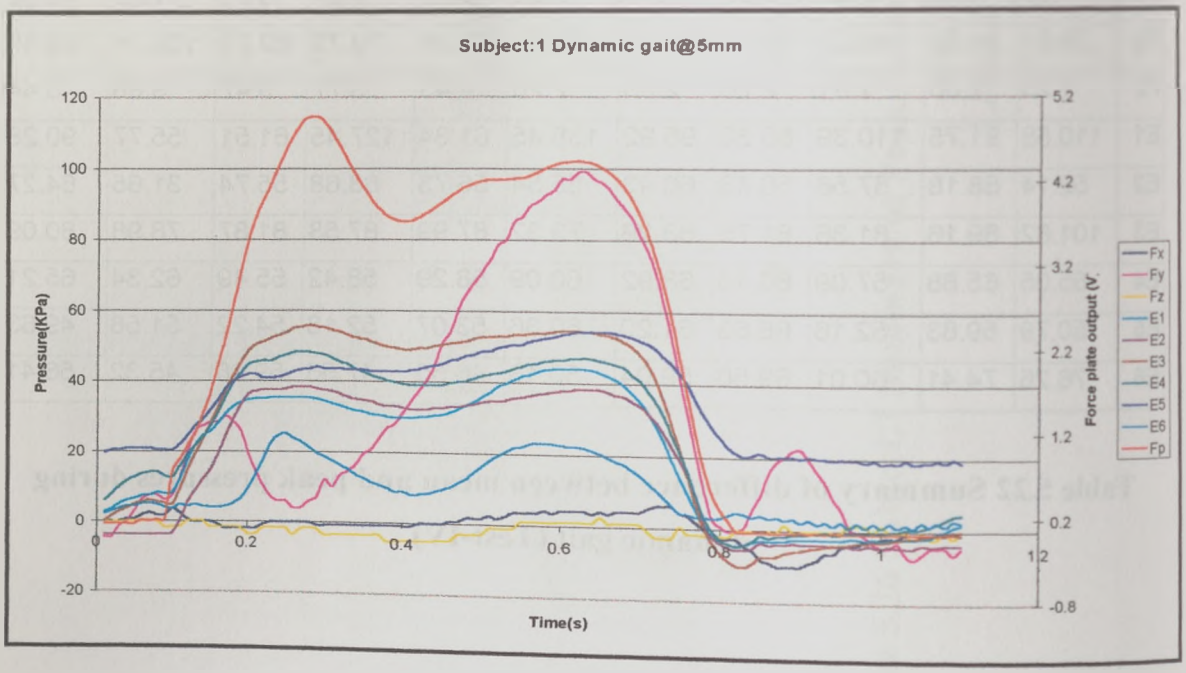

Figure 5.28 Figure 5.27 Pressure variation around the socket during dynamic gait with the patellar tendon bar displaced 5mm into the socket

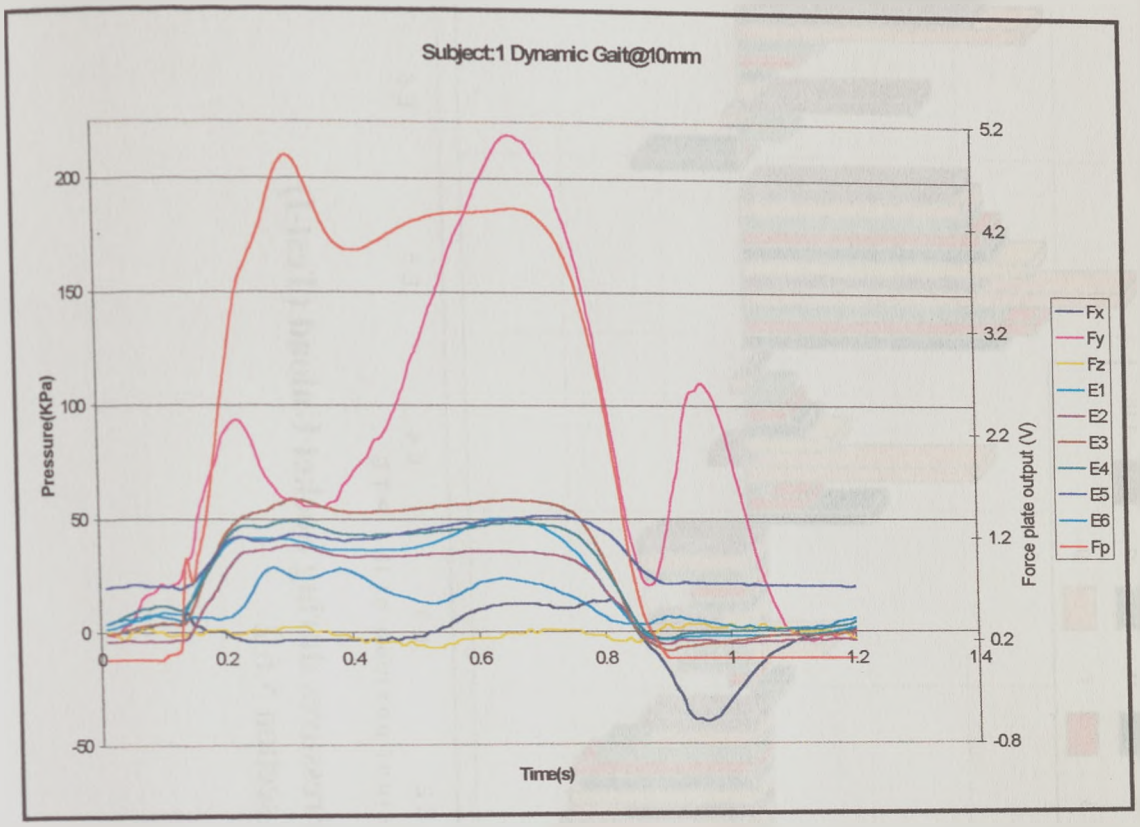

Figure 5.29 Pressure variation around the socket during dynamic gait with patellar tendon bar displaced 10mm into the socket.

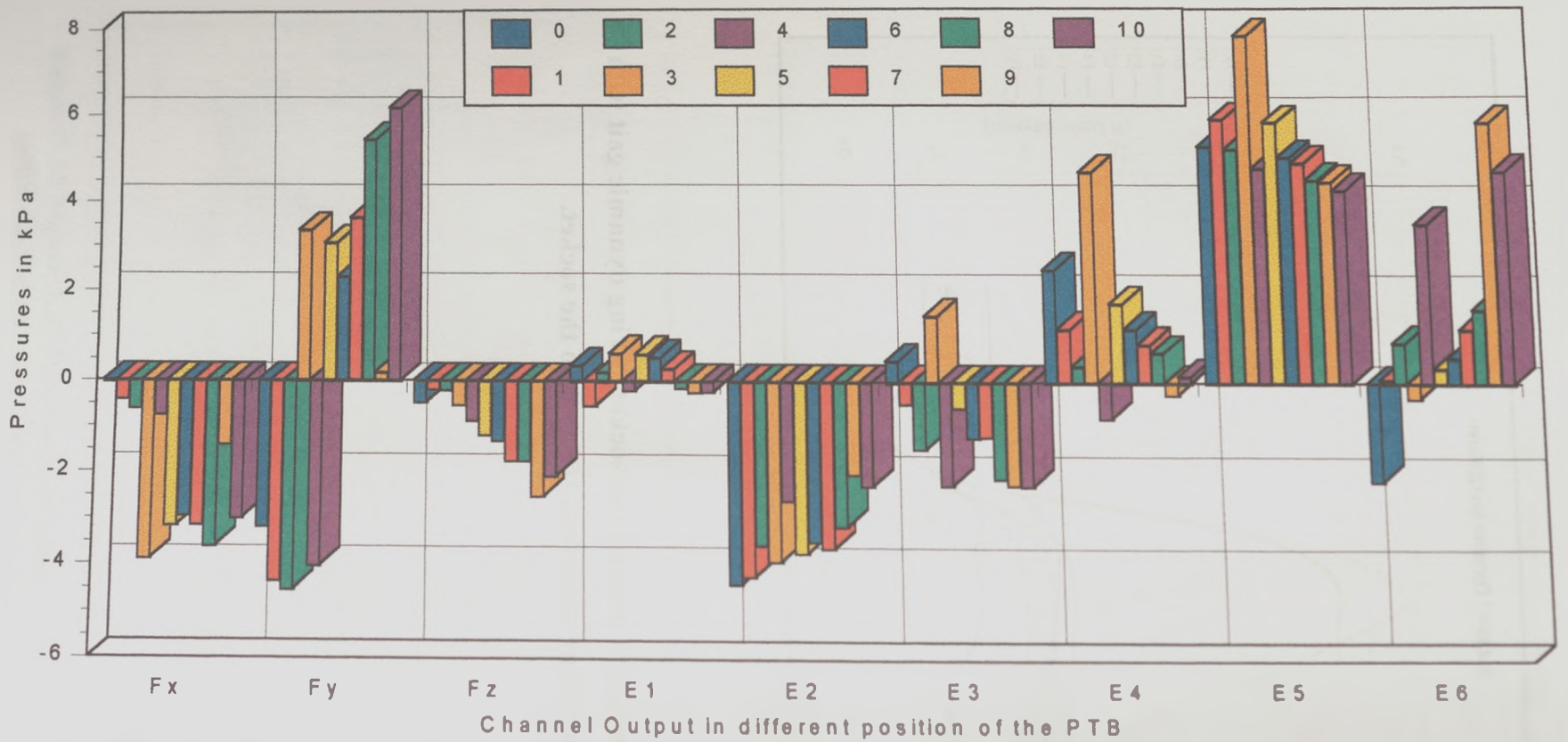

Figure 5.30 Subject:1 Summary of mean Pressures during Socket Unload (Test-I)
Legend – Refer section 5.6.2

	0mm (kPa)	1mm (kPa)	2mm (kPa)	3mm (kPa)	4mm (kPa)	5mm (kPa)	6mm (kPa)	7mm (kPa)	8mm (kPa)	9mm (kPa)	10mm (kPa)
Fx	0.00	-0.39	-0.60	-3.88	-0.74	-3.16	-2.95	-3.15	-3.61	-1.39	-2.99
Fy	-3.19	-4.34	-4.52	3.35	-4.02	3.06	2.31	3.64	5.42	0.18	6.15
Fz	-0.47	-0.19	-0.20	-0.53	-0.87	-1.18	-1.30	-1.75	-1.75	-2.51	-2.08
E1	0.35	-0.54	0.20	0.62	-0.20	0.60	0.53	0.28	-0.13	-0.23	-0.21
E2	-4.39	-4.23	-3.56	-3.92	-2.60	-3.72	-3.47	-3.63	-3.15	-2.00	-2.27
E3	0.47	-0.47	-1.46	1.47	-2.24	-0.55	-1.21	-1.18	-2.09	-2.23	-2.26
E4	2.49	1.19	0.36	4.68	-0.77	1.73	1.18	0.85	0.66	-0.26	0.15
E5	5.26	5.88	5.20	7.79	4.77	5.81	5.02	4.90	4.52	4.46	4.27
E6	-2.12	0.08	0.90	-0.31	3.53	0.33	0.57	1.21	1.63	5.79	4.69

Table 5.23 Summary of mean pressures during socket unload(Test-I)

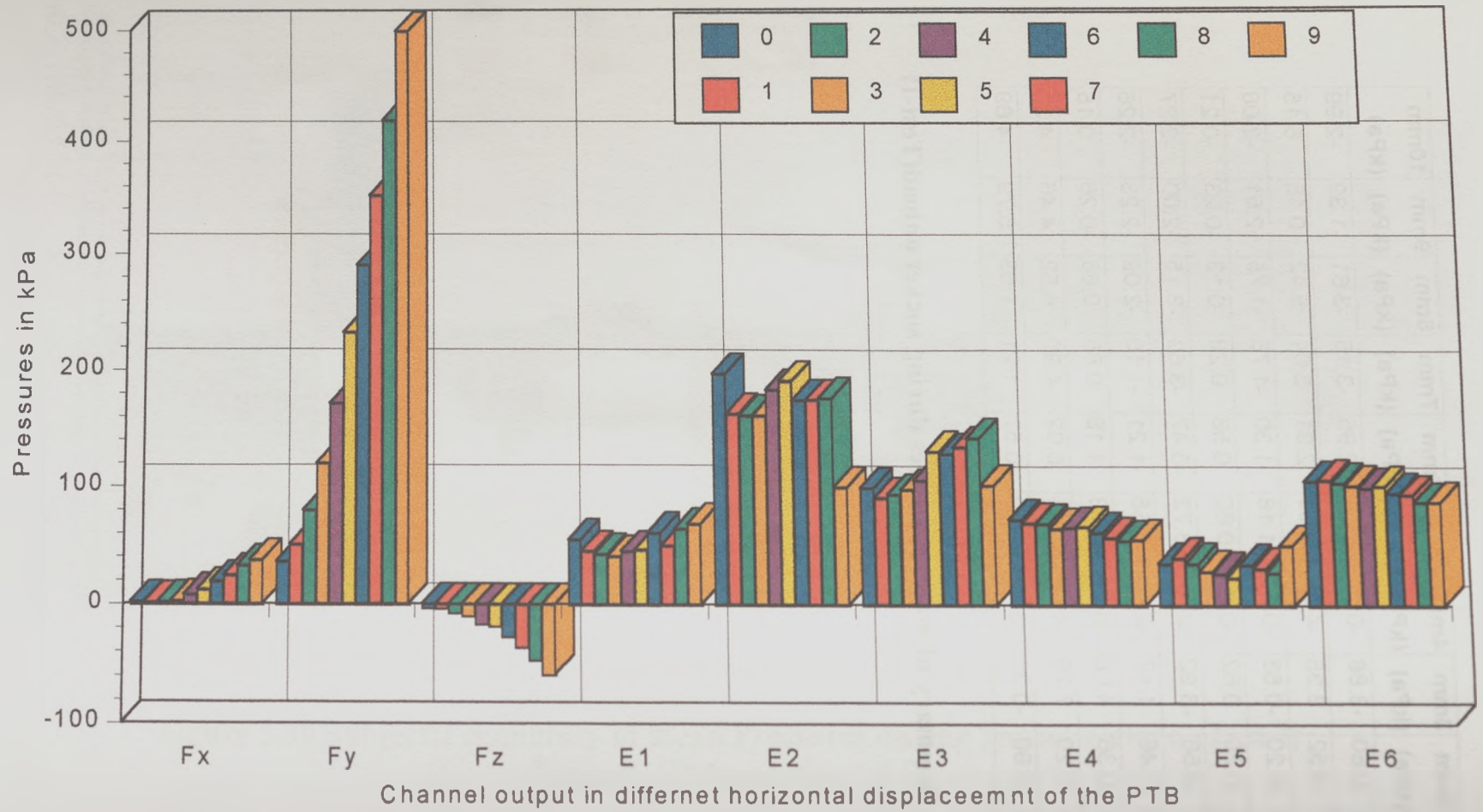

Figure 5.31 Subject:2 Summary of Mean Pressures during Single-leg Stance on prosthetic side – static test (Test-II)

Legend – Refer section 5.6.2

5.6.4 Subject: 2

This section gives the results of subject: 2 (figures 5.31 to 5.43 and tables 5.24 to 5.36). The tests performed on subject: 2 was restricted to a maximum 9mm of displacement of the patellar tendon bar, this was because of the discomfort experienced by the subject due to the advancement of the patellar tendon bar. The variations of pressure during dynamic gait have not been fully presented in this section. The pressure variations during flush position (0mm), 5mm and 10mm are presented in figures 5.40, 5.41 and 5.42 respectively.

	0mm (kPa)	1mm (kPa)	2mm (kPa)	3mm (kPa)	4mm (kPa)	5mm (kPa)	6mm (kPa)	7mm (kPa)	8mm (kPa)	9mm (kPa)
Fx	1.53	0.64	1.49	2.52	7.73	11.86	18.36	24.03	31.75	36.60
Fy	35.45	49.67	79.21	118.97	170.61	231.29	290.07	351.81	419.14	499.18
Fz	-3.03	-3.42	-7.21	-9.70	-16.62	-18.31	-27.32	-36.19	-46.56	-59.32
E1	53.93	44.19	41.57	40.22	44.12	45.33	60.18	49.02	63.40	67.54
E2	196.30	162.18	160.68	160.69	182.67	190.24	173.53	173.92	175.94	99.13
E3	98.43	90.07	93.36	97.33	105.34	130.08	127.86	133.72	141.27	101.14
E4	71.79	69.25	68.32	64.22	64.83	65.94	60.64	56.28	53.66	54.89
E5	34.86	39.82	34.94	28.65	26.90	23.17	33.81	31.36	27.43	50.02
E6	105.05	106.23	103.90	101.62	99.62	101.08	95.29	93.50	87.21	87.38

Table 5.24 Summary of mean pressures during single-leg stance on prosthetic side – static test (Test-I)

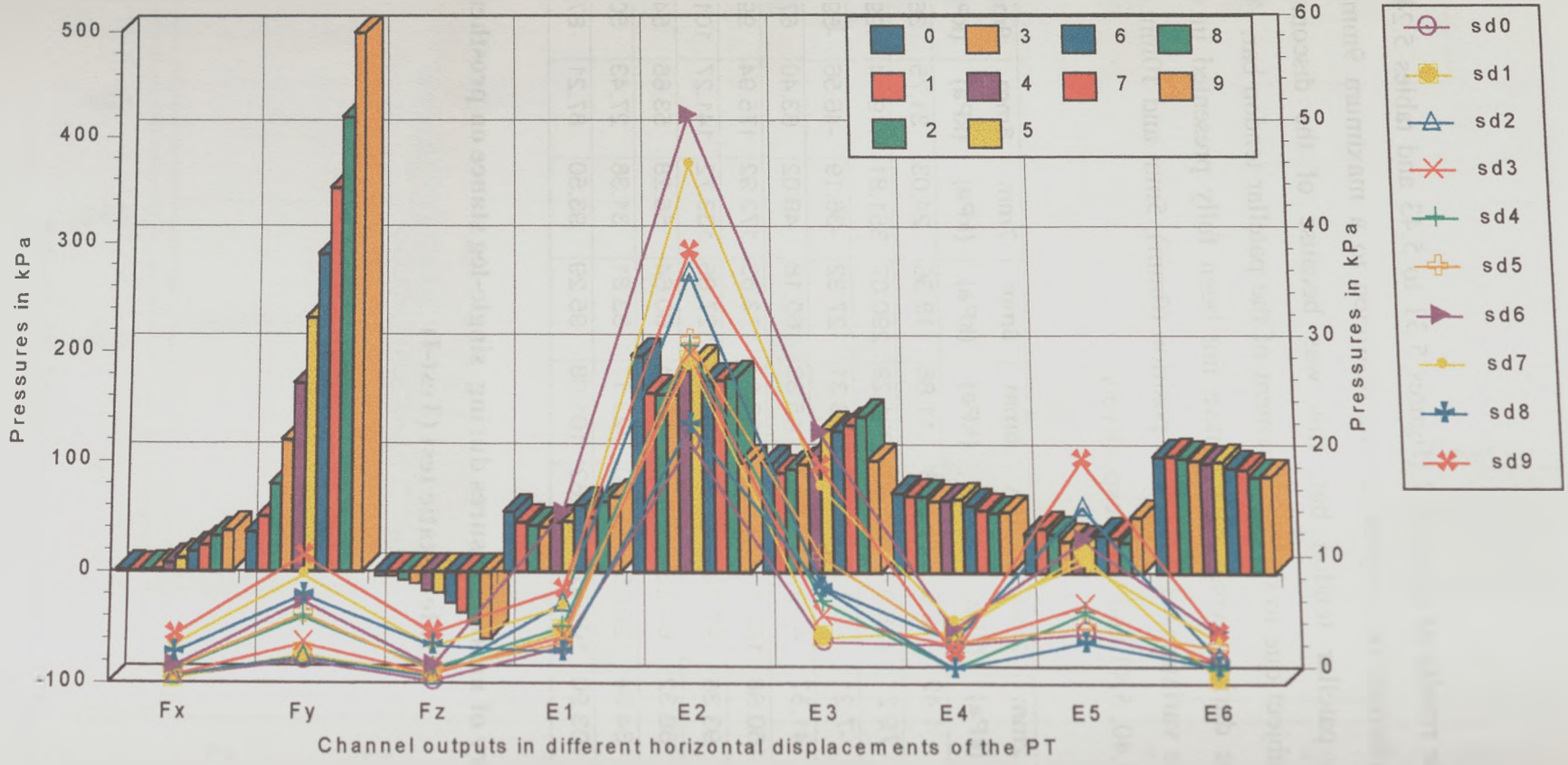

Figure 5.32 Subject:2 Summary of Mean and Standard deviation of Pressures during Single-leg Stance on prosthetic side – static test (Test-II)

Legend – Refer section 5.6.2

	0mm (kPa)	1mm (kPa)	2mm (kPa)	3mm (kPa)	4mm (kPa)	5mm (kPa)	6mm (kPa)	7mm (kPa)	8mm (kPa)	9mm (kPa)
Fx	0.51	0.37	0.61	0.62	1.22	1.24	1.45	3.38	2.68	4.23
Fy	2.02	2.49	2.31	3.55	5.88	6.19	7.29	9.64	7.86	11.36
Fz	0.18	0.79	0.56	0.85	1.30	1.11	1.50	3.24	3.35	4.48
E1	3.27	4.57	7.14	4.17	4.98	3.60	15.17	6.85	2.77	8.33
E2	21.60	29.05	37.12	29.66	30.40	30.93	51.91	47.28	23.28	39.20
E3	3.79	4.18	8.73	6.04	7.33	11.35	22.56	17.69	8.60	19.52
E4	3.52	4.75	3.94	3.46	1.43	3.76	4.94	5.59	1.41	2.73
E5	4.52	11.71	15.87	7.08	6.40	5.07	12.86	10.89	3.71	20.13
E6	1.87	0.48	2.29	1.97	1.21	3.28	4.60	3.91	1.55	4.54

Table 5.25 Summary of standard deviation of pressures during single-leg stance on prosthetic side – static test (Test-II)

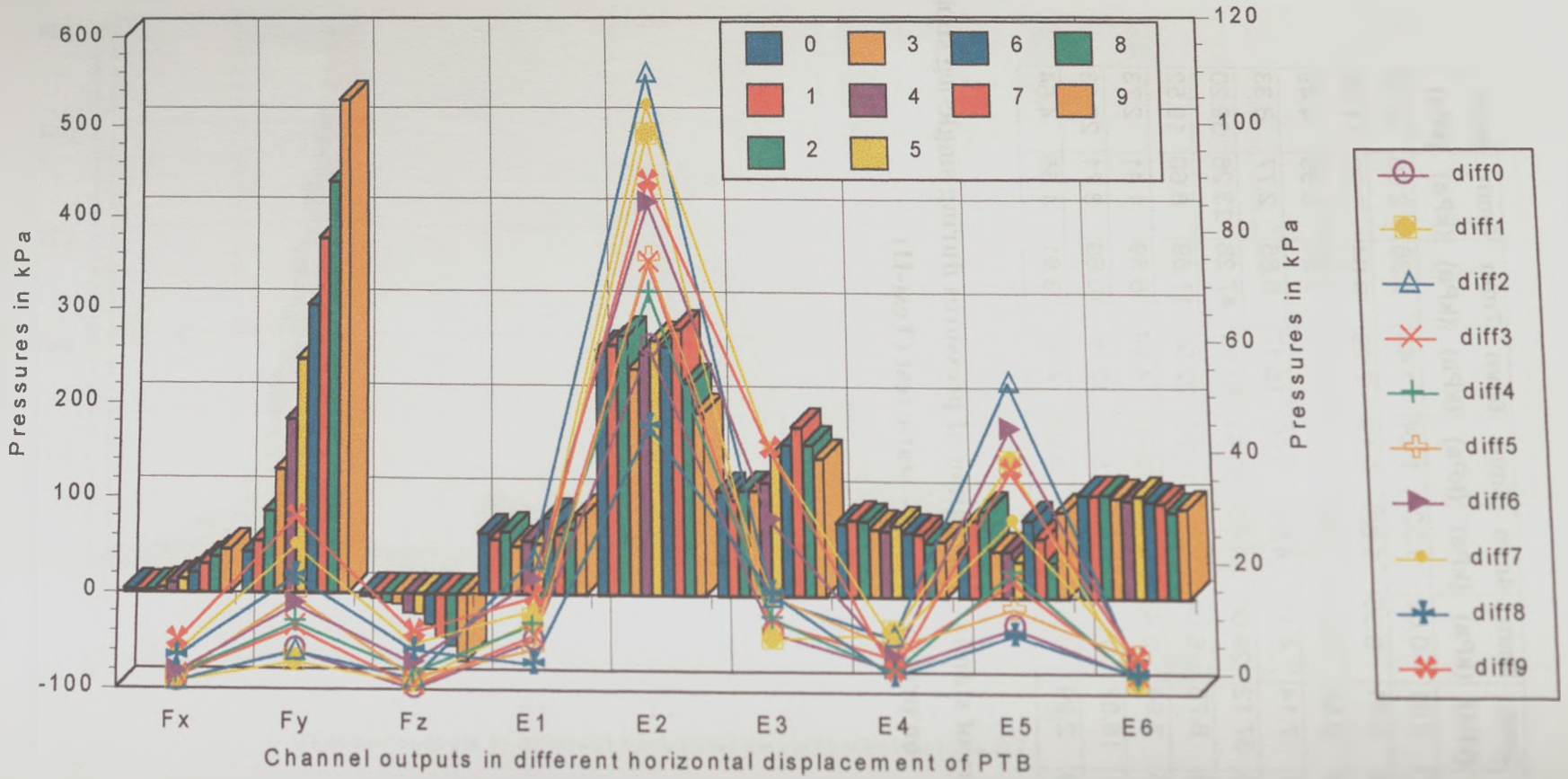

Figure 5.33 Subject:2 Summary of Peak Pressures and their differences with their mean during Single-leg Stance on prosthetic side – static test (Test-II)

Legend – Refer section 5.6.2

	0mm (kPa)	1mm (kPa)	2mm (kPa)	3mm (kPa)	4mm (kPa)	5mm (kPa)	6mm (kPa)	7mm (kPa)	8mm (kPa)	9mm (kPa)
Fx	2.61	1.90	2.70	4.56	10.17	13.85	20.95	30.24	37.31	44.84
Fy	42.14	54.41	85.80	129.87	182.31	247.61	304.96	377.26	439.09	529.68
Fz	-2.93	-4.57	-9.08	-10.28	-19.61	-20.51	-31.83	-44.29	-53.47	-69.29
E1	62.60	56.35	64.64	49.70	55.68	52.42	79.58	63.01	67.90	83.92
E2	258.12	263.25	273.36	237.91	254.47	268.22	261.76	280.65	223.33	191.35
E3	108.92	99.49	109.92	109.92	118.35	147.23	158.38	177.24	158.80	144.51
E4	75.97	79.67	78.03	70.35	68.57	74.05	66.65	65.69	56.64	58.56
E5	46.51	81.00	90.72	48.41	48.41	38.12	81.00	61.94	37.74	89.77
E6	108.17	108.17	108.47	104.80	102.19	107.40	100.96	99.43	90.55	93.46

Table 5.26 Summary of peak pressures during single-leg stance on prosthetic side – static test (Test-II)

	0mm (kPa)	1mm (kPa)	2mm (kPa)	3mm (kPa)	4mm (kPa)	5mm (kPa)	6mm (kPa)	7mm (kPa)	8mm (kPa)	9mm (kPa)
Fx	1.08	1.27	1.22	2.04	2.44	1.99	2.59	6.22	5.56	8.24
Fy	6.69	4.74	6.58	10.91	11.70	16.31	14.89	25.45	19.95	30.50
Fz	0.09	1.15	1.87	0.58	2.99	2.20	4.51	8.11	6.91	9.97
E1	8.67	12.16	23.07	9.48	11.56	7.08	19.39	13.99	4.49	16.38
E2	61.82	101.07	112.68	77.22	71.80	77.98	88.23	106.73	47.38	92.23
E3	10.48	9.41	16.56	12.59	13.01	17.14	30.52	43.52	17.53	43.37
E4	4.18	10.43	9.71	6.13	3.73	8.11	6.01	9.41	2.98	3.67
E5	11.65	41.19	55.79	19.77	21.51	14.95	47.20	30.59	10.31	39.75
E6	3.11	1.94	4.57	3.17	2.57	6.32	5.68	5.93	3.34	6.08

Table5.27 Summary of the difference between the mean and peak pressure during single-leg stance on prosthetic side – static test (Test-II)

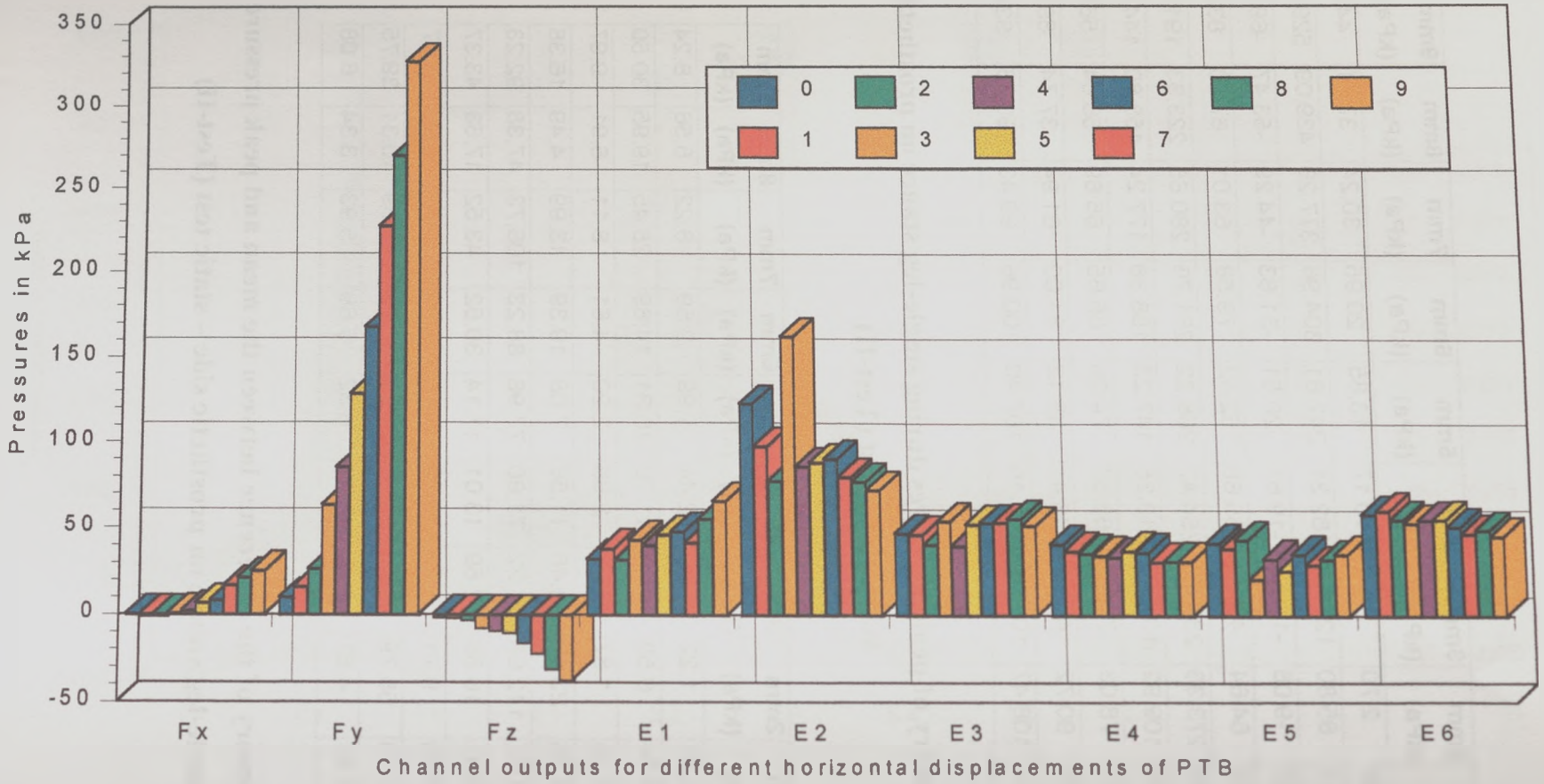

Figure 5.34 Subject:2 Summary of Mean Pressures during Double Support – Static test (Test-III)
Legend – Refer section 5.6.2

	0mm (kPa)	1mm (kPa)	2mm (kPa)	3mm (kPa)	4mm (kPa)	5mm (kPa)	6mm (kPa)	7mm (kPa)	8mm (kPa)	9mm (kPa)
Fx	0.03	-0.95	-0.64	0.48	1.84	6.31	8.19	16.72	21.22	25.09
Fy	9.76	15.87	26.34	63.32	85.07	128.18	167.49	226.98	269.93	327.30
Fz	-1.39	-1.73	-3.15	-7.63	-8.93	-10.35	-15.94	-22.13	-30.86	-37.26
E1	31.98	38.04	31.60	42.91	39.86	45.74	47.87	41.70	55.14	65.42
E2	122.16	97.40	77.44	162.06	85.48	88.12	90.22	79.73	77.02	72.01
E3	46.82	46.25	40.63	54.14	39.99	52.45	52.91	53.43	55.64	51.75
E4	41.34	37.39	36.02	34.81	33.92	37.56	36.58	31.05	31.47	31.40
E5	41.90	39.03	43.74	21.26	33.09	26.26	35.49	29.63	32.67	35.50
E6	58.56	60.75	55.62	53.40	55.33	55.66	51.52	47.58	49.30	45.89

Table 5.28 Summary of mean pressures during double support – Static test (Test-III)

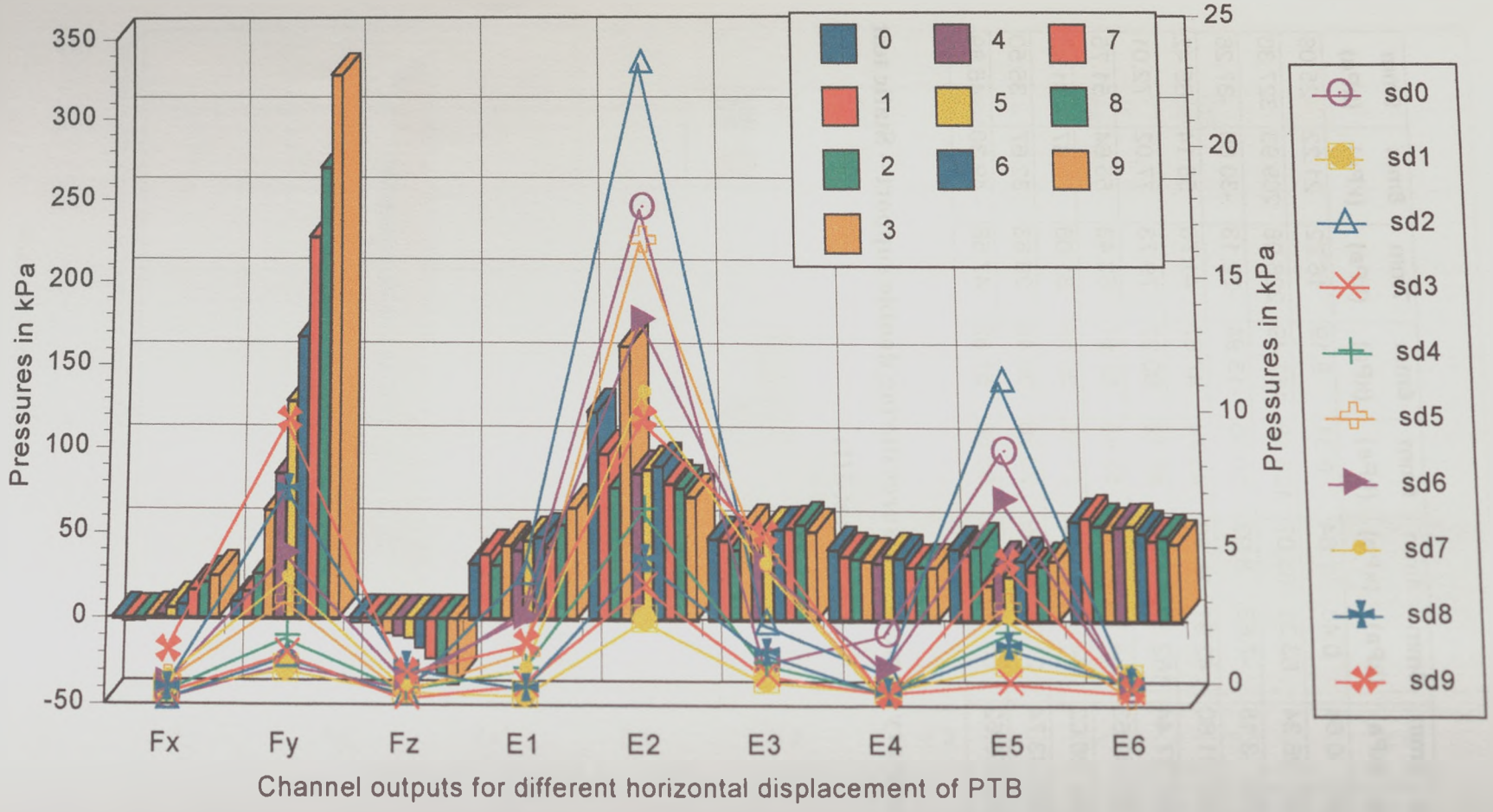

Figure 5.35 Subject:2 Summary of Mean and Standard deviation of Pressures during Double Support – Static test (Test-III)

Legend – Refer section 5.6.2

	0mm (kPa)	1mm (kPa)	2mm (kPa)	3mm (kPa)	4mm (kPa)	5mm (kPa)	6mm (kPa)	7mm (kPa)	8mm (kPa)	9mm (kPa)
Fx	0.17	0.46	0.16	0.36	0.43	0.78	0.68	0.90	0.51	1.86
Fy	1.38	1.21	1.69	1.78	2.38	3.72	5.41	4.51	7.81	10.32
Fz	0.60	0.44	0.34	0.21	0.53	0.44	0.87	0.62	1.31	1.08
E1	3.34	0.31	4.73	0.67	1.24	1.84	3.12	1.25	0.54	2.15
E2	18.39	3.05	24.02	4.30	7.05	17.15	14.17	11.41	5.27	10.39
E3	1.49	0.86	2.96	1.08	1.47	5.26	5.11	5.09	1.86	6.18
E4	2.56	0.48	1.15	0.42	0.49	0.36	1.28	0.18	0.45	0.29
E5	9.28	1.51	11.94	0.81	2.59	3.56	7.50	3.16	2.11	5.20
E6	0.54	0.96	0.94	0.46	0.81	0.32	0.67	0.68	0.82	0.53

Table 5.29 Summary standard deviations of pressures during double support Static test (Test-III)

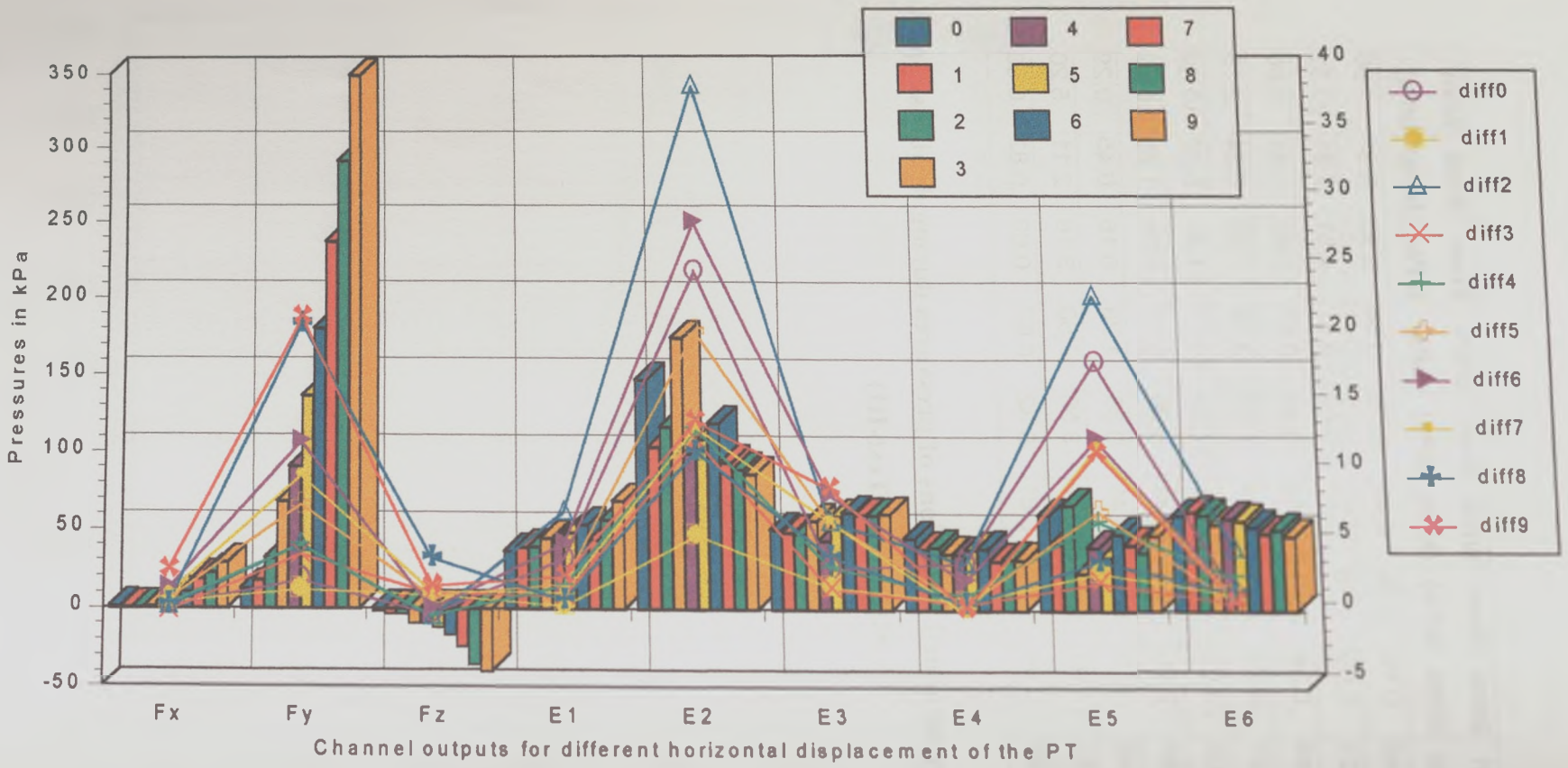

Figure 5.36 Subject:2 Summary of Peak Pressures and their differences with their mean during double support – Static test (Test-III)

Legend – Refer section 5.6.2

	0mm (kPa)	1mm (kPa)	2mm (kPa)	3mm (kPa)	4mm (kPa)	5mm (kPa)	6mm (kPa)	7mm (kPa)	8mm (kPa)	9mm (kPa)
Fx	0.75	0.05	0.05	0.88	2.71	7.50	10.13	18.26	22.07	28.35
Fy	12.35	17.78	31.44	67.68	90.14	136.14	180.03	237.08	291.16	348.93
Fz	-1.58	-3.29	-3.14	-9.34	-9.03	-11.84	-16.50	-23.95	-35.07	-39.44
E1	36.12	38.84	39.11	44.40	42.10	48.07	53.10	43.45	56.35	68.30
E2	147.28	103.21	116.47	174.78	99.07	108.85	118.95	93.44	88.97	86.15
E3	50.31	48.46	47.46	56.17	43.60	59.32	61.75	60.32	60.03	61.03
E4	45.25	38.53	39.91	35.79	35.52	38.53	39.22	31.40	32.50	32.09
E5	60.42	42.31	67.09	23.82	40.03	33.93	48.41	41.93	36.79	47.46
E6	60.21	62.51	60.67	54.54	58.37	56.84	53.16	49.03	51.17	47.19

Table 5.30 Summary of peak pressures during double support- Static test (Test-III)

	0mm (kPa)	1mm (kPa)	2mm (kPa)	3mm (kPa)	4mm (kPa)	5mm (kPa)	6mm (kPa)	7mm (kPa)	8mm (kPa)	9mm (kPa)
Fx	0.73	1.00	0.70	0.40	0.87	1.19	1.94	1.54	0.85	3.26
Fy	2.58	1.91	5.10	4.37	5.07	7.96	12.54	10.10	21.24	21.63
Fz	0.19	1.56	-0.01	1.71	0.10	1.49	0.56	1.82	4.21	2.18
E1	4.14	0.79	7.50	1.50	2.23	2.33	5.22	1.75	1.21	2.88
E2	25.12	5.81	39.03	12.73	13.60	20.72	28.74	13.71	11.95	14.14
E3	3.49	2.21	6.82	2.04	3.61	6.87	8.84	6.89	4.40	9.28
E4	3.92	1.15	3.89	0.98	1.59	0.97	2.64	0.35	1.03	0.69
E5	18.52	3.28	23.35	2.57	6.94	7.67	12.92	12.30	4.12	11.96
E6	1.65	1.76	5.06	1.14	3.04	1.18	1.64	1.45	1.87	1.30

Table 5.31 Summary of difference in mean and peak pressures during double support- Static test (Test-III)

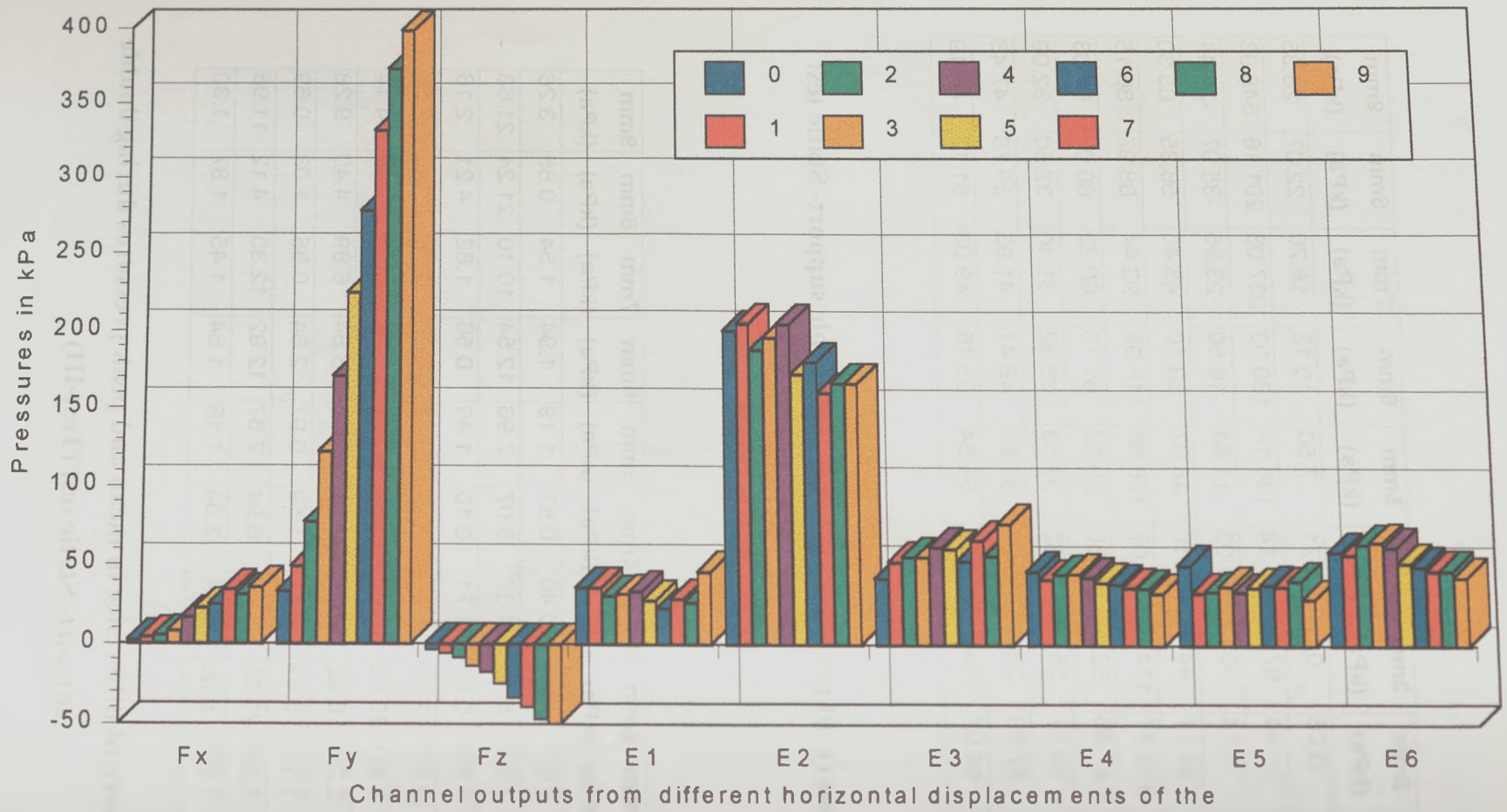

Figure 5.37 Subject:2 Summary of Mean Pressures during Dynamic Gait – Stance phase (Test-IV)
Legend – Refer section 5.6.2

	0mm (kPa)	1mm (kPa)	2mm (kPa)	3mm (kPa)	4mm (kPa)	5mm (kPa)	6mm (kPa)	7mm (kPa)	8mm (kPa)	9mm (kPa)
Fx	2.35	3.17	4.10	5.87	8.23	11.09	12.12	19.08	22.64	24.03
Fy	29.61	35.18	47.15	67.48	92.19	129.93	157.51	196.52	230.73	254.73
Fz	2.19	3.39	5.11	6.83	8.95	13.10	17.47	22.69	27.79	27.55
E1	13.98	17.48	12.86	15.27	19.31	13.76	12.20	21.70	14.69	32.97
E2	100.99	113.13	105.60	96.43	101.38	92.61	90.68	98.95	96.76	112.93
E3	26.81	33.05	35.49	35.32	41.79	42.68	35.22	51.60	41.79	58.53
E4	16.68	17.08	20.26	18.69	17.68	15.74	15.97	16.47	16.28	14.28
E5	26.97	23.16	20.30	20.51	20.32	21.23	23.97	24.84	24.14	17.03
E6	31.07	30.15	33.46	32.73	33.23	27.73	25.30	28.94	28.17	28.72

5.33 Summary of standard deviations of pressures during dynamic gait – Stance phase (Test-IV)

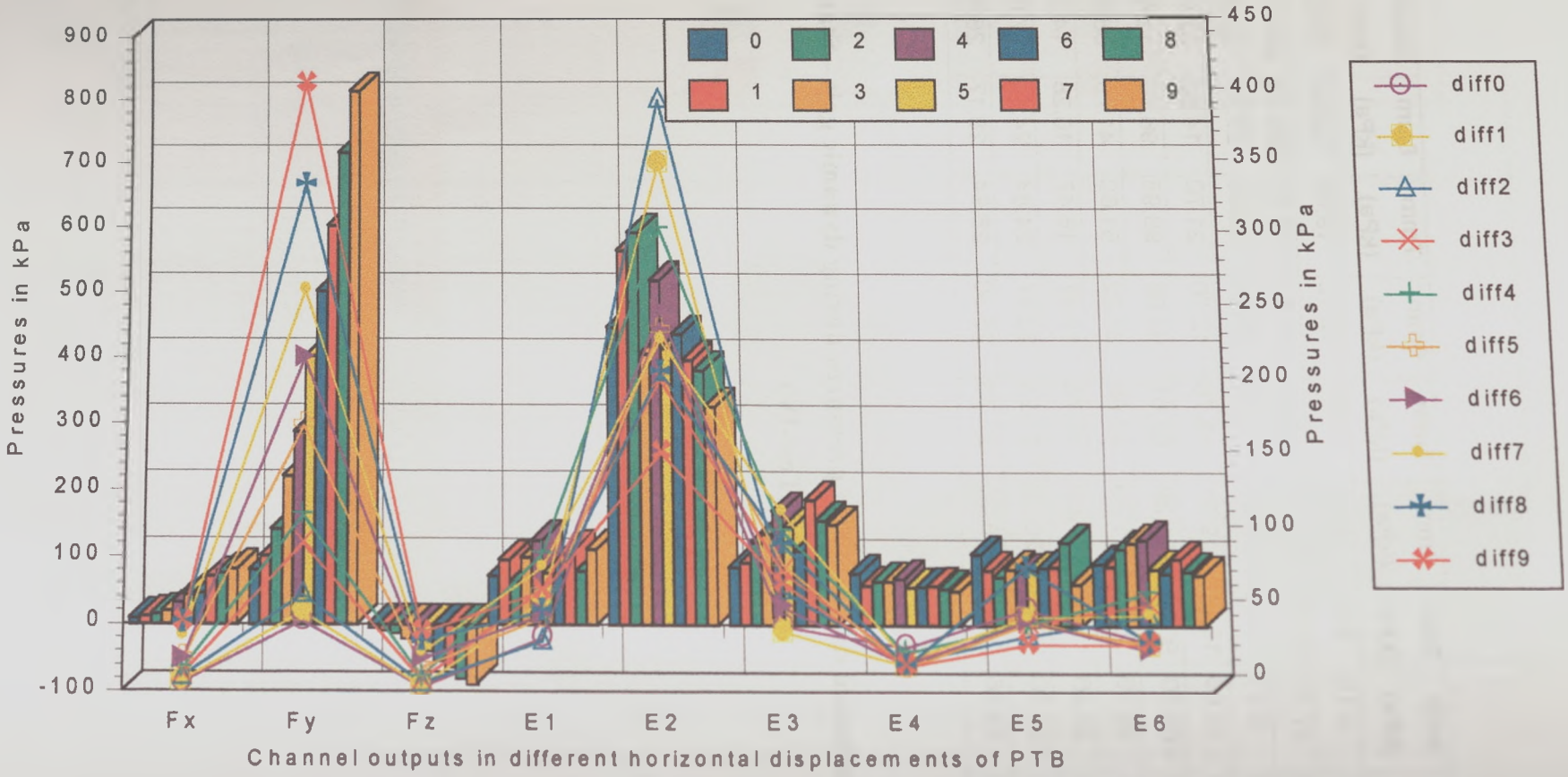

Figure 5.39 Subject:2 Summary of Peak Pressures and their differences with their mean during dynamic gait – Stance phas (Test-IV)

Legend – Refer section 5.6.2

	0mm (kPa)	1mm (kPa)	2mm (kPa)	3mm (kPa)	4mm (kPa)	5mm (kPa)	6mm (kPa)	7mm (kPa)	8mm (kPa)	9mm (kPa)
Fx	2.43	4.13	5.16	8.10	16.70	22.31	24.84	34.05	31.22	35.81
Fy	33.21	49.00	76.59	121.72	170.34	224.21	277.82	331.32	372.59	398.60
Fz	-2.93	-5.42	-7.96	-13.33	-17.15	-24.42	-33.03	-38.70	-46.18	-49.53
E1	35.84	35.92	30.43	31.46	33.52	27.46	22.32	28.34	26.15	45.75
E2	199.87	204.75	187.42	195.72	204.29	171.85	179.80	160.11	166.07	166.10
E3	41.87	52.19	55.31	55.38	61.75	60.59	53.20	66.10	56.36	76.92
E4	46.86	41.66	44.69	45.30	42.97	39.83	38.72	36.65	35.96	33.13
E5	51.12	33.51	34.19	37.66	33.67	36.86	38.53	37.72	40.90	29.27
E6	59.17	57.66	64.19	65.22	62.43	52.37	50.36	47.59	47.52	43.38

Table 5.32 Summary mean pressures during dynamic gait – Stance phase (Test-IV)

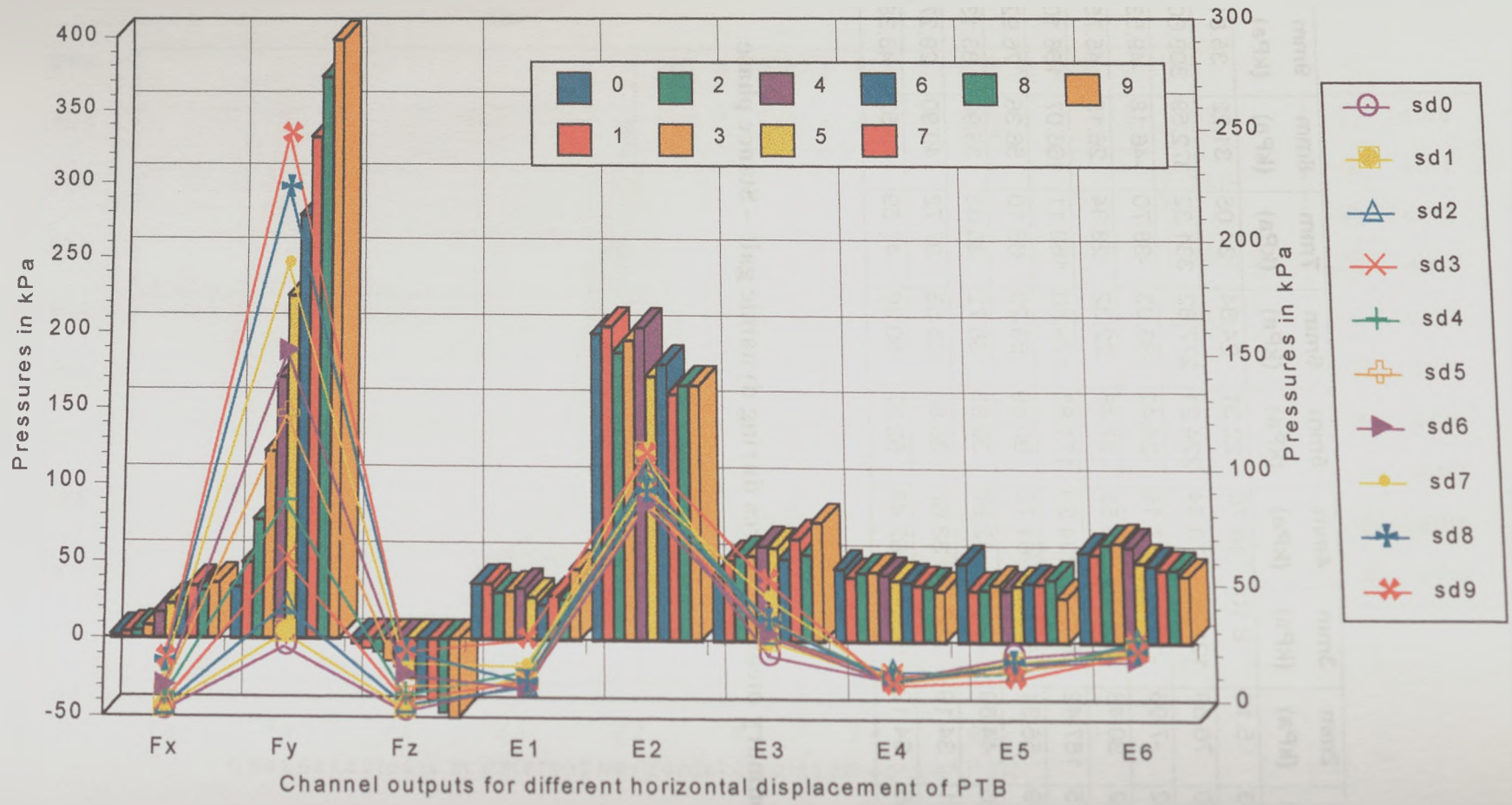

Figure 5.38 Subject:2 Summary of Mean and Standard deviation of Pressures during Dynamic Gait – Stance phase (Test-IV)

Legend – Refer section 5.6.2

	0mm (kPa)	1mm (kPa)	2mm (kPa)	3mm (kPa)	4mm (kPa)	5mm (kPa)	6mm (kPa)	7mm (kPa)	8mm (kPa)	9mm (kPa)
Fx	8.13	10.72	14.44	18.94	31.44	43.32	45.37	70.31	76.03	81.65
Fy	80.11	101.79	140.78	220.59	287.91	402.46	502.16	602.80	716.88	815.26
Fz	-5.81	-8.61	-13.28	-20.62	-26.40	-40.06	-54.24	-64.09	-79.72	-88.56
E1	71.56	96.14	63.96	99.40	125.61	76.59	72.92	111.35	79.58	112.03
E2	447.32	564.28	591.78	405.73	518.06	415.34	436.38	397.61	381.05	326.37
E3	85.48	92.20	122.50	135.79	169.24	145.94	109.63	186.39	155.23	148.94
E4	76.66	58.97	65.00	65.00	69.25	56.22	56.91	58.28	53.89	50.19
E5	106.16	81.96	71.66	83.29	79.10	82.34	86.15	87.48	124.27	60.99
E6	92.08	88.25	115.21	123.79	128.70	84.57	78.14	99.43	81.20	75.53

Table 5.34 Summary of peak pressures during dynamic gait – Stance phase (Test-IV)

	0mm (kPa)	1mm (kPa)	2mm (kPa)	3mm (kPa)	4mm (kPa)	5mm (kPa)	6mm (kPa)	7mm (kPa)	8mm (kPa)	9mm (kPa)
Fx	5.70	6.59	9.28	10.84	14.74	21.01	20.52	36.27	44.81	45.84
Fy	46.90	52.79	64.19	98.86	117.57	178.25	224.34	271.48	344.29	416.66
Fz	2.87	3.20	5.33	7.29	9.26	15.65	21.21	25.39	33.54	39.02
E1	35.72	60.22	33.53	67.94	92.09	49.13	50.60	83.01	53.42	66.28
E2	247.44	359.53	404.36	210.01	313.77	243.49	256.58	237.51	214.97	160.28
E3	43.60	40.01	67.18	80.41	107.48	85.35	56.43	120.30	98.88	72.02
E4	29.80	17.31	20.31	19.70	26.28	16.40	18.19	21.63	17.93	17.06
E5	55.04	48.45	37.48	45.63	45.43	45.47	47.62	49.76	83.37	31.72
E6	32.91	30.59	51.02	58.58	66.27	32.21	27.78	51.84	33.69	32.16

5.35 Summary of difference between mean and peak pressures during dynamic gait – Stance phase (Test-IV)

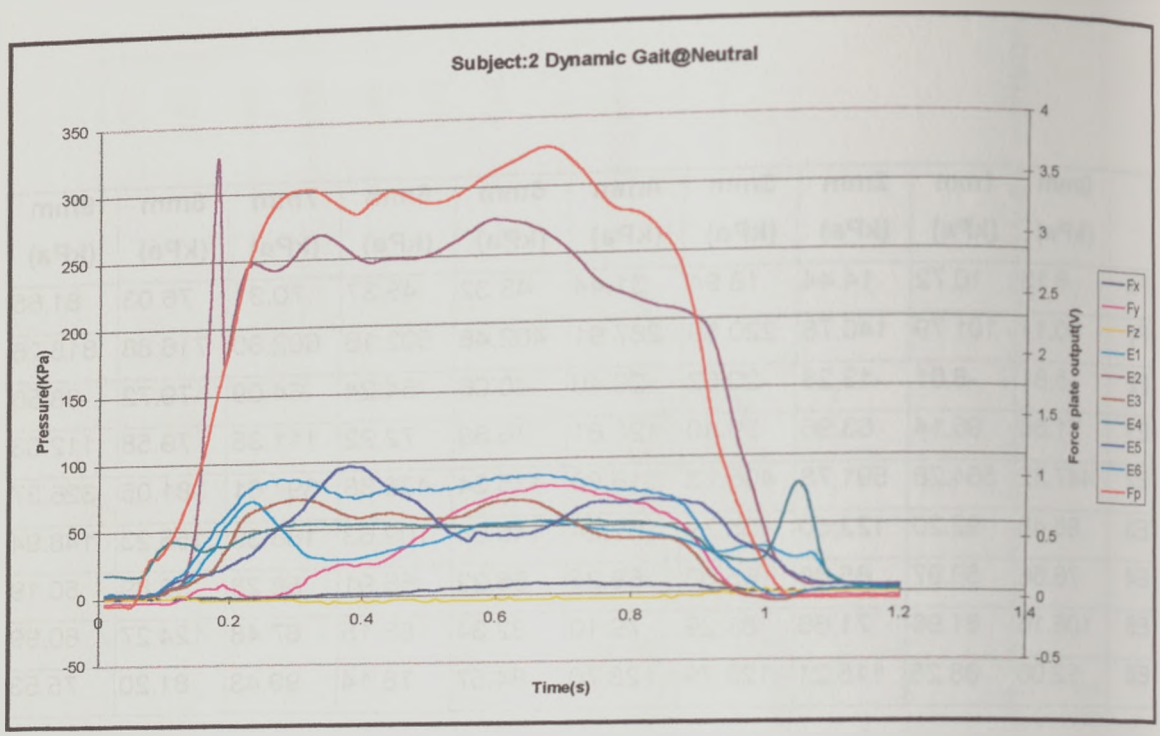

Figure 5.40 Pressure variations around the socket during dynamic gait (Test-IV) at flush position of the patellar tendon bar with the socket wall

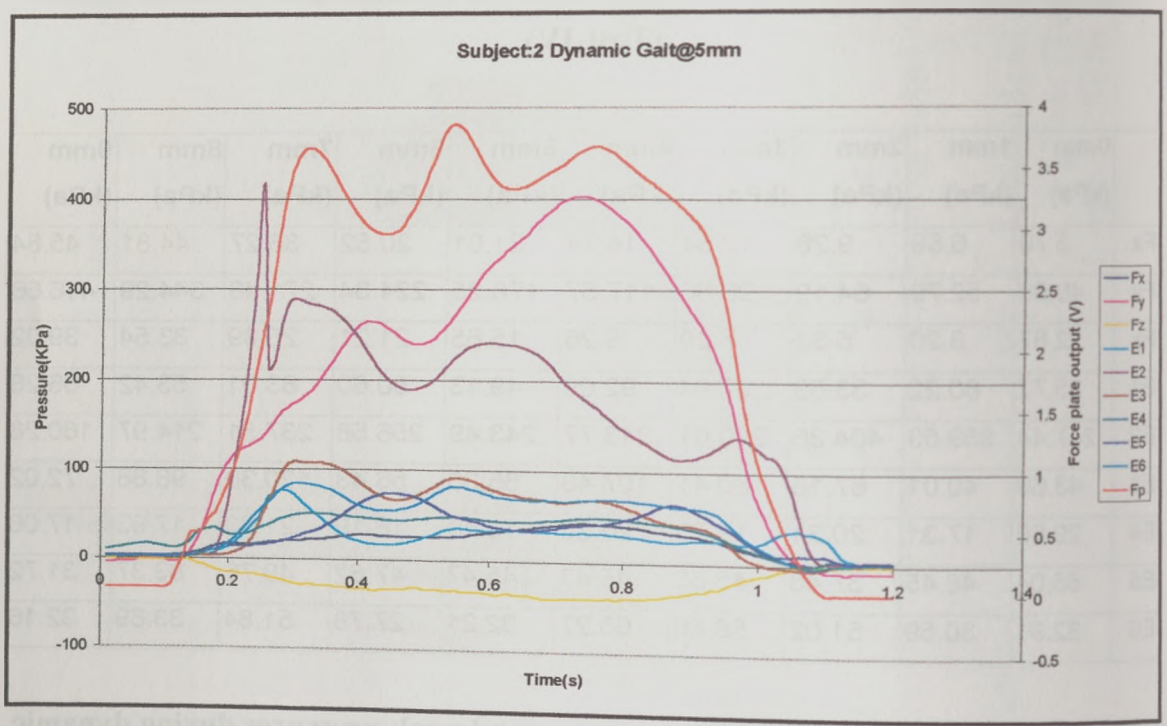

Figure 5.41 Pressure variation around the socket during dynamic gait (Test-IV) at 5mm displacement of the patellar tendon bar into the socket

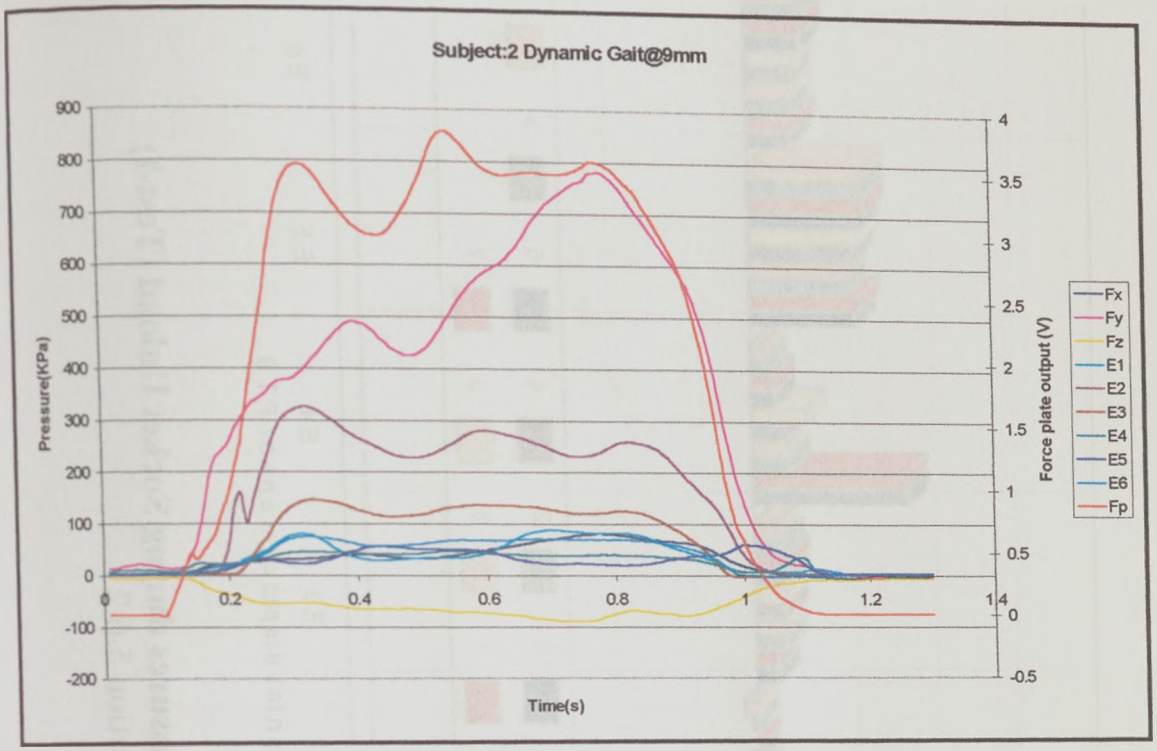

Figure 5.42 Pressure variations around the socket during dynamic gait (Test-IV) at 9mm displacement of the patellar tendon bar into the socket

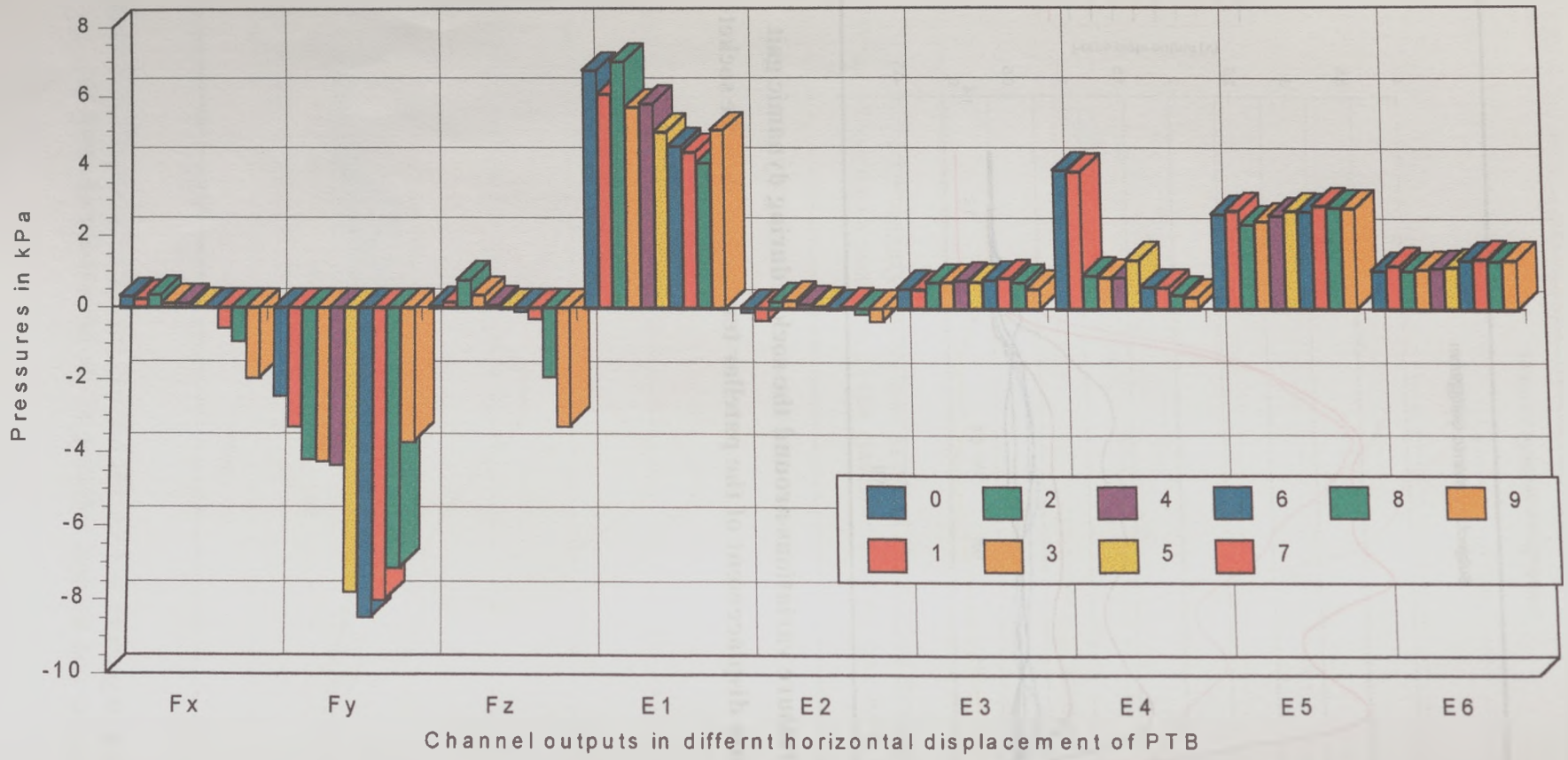

Figure 5.43 Subject:2 Summary of Mean Pressures during Socket Unload (Test-I)
Legend – Refer section 5.6.2

	0mm (kPa)	1mm (kPa)	2mm (kPa)	3mm (kPa)	4mm (kPa)	5mm (kPa)	6mm (kPa)	7mm (kPa)	8mm (kPa)	9mm (kPa)
Fx	0.30	0.24	0.36	0.12	0.13	0.02	-0.01	-0.54	-0.92	-1.94
Fy	-2.43	-3.28	-4.17	-4.23	-4.32	-7.76	-8.45	-7.98	-7.12	-3.69
Fz	0.04	0.15	0.78	0.35	0.08	-0.03	-0.09	-0.28	-1.90	-3.26
E1	6.72	6.06	6.98	5.68	5.78	4.98	4.57	4.40	4.08	5.02
E2	-0.10	-0.31	0.19	0.23	0.11	0.06	-0.02	0.05	-0.13	-0.32
E3	0.56	0.53	0.73	0.73	0.78	0.73	0.80	0.84	0.72	0.55
E4	3.87	3.84	0.91	0.86	0.87	1.35	0.59	0.58	0.38	0.31
E5	2.63	2.73	2.34	2.43	2.59	2.73	2.71	2.89	2.83	2.82
E6	1.06	1.20	1.06	1.10	1.13	1.17	1.35	1.40	1.34	1.37

5.36 Summary of mean pressures during socket unload (Test-I)

Chapter: 6

Discussion and Analysis of Results

6.1 Introduction

The results of this study are discussed in the order that they were presented in chapter:5.

6.2 Validation of the Rincoe socket fitting system

These tests were mainly carried out to provide an insight into the accuracy of the Rincoe pressure measurement system. The author believed that the results obtained from this system required to be analysed in full consideration of its errors to avoid losing the objective of using the system i.e. to identify areas of high pressure. Through this process, the accuracy error of the system was found to be 15.27 % and had an average deviation of 5.33 %, the hysteresis error was found to be 9.05 % and a average deviation of 1.34%. The Rincoe system as described in section 3.1.4 has poor resolution of pressure in its measurement range, which is between 0-12 psi. The first reading obtained after 0 is 1.5 psi, and thereafter until 4 psi it has a resolution of 0.5 psi and from 4 – 12 psi its resolution is 1 psi. This leads to the system rounding up pressures to the nearest value and this could possibly be the reason for its large errors. The results obtained in this study were in contrast to validation studies carried out by Polliack et al. (2000), who had reported an accuracy error of 24.7 %.

In the present study, it was noted that above 12 psi of pressure the Rincoe system returned a value of 99.9 psi, and sometimes even at lower pressures such as 10 psi some sensors saturated and showed a reading of 99.9 psi. This value when included in the calculations skewed the data and produced difficulties in interpretation. Therefore the value of 99.9 psi was assumed to be a pressure reading over 12 psi and was given an arbitrary value of 12.1. In the study carried out by Polliack et al (2000), this problem was not addressed, and the author believes that this could be a reason for large difference in the accuracy error. It should be noted that in the present study

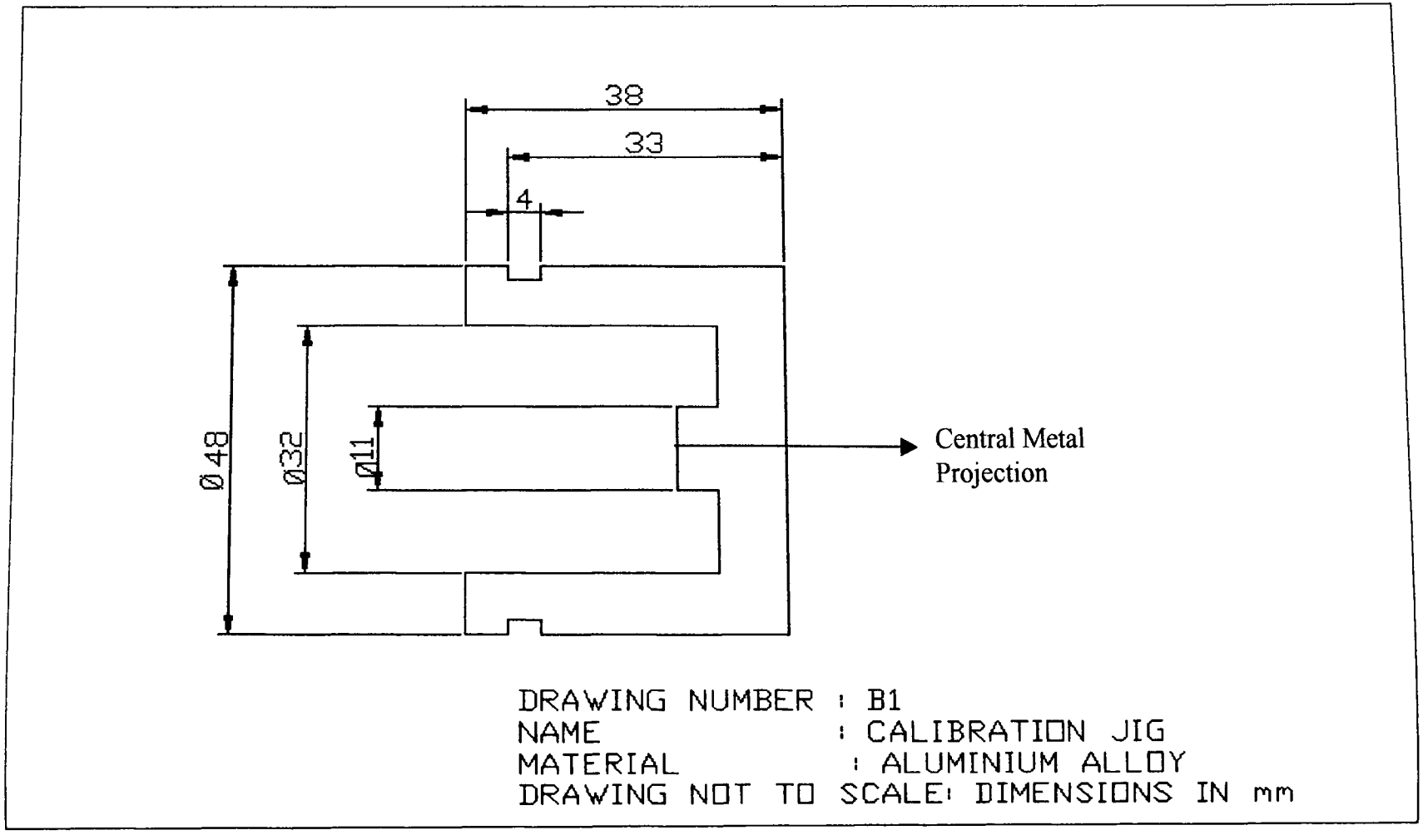

Figure 6.1 Calibration jig with the central metal projection

the validation of the sensors was performed by just one cycle of loading and unloading due to time constraints and it is recognised that this methodology is not adequate to give a clear picture of the accuracy errors involved.

6.3 Calibration of the PTB mark-II transducer

The results of the PTB mark-II transducer (figures 5.2 – 5.6, Tables 5.2 – 5.6) calibration show a high linearity in all the three channels (R^2=0.99). The cross talk was also minimal during shear calibration. However it should be noted that these results were presented from the second calibration test performed with a modified calibration jig. The results of the initial calibration tests are presented in appendix :3 The comparison of both sets of results showed that the calibration jig attached to the strain gauged piston through a central metal projection (figure 6.1) resulted in significant Fy cross talk during the calibration of the shear channels Fx and Fy. The author believes that this central metal projection had been applying a considerable amount of strain over the Fy channel during the shear calibration and thus caused the cross talk from the Fy channel during the shear calibration. However following the removal of the central metal projection in the calibration jig, and after securing the strain gauged piston by means of screws to the bottom of the calibration jig, it resulted in reduction of cross talk from the Fy channel. This would have had a considerable effect on the earlier studies done by Osman (1999) and Wandrum (2000) as the same calibration jig had been originally designed by Osman (1999) and later used by Wandrum (2000).

6.4 Calibration of the Entran Transducer

The calibration results of the entran transducers were presented in section 5.4. The results have been presented both as numerical data and as calibration graphs (table 5.7 and figures 5.7 to 5.12). The responses of the transducers as evident from the graphs, showed good linearity and minimal hysteresis, with transducer 6 diplaying the greatest amount of hysteresis (figure 5.12). They also showed high repeatability and sensitivity. The maximum output at a fully loaded position was almost the same

in transducers 1,3,4, and 6 (1.033V on average), however transducer 2 and 5 had a slightly lesser output (0.8858V and 0.7738 respectivly). These decreased outputs would not possibly affect the final results of the study, as each transducer has been calibrated separately, and calibration co-efficients for each of the transducer has been determined, from which the loads would be computed.

6.5 Results of Rincoe Test

The placement of the Entran transducers around the socket both in subject:1 and subject:2 followed from the analysis of the Rincoe test results. Figures 5.13 and 5.14 show these sites in subject: 1 and figures 5.15 and 5.16 show the sites chosen in subject:2. From the data presented in table 5.9 for subject: 1 and table 5.10 for subject: 2 it can be seen that the accuracy and hysteresis errors of the sensors that monitored these sites are really high and vary about 4 – 19% of the full-scale outputs. So the pressures monitored were only used to compare with the other sensor recordings in terms of their errors and were chosen. However this has provided only an approximate picture of the distribution of areas of high pressure around the socket. It should be also noted that the spacing between each of the sensors was 2.3cms (figure 3.2). This cannot satisfy the claim that areas of high pressure can be monitored completely around the socket and hence rises the question of pressures in the areas between the sensors.

The sensor strips used were also stored for considerable amount of time before use, and hence the output from these sensors may not be accurate. Polliack et al (2000) have stated that physical conditions of the sensors deteriorate after significant use of 90 days. But the sensors used in this study were not used before, although they were stored for a considerable amount of time. However in the scope of the present study the results of these tests were treated with utmost caution and sites of high pressure were decided only by picking the sensors with the highest responses and low errors.

6.6 Results of interface pressure measurements

The results of both the subjects are discussed under four different situations i.e single leg stance, double support, dynamic gait and socket unload.

6.6.1 Single-leg stance (static)

The subjects during this test were asked to weight bear only using their amputated limb loading their sockets completely with their body mass. The results of subject:1 are shown in Fig 5.18 – 5.20 The distribution of pressure in subject:1 was found in the patellar tendon region and in the region of Entran transducer :1 (fig 5.13). This reveals a pattern that during these tests the subject had been taking considerable amount of pressure on the lateral side of the stump. This can be explained as a force on the lateral side of the stump, which counteracts the effects of the centre of mass of the body, which acts medial to lateral, and acts totally only on the prosthetic side. It is also clear that the pressure tends to increase in the axial direction in the patellar tendon bar area as the patellar tendon bar is advanced into the socket and has a mean pressure of 148 kPa in subject:1. Although there was an increase in pressure at the patellar tendon region the standard deviation is 7 kPa at 10mm of advancement into the socket. However the Entran transducer :1 recorded a maximum pressure of 160 kPa and shows a large standard deviation (52.54 kPa) which shows the huge variation of pressure. This signifies that the pressure in this area varies considerably.

A similar pattern of pressure was also found in subject: 2 (Figure 5.31 –5.33). But the magnitudes are much higher compared to that of subject: 1. The author believes that these high pressures may be due to the bony and shorter stump of subject:2, as explained in section: 4.4. This reduces the area of distribution of pressure considerably and causes areas of concentration and the lack of soft tissue cover exposes the stump to high pressures. Subject:2 showed a mean pressure of 499 kPa in the axial direction at the patellar tendon region at 9mm advancement of the patellar tendon bar into the socket. The pressure in the axial direction seems to be considerably increasing with each 1mm advancement of the patellar tendon bar. The

pressures however in subject:2 around the socket are also slightly elevated compared to subject:1. The pressure at the transducer site of Entran :2 (Figure 5.15) which was over the distal end of the fibula shows considerably high pressures of 280 kPa during 7mm displacement of the PTB bar. The standard deviations of these pressures were higher (52 kPa) as in subject:1

On the whole it was observed in both subjects that there tends to exist high pressure predominantly on the lateral side of the socket during single-leg stance and the pressure at the patellar tendon region increases considerably with forward advancement of the patellar tendon bar. The shear channels have also shown considerable shear stresses at the patellar tendon region. The shear force in the Fx direction acts downwards as the patellar tendon bar was advanced forwards. This was due to the subject tending to weight bear on it and displace it downwards. A lateral displacement of the patellar tendon bar was also seen as it is advanced into the socket.

The pressures recorded in this study are much higher compared to previous, similar studies (Osman, 1999 and Wandrum 2000). The pressures observed in these studies at the patellar tendon bar during single-leg stance had a peak pressure of 355 kPa in the axial direction. The author believes that this could be due to the use of a hard socket for testing in the present study to eliminate the effects of the liner which could have caused a considerable increase in the pressures. The mean pressure reported in a hard socket was about 280 kPa with a peak of about 420 kPa (Rae and cockrell, 1971). But pressures as high as 800 kPa were also reported in their study at the kick point. Pearson et al (1973) have investigated pressures in critical areas of the patellar tendon bearing prostheses and have carried out a similar methodology to the present study where pressures during single leg stance was monitored. It is worthwhile noting that in the study done by Pearson et al (1973), they observed the pressure distribution with both the stump muscles tensed and relaxed during single leg stance. Pearson et al (1973) noted that tensing of the stump muscles could have a significant effect upon the interface pressure. This parameter however was not taken into account in the present study and hence the fluctuation of the pressures around the

socket may be due to the active contraction and relaxation of muscles, as reported by Pearson et al (1973).

6.6.2 Double support Results

The results obtained from the double support test for subject: 1 were presented in figures 5.21 – 5.23. During double support the subjects were asked to distribute their weight equally between both the legs. This was quite evident in the case of subject:1 as shown in figure 5.21. The mean pressures were found to be nearly half (65 kPa in axial loading in the patellar tendon region) of what had been recorded during single-leg stance. This could be directly attributed to the fact that the subject is now distributing his body mass almost equally between both the legs. It was noted that the pressure distribution around the socket was also even during the double support test. However the forward displacement of the patellar tendon bar only produced a steep raise in pressure in the axial direction (0.3 kPa to 65 kPa) from 0 to 10mm. Further to that there was no strong evidence that the pressures around the socket reduced with increasing pressures at the patellar tendon region. The Entran transducer 1-4 (figure 5.13) showed a very similar mean and peak pressure in the range of 17-20 kPa, throughout the displacement of the patellar tendon bar from 0-10mm of forward displacement. All these transducers as shown in figure 5.13 were placed more towards the lateral side of the socket. On the medial side the pressure recordings were not equally distributed. The Entran transducer 5 (Figure 5.14) showed a much higher pressure (29-34 kPa) compared to the Entran transducer 6 (Figure 5.14) which showed pressures in the range of 6-12 kPa. This clearly showed that the interface pressures were mostly confined to the medial superior aspect of the socket rather than the distal end. The author believes that this sort of reversal in action of pressures in double support is due to a wider base of support. This wider base of support offers better stability compared to that of single leg stance, explained in section 6.6.1. This results in equal distribution of the mass of the body, which literally eliminates the need of a stabilising lateral force.

It was also further noted that Entran transducer: 6 (figure 5.14) showed a slight decrease in pressure (11-6 kPa) with advancement of the patellar tendon bar which may make a point that the patellar tendon bar sitting proud into the socket actually prevents the stump from moving into the socket and thus prevents end bearing, but this happens at the cost of a high pressure at the patellar tendon area. The standard deviations in subject:1 seem to be within the range of 0-4 kPa. As pointed out in section 6.6.2 this could be either due to the postural sway of the patient or due to the contraction of the muscles within the socket

The results of subject:2 are presented in figures 5.34 – 5.36. The mean pressures of subject:2 were 327 kPa, which was a little more than half of the pressures observed during single-leg stance. The pressures around the socket during various displacements of the patellar tendon bar still showed a higher pressure on the lateral side compared to the medial side. However it was also noted that the pressures on the lateral side (72 –162 kPa) at Entran transducer: 2 (figure 5.15) were reduced compared to pressures monitored during single leg stance. The standard deviations of pressure at the patellar tendon was found to be 10 kPa in the axial channel (Fy) in maximum displacement of the patellar tendon bar. Higher standard deviations were found to mainly occur at the Entran transducer :2 (24 kPa) and entran transducer: 5 on the medial side (11 kPa). It was interesting to note that these large standard deviations were both detected at 2mm of the patellar tendon bar. The author believes that this may not signify anything in particular, but would have occurred due to postural sway of the subject.

The results obtained in this study do not agree with the results obtained during double support in a similar study (Osman 1999). The peak pressures recorded by Osman (1999) were 158 kPa in the Fy direction at the patellar tendon region. In the present study subject:2 has shown almost twice the pressure (350 kPa) at maximum displacement of the patellar tendon bar. The author believes the reasons for this high pressures is due to the same reasons quoted in section 6.6.1 of this chapter which are to do with stump configuration. On the whole both subjects have shown significant reduction of pressures in double support compared to single leg stance. The

distribution of pressures between the medial and lateral side in both subjects varies, but it should be noted that the pressures on the lateral side decrease in both subjects and this could be due to the broader base assumed by subjects during double support. The shorter stump in subject:2 could still be unstable during the double support period and coupled with the presence of a prominent end of fibula could have possibly given rise to high pressures at the Entran transducer :2. However in both subjects there was no significant decrease in the pressures around the socket with advancement of the patellar tendon bar.

6.6.3 Results of Dynamic gait

The results of dynamic gait are presented in Figures 5.24 – 5.26 in subject :1. The variations of pressure at the patellar tendon bar and around the socket throughout the gait cycle at Neutral or the flush position, 5 mm and 10mm displacement of the patellar tendon bar have been shown in figures 5.27 – 5.29. A mean pressure of 105kPa was obtained in the axial Fy direction in the patellar tendon region during maximum displacement of (10mm) the patellar tendon bar. It was interesting to note the average mean pressure in the axial direction (Fy) in the patellar tendon bar region of single leg stance of subject:1 with maximum displacement of the patellar tendon bar (148 kPa) was higher than that of pressures during dynamic gait. But the peak pressures at the patellar tendon bar in the Fy direction are much higher (227 kPa) during dynamic gait compared to that of (171 kPa) during single-leg stance. This clearly implies that there is a fast pressure build up during dynamic gait compared to a constant high pressure in the region during single – leg stance. This ratifies further analysis of the variations of pressures at the patellar tendon region. The pressure variations at the patellar tendon region at various points of the gait cycle in different displacements of the patellar tendon bar can be seen in figures (5.27 – 5.29) at neutral, 5mm and 10mm of horizontal displacements. The axial force in the patellar tendon region increases with displacements of the patellar tendon bar into the socket. At heel strike the first peak occurred in the axial directions with pressure recording of just 5 kPa at the neutral or flush position of the patellar tendon bar and at 5 mm displacement there was a slow increase in pressure to just over 20 kPa but at 10mm

displacement of the patellar tendon bar this peaked at 100 kPa. During midstance the pressures dropped down and the maximum pressure in the axial direction in the patellar tendon region started building up just before and during push-off and climbed to the highest pressure of 227 kPa at 10mm displacement of the patellar tendon bar.

The author tends to justify this 'uneven double peak' with the biomechanical concepts put forward by Radcliffe and Foort (1961). The smaller peak during heel strike is due to the controlled knee flexion that an amputee executes during heel strike as the line of action acts anterior to the knee joint. So the interface pressure showed a short peak during heel strike which occurs due to the patellar tendon bar hitting back on the stump, due to the rotation of the prosthesis in an anti-clockwise direction (right side) about its point of contact at the heel due to the line of action passing anterior to the knee. The author also believes that during the swing phase there is pistoning occurring in the socket, and complete loading of the socket does not take place immediately after heel strike as still most of the areas of the stump are still away from their points of contact. However during midstance the pressures drop in the patellar tendon region and all around the socket (figure 5.27- 5.29) as the line of action directly passes through the knee. At the end of midstance when the heel was about to leave the ground the pressure once again starts building in the patellar tendon region. This was due to the line of action now acting posterior to the knee causing moment which tends to flex at the knee. The amputee now has to overcome this moment and maintain the knees in extension. This brings about an active quadriceps contraction tending to extend the knee. The short stump now needs to keep the knee in extension and this in a normal gait is usually assisted by the dorsiflexors during push off. A lack of this dorsi flexor action totally tends to make the amputee rely upon the quadriceps and hip extensor action which uses the patellar tendon region as the main point of contact around which the stump is rotated and this resulted in a much higher second peak with peak pressures of 227 (kPa) during push –off. It is also interesting to note in subject:1 that a peak occurs once again during the swing phase in the axial direction, the author believes that this could be the patellar tendon bar which is now sitting proud into the socket pushing itself against

the stump during swing phase, but the position and behaviour of this peak could be a possible artefact occurring during data collection. However, the information acquired from just two steps is not adequate to conclude.

The shear channels Fx and Fz did not record high shear stress during the gait cycle. However on advancement of patellar tendon bar into the socket caused the Fx to increase in magnitude due to weight bearing of the stump on to the patellar tendon bar and pushing it downwards. The medial –lateral shear does not show any significant changes throughout the gait cycle, showing minimal displacement of the patellar tendon bar in the lateral direction

Similar results were also observed in subject:2 and are presented in figures 5.37-5.42. However the pressures observed were much higher in the patellar tendon region compared to subject:1. The two uneven double peaks observed during the axial loading of the patellar tendon bar in the case of subject:1 were also observed in subject:2 but were found to be less distinctive. This is due to the pressure constantly building up in the patellar tendon region throughout the stance phase. The stance phase duration is also a little longer than that of subject:1. A second area of high pressure at the entran transducer:2 (figure5.15) of about 590 kPa was also observed in subject:2 during 2mm displacement of the patellar tendon bar. It was observed that all pressures dropped almost completely to zero during swing phase in subject:2 compared to subject:1, this is to be expected during swing phase as the load is removed off the stump. This may also signify the presence of pistoning of the stump during swing phase, and during heel strike the stump pistons into the socket causing a sharp jump in the pressure at the entran transducer :2. The author believes that this impact is brought about by the end of fibula impacting against the entran transducer:2 however this was noted to decrease with the forward displacement of the patellar tendon bar into the socket. This happens because of the patellar tendon bar holding on to the stump during swing phase and preventing extensive pistoning and to validate this further a negative pressure is read in swing phase from the axial channel of the patellar tendon bar which is due to the socket suspending itself from the stump by means of the patellar tendon bar.

Both subjects have displayed an almost even distribution of pressures around the socket, except for the Entran transducer site (Entran 2) which has displayed high pressures in subject:2. The standard deviations were also quite high 255 kPa in subject:2) in all areas of high pressure in the socket signifying a sudden loading up of pressure from a very small magnitude to a large magnitude.

The results from this study cannot be used as a stand alone case due to a number of reasons. The high pressures in subject:2 cannot be properly explained due to the limited data collection due to time constraints i.e. two steps for each displacement of the patellar tendon bar. The incorporation of force plate as a switch to indicate various phases of the gait cycle although proves advantageous from one point of view, proves to be highly disadvantageous, because although proper instructions were given, the subjects still tend to anticipate the force plate and alter their gait which could have a significant effect on the results. The results of this study may also have been influenced by the use of hydrocast sockets.

Chapter:7

Conclusions and Recommendations for future work

6.1 Outcome and conclusion

The aims and objectives of this study were to primarily optimise an existing design of patellar tendon bar transducer, and to identify areas of high pressure around the socket and study the distribution of pressures for various displacements of the patellar tendon bar. It was also an aim to carry out this study in more than one subject.

The study had met its initial objectives of optimising the patellar tendon bar transducer. As explained in the discussion analysis section of the thesis, the characteristics of the PTB mark-II transducer have been proven to be excellent. However the technique of transducer fixation to the socket could be imporved.

The Rincoe system used in detecting areas of peak pressures had limitations in terms of its accuracy. The areas of high pressure were chosen while acknowledging these limitations. However it cannot be said that all the areas of high pressure have been identified, and the conclusions and results of this study must always be considered under these conditions.

The interface pressure measurements have shown a few similar patterns of pressure distribution, between the two subjects. It is also quite evident from this study that the distribution of pressure around the socket is not significantly altered by the position of the patellar tendon bar. However maximum displacement of the patellar tendon area into the socket by modification during socket fabrication may lead only to significantly high pressures concentrating in the patellar tendon region, which is actually not required under any circumstances. It is also worthwhile noting that the pressures experienced in a shorter stump is quite higher compared to a longer one. If this is the case, socket fabrication of amputees with shorter stump must be addressed adequately, because even a minor indentation in the socket can give rise to high

pressure and stress concentrations. Therefore it may require more accuracy, and better understanding in the distribution of pressures

These observations however need to be ratified by a further intensive study with more subjects. However this exploratory study has opened up avenues to study the behaviour of pressure in stump socket interface in various scenarios such as longer and shorter stumps, amputees who have used prostheses for longer time and shorter time etc.

7.2 Suggestion for future studies

This study has opened up a channel for further work to be mainly undertaken in further identifying the behaviour of pressures around the socket. Future studies might need to concentrate on the following lines

- Better fixation techniques of the PTB mark-II transducer onto the socket
- Test more than two subjects and possibly have two groups of subjects i.e. one group of subjects with normal or longer stumps and one group with short stumps, and compare the results between the two groups
- Use a more accurate system to identify areas of high pressure and use statistical methods to choose areas of high pressure to avoid any significant errors
- Use sensitive load cells like entran transducers, but with a higher operating range to monitor pressures around the socket. The present study has measured pressures of more than 600 kPa and repeated loading may lead to permanent plastic deformation of the transducer may occur although a possible overload up to approximately 700 kPa is possible
- Electronic goniometers or similar instruments can be used to detect the phases of gait cycle rather than force plates to get more accurate results
- Shear measurements around the socket would give a much better picture of load distribution around the socket and possibly a transducer could be designed to meet these criteria.

References

Appoldt FA and Bennett L (1967): A preliminary report on dynamic socket pressures. Bulletin of Prosthetic Research: 10-8 pp20-55

Bader D.L.(1990): Pressure Sores: Clinical Practice and Scientific Approach: Macmillan Press pp 191-201

Bennet L, KavnerD, Lee BK, Trainor FA(1979): Shear Vs Pressure as causative factors in skin blood flow occlusion. Archives of Physical Medicine and Rehabilitation:60 pp309-14

Berbrayer EKN, Hunter GA, Berbrayer D (1996): Transtibial Amputation: Preoperative Vascular Assessment and Functional Outcome. Journal of Prosthetics and Orthotics: Vol.8 (4) pp. 123-129.

Briggaman R.A., Wheeler C.E (1975) : The epidermal-dermal junction . Journal of Investigative dermatlogy: 65(1) pp71-84

Buis A.W.P (1997) Dynamic interface pressure measurement – comparing two trans-tibial socket concepts. PhD Thesis, National centre for education in Prosthetics and Orthotics, University of Strathclyde, Glasgow.

Buis A.W.P and Convery P (1997): Calibration problems encountered while monitoring stump/socket interface pressures with force sensing resistors: techniques adopted to minimise inaccuracies. Prosthetics and Orthotics International :21: pp179-182

Burgess EM and Moore AJ (1977) : A study of interface pressures in the below-knee prostheses (physiological suspension: an interim report). Bulletin of Prosthetic Research: 10-28 pp58-70

Clark R.A. (1985): Cutaneous tissue repair: Basic biological considerations. Journal of American Academy of Dermotology: 13(5) pp701-25

Convery P, Buis AWP (1998): Conventional patellar tendon bearing socket/stump interface dynamic pressure distribution recorded during prosthetic stance phase of gait of a trans-tibial amputee. Prothetic and Orthotic International: 22: pp193-8

Convery P, Buis AWP (1999): Socket/stump interface dynamic pressure distribution recorded during the prosthetic stance phase of gait of trans-tibial amputee wearing a hydrocast socket: Prosthetic and Orthotic International: 23 : pp107-12

Daly CH (1982): Biomechanical properties of dermis : Journal of investigative dermatology 79: Suppl 1: ppS17-S20

Daniel RK, Priest DL, Wheatley DC (1981): Etiological factors in pressure sores: an experimental model. Archives of Physical Medical and Rehabilitation:62: pp492-8

Hughes J (1969): Below-knee amputation-Biomechanics. In: Murdoch G: Editor; Prosthetics and Orthotics practice. Edward Arnold Ltd., pp 61-68

Hunter R (1996): Laboratory and clincal evaluation of a commercial stump socket interface pressure measurement system. MSc Thesis, Bioengineering Unit, University of Strathclyde, Glasgow.

Husain T (1953): An experimental study of some pressure effects on tissues, with reference to the bed-sore problem. Journal of Path bact: 66: pp347-58.

Krouskop TA, Noble PC, Garber SL (1983): The effectiveness of preventive management in reducing the occurance of pressure sores. Journal of Rehabilitation Research and Development: 20(1): pp74-83.

Levy SW (1980): Skin problems of the leg amputee, Prothetic and Orthotics international: 4: pp 37-44.

Mak AFT, Zhang M, Boone DA (2001): State-of-the-art research in lower limb prosthetic biomechanics-socket interface: A review: Journal of Rehabilitation Research and Development: Vol.38 No.2 : pp 161-174.

Michel CC, Gillott H (1990): Microvascular mechanisms in stasis and ischemia. In: Bader DL, Editor: Pressure Sores: Clinical Practice and scientific approach: London:Macmillan Press. pp 153-63.

Murdoch G (1969), Prosthetic and Orthotic Practice : London : Edward Arnold Ltd., London

Naeff M, Van Pijkeren T (1980): Dynamic pressure measurements at the interface between residual limb and socket-the relationship between pressure distribution, comfort, and brim shape . Bulletin of Prosthetic Research: 10-33: pp35-50

Naylor PFD (1955): Experimental frictional Blisters. British journal of Dermatology :67:327-42

Nola GT, Vistnes LM (1980): Differential response of skin and muscle in the experimental production of pressure sores. Plastic and Reconst Surgery:66: pp728-33

Oberg K, Kofman J, Karisson A, Lindstrom B, Sigblad G (1989): The CAPOD System-A Scandinavian CAD/CAM System for Prosthetic Sockets. Journal of Prosthetics and Orthotics; Vol.1(3); pp 139-148

Osman NAA(1999): Study of the pressure distribution at the stump/socket interface in a below knee prosthesis, MSc Thesis, Bioengineering Unit, University of Strathclyde, Glasgow

Pritham CH (1979): Suspension of the below knee prosthesis: an overview. Orth. Prosthet.:33(2): pp1-19

Pearson JR, Holmgren G, Marsh L (1973): Pressures in critical regions of the below-knee patellar tendon bearing prosthesis; Bulletin of Prosthetic Research:10-19: pp52-76

Polliack AA, Seih Rc, Craig DD, Landsberger S, McNeil DR, Ayyappa E (2000): Scientific validation of two commercial pressure systems for prosthetic socket fit. Prosthetic and Orthotic Interantional:24:63-73

Radcliffe CW, Foort J(1961): The patellar-tendon-bearing below-knee prosthesis. Biomechanics Laboratory: University of California. Berkeley.

Rae JW and Cockrell JL (1971): Interface pressure and stress distribution in prosthetic fitting: Bulletin of Prosthetic Research: 10-15: pp 64-111

Robinson KP (1991): Historical aspects of amputation. Annals of the Royal College of Surgeons of England:73(3): pp 134-6.

Sanders J.E., Goldstein B.S., Leotta D.F (1995): Skin Response to mechanical stress: Adaptation rather than breakdown – A review of Literature. Journal of Rehabilitation Research and Development: 32(3):pp 214-226.

Sanders JE and Daly CH (1993a): Measurement of stresses in three orthogonal direction at the residual limb or prosthetic socket interface. IEEE Trans. Rehab. Eng: 1(2): pp79-85

Sanders JE and Daly CH (1993b): Normal and shear stresses on a residual limb on a prosthetic socket during ambulation: comparison of finite element results with experimental measurements. Journal of Rehabilitation Research and Development: 30(2): pp191-204

Sanders JE, Daly CH, Burgess EM (1992): Interface shear stresses during ambulation with prosthetic limb. Journal of Rehabilitation Research and Development: 29(4) pp1-8.

Sanders JE, Daly CH, Burgess EM (1993): Clinical measurement of normal and shear stresses on a transtibial stump: characteristics of wave-form shapes during walking. Prosthetics and Orthotics International:17: pp38-48

Sanders JE, Daly CH (1999): Interface pressures and shear stresses: sagittal plane angular alignment effects in three trans-tibial amputee case study. Prothetics and Orthotics international:23: pp21-9

Sanders JE, Daniel MB, Okumura RM, Dralle AJ (1998): Effects of alingment changes on stance phase pressures and shear stresses on transtibial amputees: Measurement from 13 transducer sites; IEEE trans Rehab. Eng.:6(1): pp21-31

Sanders JE (1995): Interface mechanics in external prosthetics: Review of interface stress measurement techniques. Med Biol Eng comput:33: pp509-16

Shem KL, Breahey JW, werner PC (1998): Pressures at the residual limb-socket interface in transtibial amputees with thigh lacer-side joints. Journal of Prosthetics and Orthotics:10: pp51-5

Silver-Thorn MB, Steege JW, Childress DS (1996): A review of prosthetic interface stress investigations. Journal of Rehabilitation Research and Development:33(3): pp253-66

Snell R.S. (1992): Clinical anatomy for medical students: 4th Edition: Little, Brown and company, Boston/London/Toronto, pp 5-8.

Solomon L, Warwick D(2001): Apley's system of Orthopaedics, 8th edition, Edward Arnold, Ltd.London.

Sonck WA, Cockrell JL, Koepke GH (1970): Effect of liner materials on interface pressures in below knee prostheses. Archives of Physical Medicine and Rehabilitation:51: pp666-9

Tappin JW, Pollard JP, Beckett EA (1980); Method of measuring shearing forces on the side of the foot. Clin Phys. Physiol. Meas1: pp 83-85

Torres-Moreno R (1991): Biomechanical analysis of the interaction between the above knee residual limb and the prosthetic socket. PhD thesis, Bioengineering Unit, University of Strathclyde, Glasgow.

Van Pijkeren T, Naeff M, Kwee HH (1980) : A new method for the measurement of normal pressure between amputation residual limb and socket; Bulletin of Prosthetic Research: 10(33): pp 31-34.

Versluysen MJ (1985): Pressure sores in elderly patients: The epidemiology related to hip operations. Journal of Bone and joint surgery:67: pp10-13

Wandrum DJ (2000): A comparative stump-socket interface pressure distribution study between two trans-tibial prosthetic sockets, MSc Thesis, Bioengineering Unit, University of Strathclyde, Glasgow.

Williams RB, Porter D, Roberts VC (1992): Triaxial force transducer for investigating stresses at the stump/socket interface. Med. and Biol. Eng. and Comput.:30: pp89-96

Web sites

Tekscan prosthetic systems
http://www.tekscan.com/medical/system_prosthetic.html (May 2001)

Rincoe Socket fitting system
http://www.masson.com.au/wwps.htm

Fundamentals of Anatomy and Physiology by Ric martini (1999-2000)
http://cw.prenhall.com/bookbind/pubbooks/martini7/

Appendix :1

Auto-Cad Drawing of

PTB Mark-II Transducer & Calibration Jig

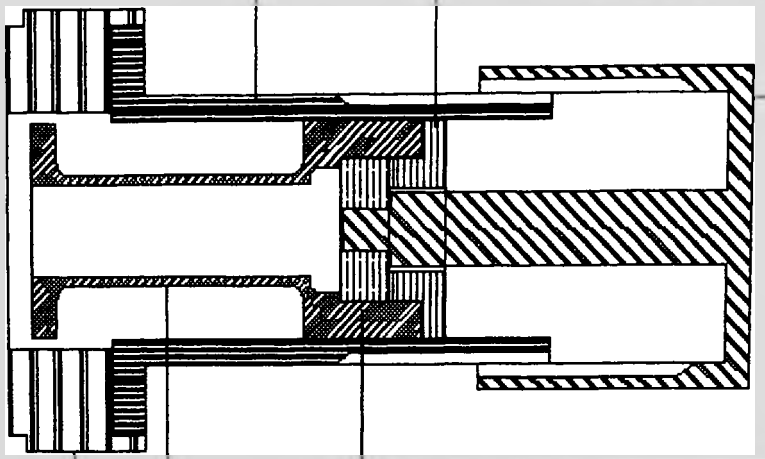

DRAWING NUMBER: A1
NAME : PTB TRANSDUCER
DRAWING NOT TO SCLAE

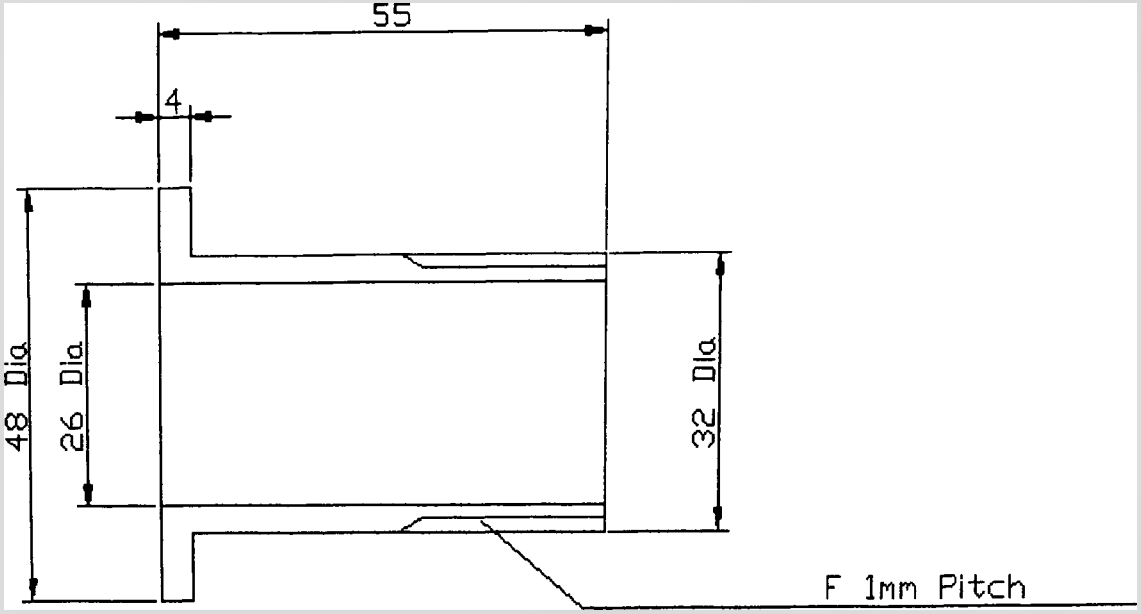

DRAWING NUMBER : A2
NAME : OUTER HOUSING
MATERIAL : ACETAL
DRAWING NOT TO SCALE-DIMENSIONS IN mm

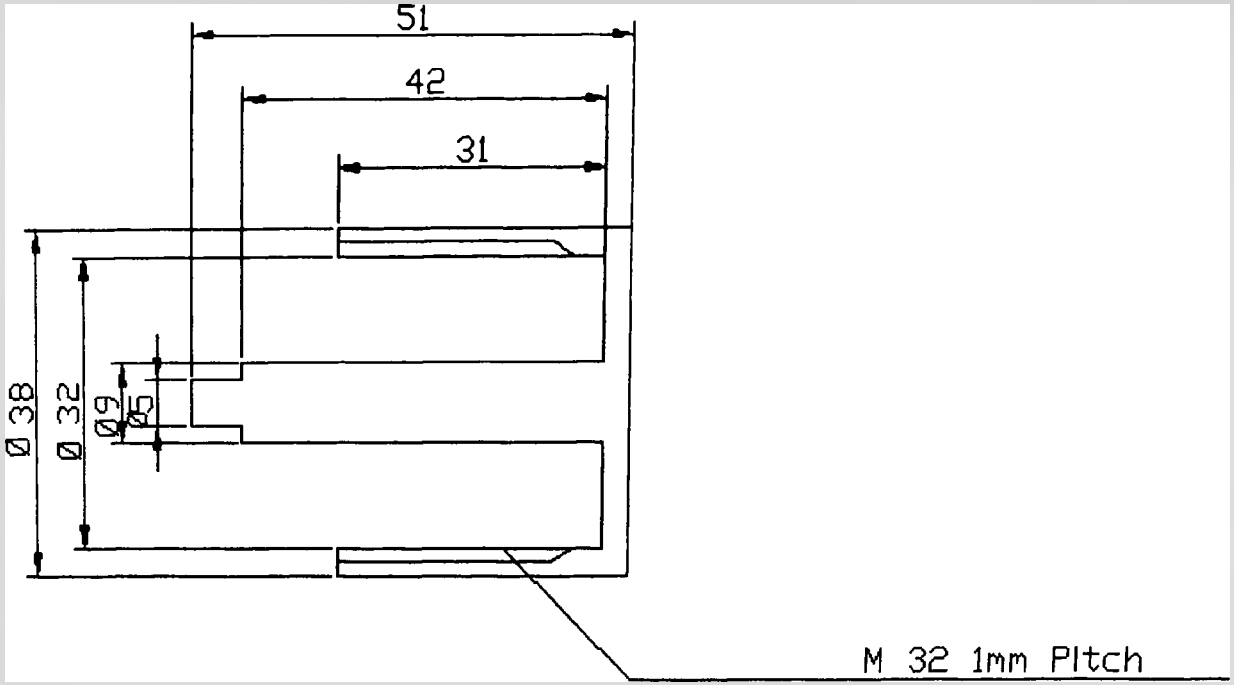

DRAWING NUMBER: A3
NAME : CONTROL KNOB
MATERIAL : ACETAL
DRAWING NOTT TO SCALE -DIMENSIONS IN mm

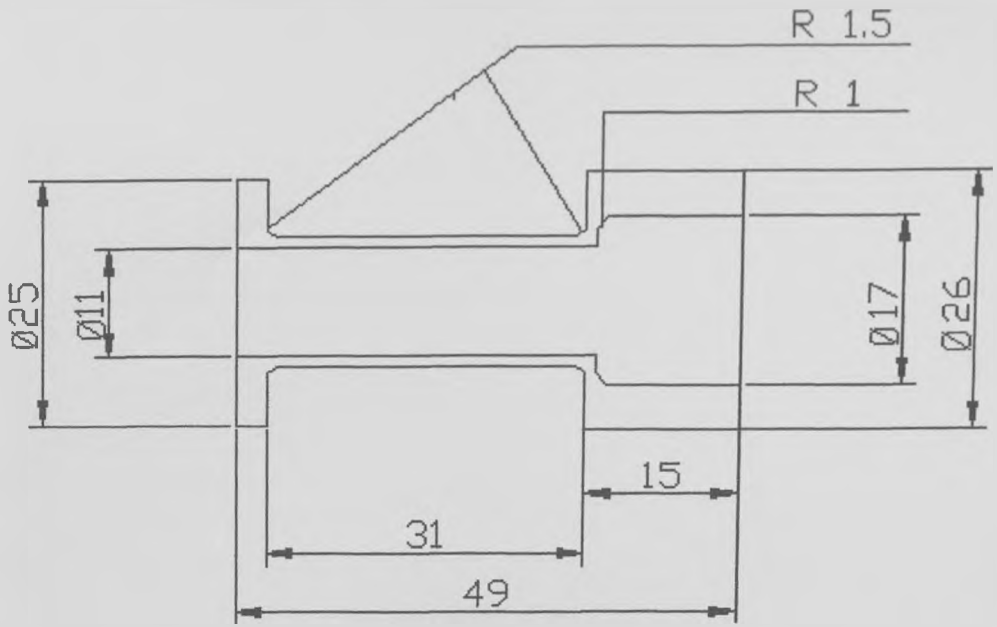

DRAWING NUMBER : A4
NAME : STRAIN GAUGE PISTON
MATERIAL : ALUMINIUM ALLOY
DRAWING NOT TO SCALE - DIMENSIONS IN mm

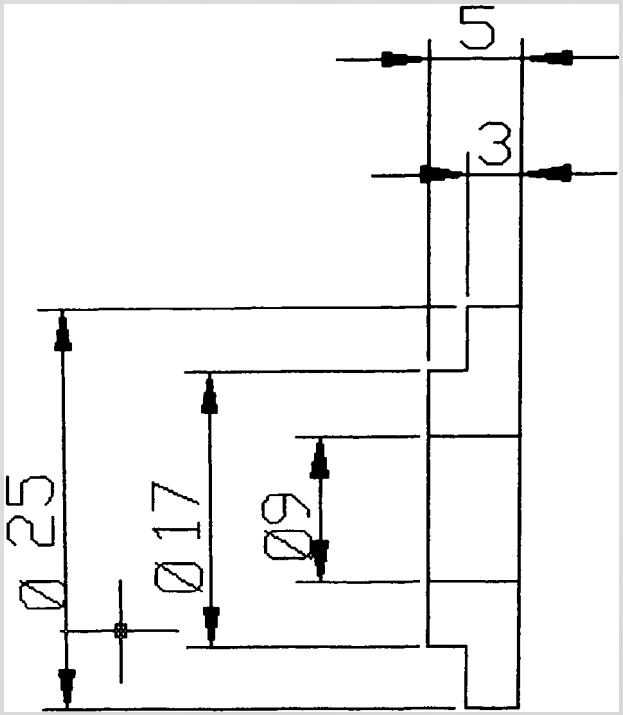

DRAWING NUMBER : A5
NAME : SPACER 1
MATERIAL : ALUMINIUM ALLOY
DRAWING NOT TO SCALE - DIMENSIONS IN mm

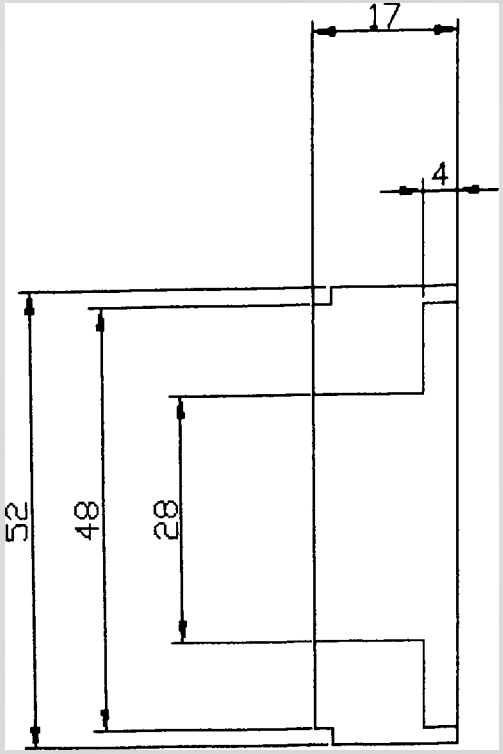

DRAWING NUMBER : A 6
NAME : HOUSING EXTENSION
MATERIAL : ACETAL
DRAWING NOT TO SCALE - DIMENSIONS IN mm

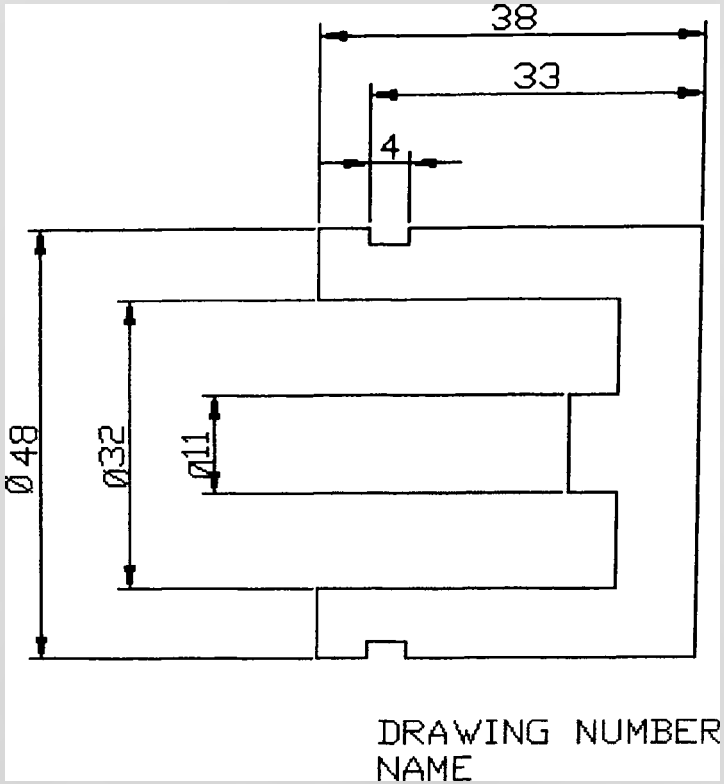

DRAWING NUMBER : B1
NAME : CALIBRATION JIG
MATERIAL : ALUMINIUM ALLOY
DRAWING NOT TO SCALE: DIMENSIONS IN mm

Appendix :2

Lab-View Programs

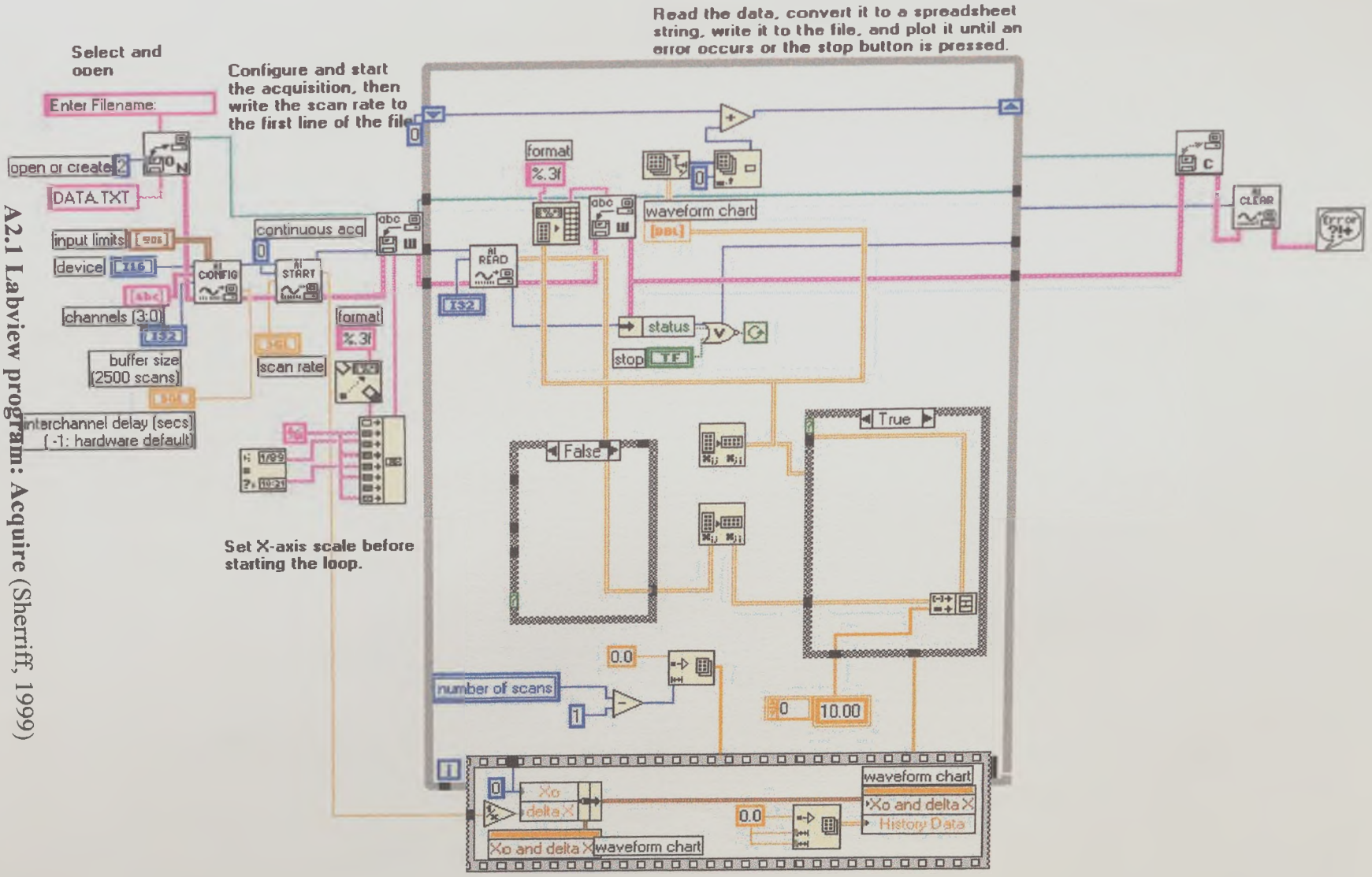

A2.1 Labview program: Acquire (Sherriff, 1999)

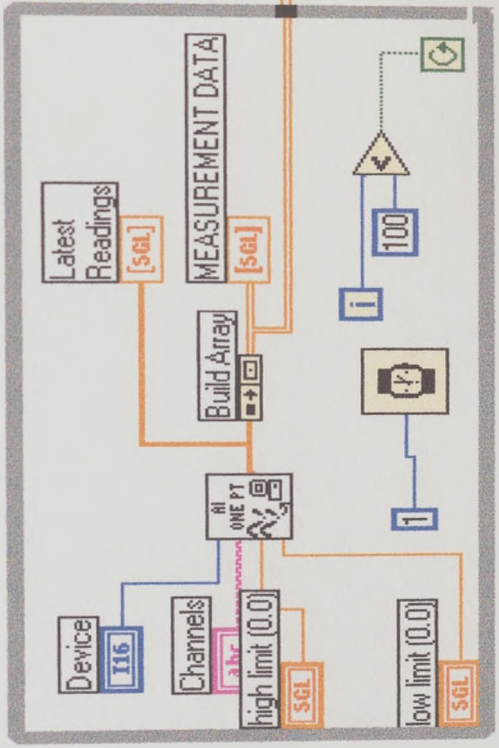

Labview program used for calibration

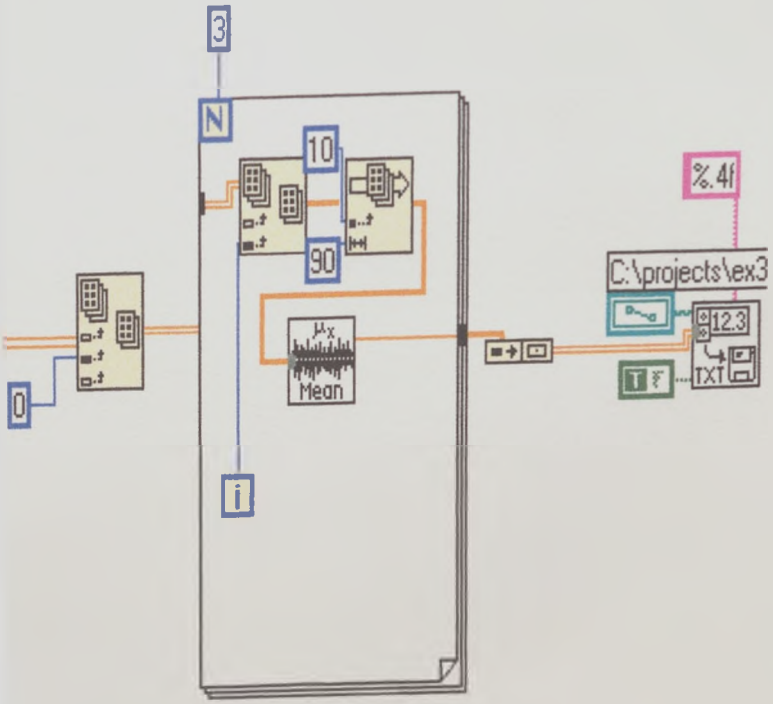
3
N
10
90
0
i
Mean
%.4f
C:\projects\ex3
12.3
TXT

APPENDIX: 3

Calibration results of shear channels without modification of calibration jig

load(N)	Fx(V)	Fy(V)	Fz(V)
0	0.0018	-0.0253	0.00036
5.54	0.0484	-0.1401	0.001
14.58	0.11272	-0.27384	-0.00018
23.63	0.1758	-0.39598	-0.00146
32.66	0.23852	-0.50352	-0.00466
42.73	0.3114	-0.63896	-0.00354
52.68	0.38036	-0.75076	-0.00396
62.7	0.4481	-0.8597	-0.00628
71.76	0.50838	-0.95182	-0.00872
62.7	0.45414	-0.88624	-0.0056
52.68	0.39036	-0.80824	-0.0035
42.73	0.32422	-0.71628	-0.0016
32.66	0.25362	-0.61092	-0.00068
23.63	0.1891	-0.48786	0.00086
14.58	0.12164	-0.33402	0.00128
5.54	0.05372	-0.17622	0.00086
0	0.00258	-0.03606	-0.00002

Table A3.1 Calibration Data: Channel Fx

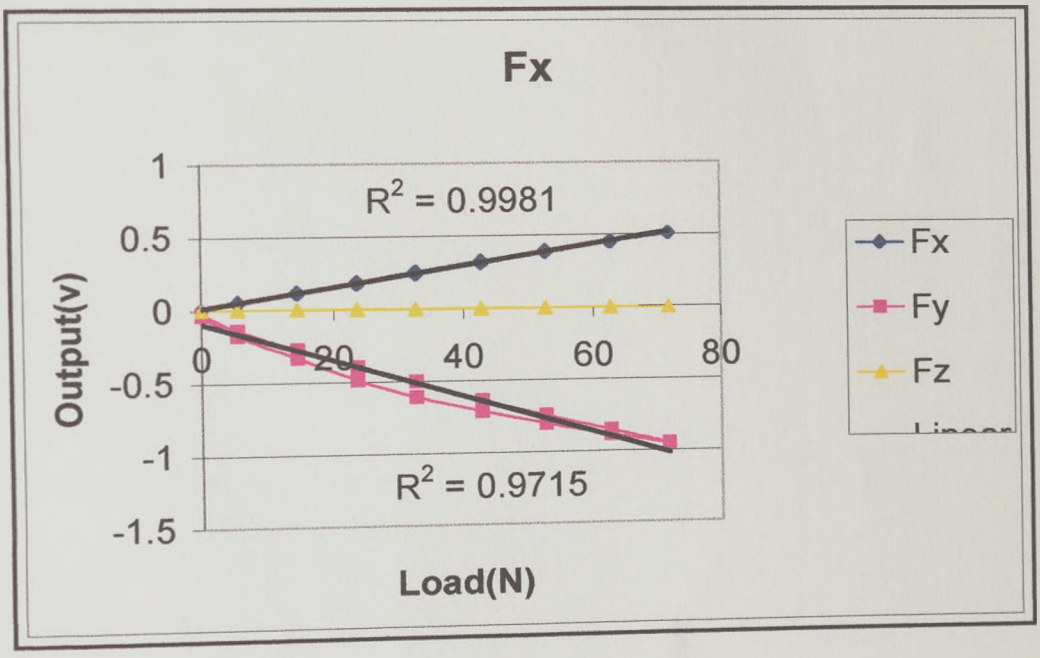

Figure A3.1 Calibration graph of channel Fx

load(N)	Fx (V)	Fy (V)	Fz (V)
0	-0.00076	-0.01382	-0.00056
5.54	-0.04674	-0.05966	-0.00822
14.58	-0.11182	-0.14262	-0.01574
23.63	-0.1756	-0.21972	-0.02278
32.66	-0.23974	-0.31758	-0.02766
42.73	-0.30836	-0.41948	-0.03136
52.68	-0.37328	-0.50504	-0.03198
62.7	-0.43762	-0.5708	-0.03314
71.76	-0.49526	-0.62424	-0.03514
62.7	-0.4427	-0.58548	-0.03558
52.68	-0.38328	-0.53148	-0.0358
42.73	-0.32244	-0.47282	-0.03558
32.66	-0.25712	-0.38998	-0.03472
23.63	-0.19074	-0.27974	-0.0296
14.58	-0.1199	-0.17312	-0.02046
5.54	-0.0507	-0.07668	-0.01042
0	-0.0012	-0.01946	-0.0014

Table A3.2 Calibration Data: Channel -Fx

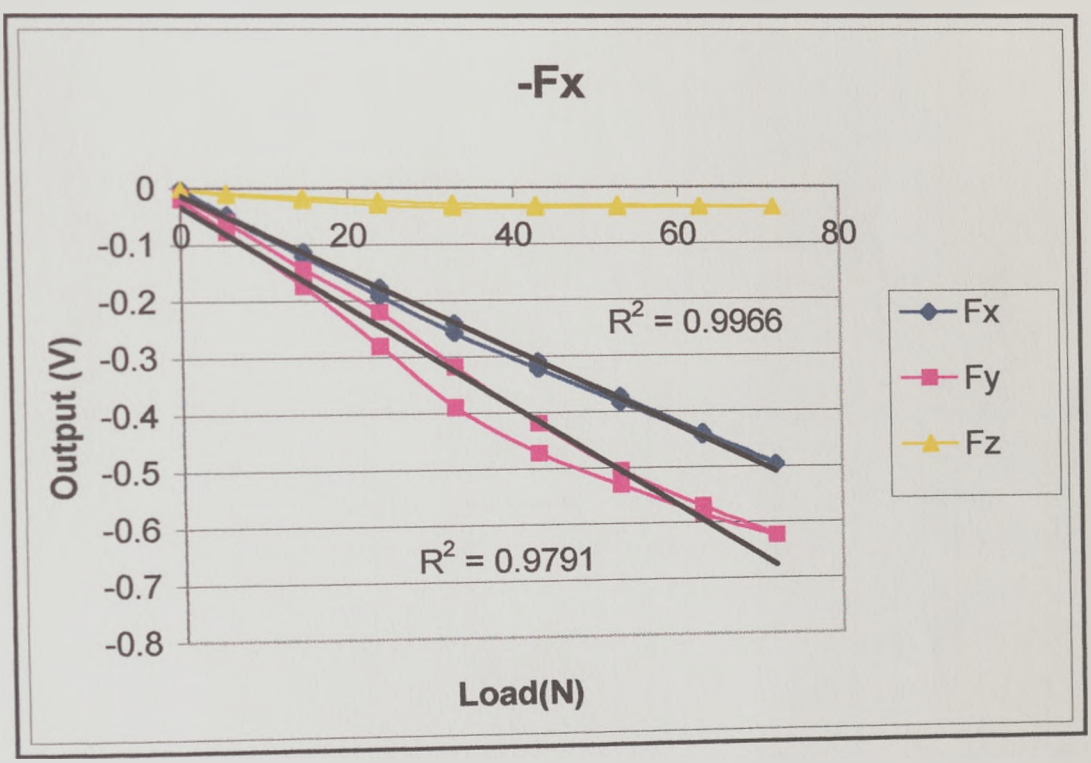

Figure A3.2 Calibration graph of channel -Fx

load(N)	Fx (V)	Fy (V)	Fz (V)
0	-0.00168	-0.02552	0.00236
5.54	-0.008	-0.04796	0.04576
14.58	-0.01492	-0.10418	0.11128
23.63	-0.01954	-0.1862	0.17688
32.66	-0.02394	-0.25048	0.24128
42.73	-0.02694	-0.35042	0.31442
52.68	-0.03046	-0.4368	0.38214
62.7	-0.03182	-0.5078	0.45028
71.76	-0.03256	-0.56184	0.51002
62.7	-0.03312	-0.51672	0.45524
52.68	-0.03538	-0.4502	0.39184
42.73	-0.03646	-0.38126	0.3279
32.66	-0.03456	-0.28896	0.2566
23.63	-0.02952	-0.17966	0.18772
14.58	-0.02114	-0.1036	0.11846
5.54	-0.01094	-0.0492	0.04884
0	-0.00222	-0.03282	0.00336

Table A3.3 Calibration Data: Channel Fz

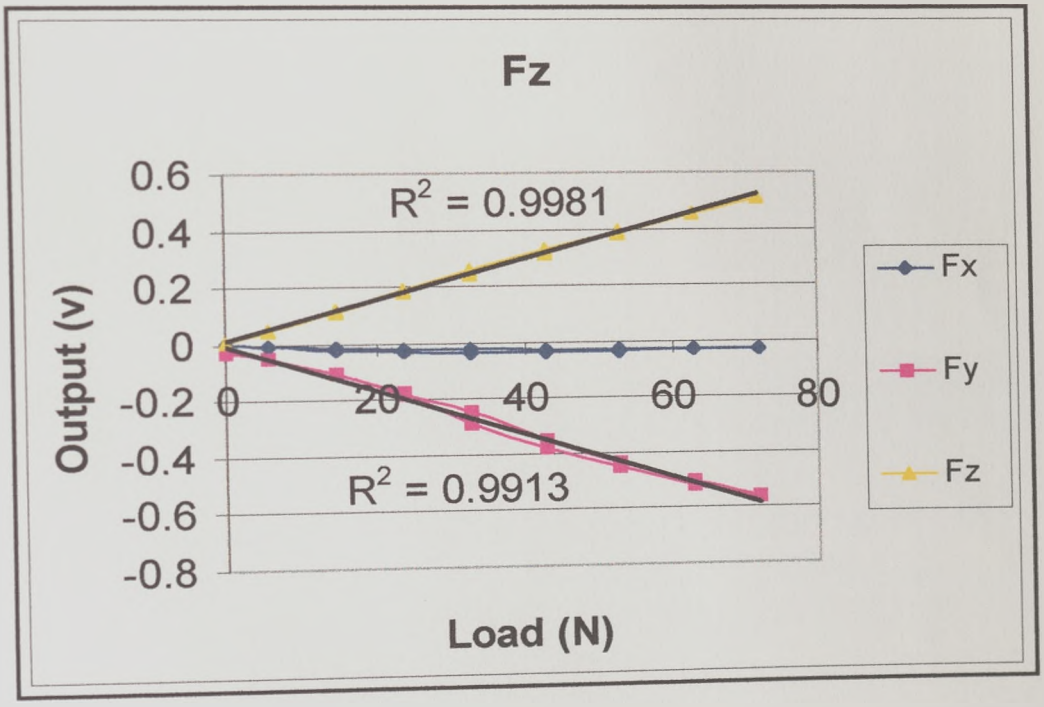

Figure A3.3 Calibration graph of channel Fz

load(N)	Fx (V)	Fy (V)	Fz (V)
0	0.00762	-0.0592	-0.00934
5.54	0.01374	-0.14166	-0.05912
14.58	0.0213	-0.25452	-0.12814
23.63	0.0279	-0.37862	-0.19684
32.66	0.03304	-0.50598	-0.26528
42.73	0.03772	-0.6413	-0.3391
52.68	0.04004	-0.77756	-0.40944
62.7	0.04018	-0.89632	-0.47884
71.76	0.03746	-1.00066	-0.54074
62.7	0.03888	-0.91708	-0.48516
52.68	0.0385	-0.829	-0.41904
42.73	0.03748	-0.70714	-0.35046
32.66	0.0357	-0.56852	-0.2763
23.63	0.03086	-0.43124	-0.20696
14.58	0.02274	-0.2988	-0.13342
5.54	0.01554	-0.17094	-0.06256
0	0.00792	-0.0864	-0.01162

Table A3.4 Calibration Data: Channel -Fz

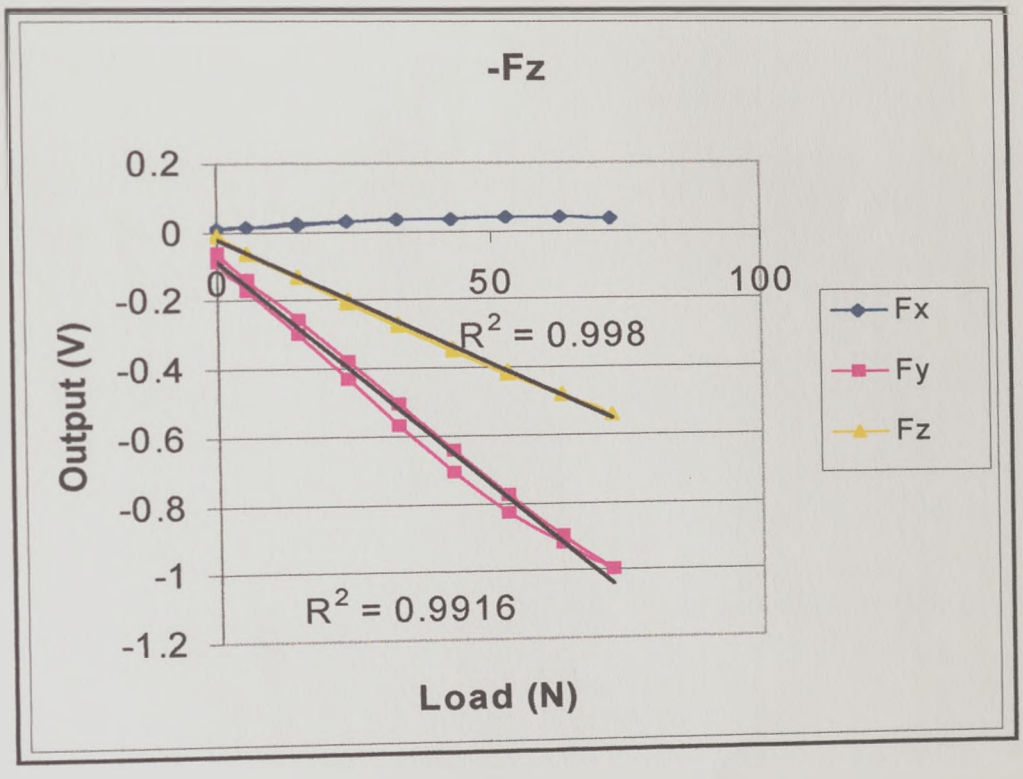

Figure A3.4 Calibration graph of channel –Fz

APPENDIX: 4

Example of calibration factor calculation

Calculation of calibration co-efficient on Fx loading

Load(N)	Fx (V)	Fy (V)	Fz (V)
0	0.00328	0.0064	-0.00068
71.76	0.40308	0.01508	-0.01358

Formula:

M_{11} = [(Slope of forces for Fx)] / [Slope of load] V/N

M_{21} = [(Slope of forces for Fy)] / [Slope of load] V/N

M_{31} = [(Slope of forces for Fz)] / [Slope of load] V/N

Calculation:

M_{11} = [(0.40308-0.00328)] / [71.76-0]

= .00557 V/N

M_{21} = [(0.01508-0.0064)] / [71.76-0]

= 0.00012 V/N

M_{31} = [(-.0.01358+0.00068)] / [71.76-0]

= -0.00018 V/N

The average of both the co-efficient of Fx and –Fx was then calculated to give the final M_{11}, M_{21} and M_{31}, co-efficient.

APPENDIX : 5

Patient Evaluation Form

Name: **Date:**
Age/DOB:
Sex:
Address:

Date of amputation:
Type of amputation: **Side:**
Type of Test socket:

Brief History:

Examination:

Inspection:

Sensory Evaluation:

Palpation:
Tenderness:

Adherent scars:

Odema:

ROM:

Muscle power:

	R	L		R	L
Hip F			Knee F		
E			E		
Ab			Ankle DF		

Ad **PF**
Irot
Erot

LLD:

Stump dimensions:

Length:

Proximal circumference (tibial Plateau):

Distal Circumference :

Other findings/Comments:

APPENDIX:6
SOUTHERN GENERAL HOSPITAL NHS TRUST

CONSENT FORM

PATENT NAME.....DATE OF BIRTH.....

To be completed by the patient

	Please Tick Yes	No
Have you read the Patient information?	☐	☐
Have you heard an opportunity to ask questions and discuss this study?	☐	☐
Have you received satisfactory answers to all your questions?	☐	☐
Have you received enough information about the study?	☐	☐

Who have you spoken to? Dr/Mr/Ms_____

Do you understand that you are free to withdraw from the study –

- At any time
- Without having given a reason
- And without affecting your future medical care? ☐ ☐
- Do you agree to take part in this study? ☐ ☐

Do you have any reason to believe you are or may be pregnant?	
YES, I may be pregnant	☐
NO, I am not pregnant	☐

Signed..... Date.....

Name in Block Letters.....

Signature of Witness..... Date.....

Name in Block letters.....